ENGINEERING MULTIVALENT VIRAL VACCINES

A Dissertation
Presented to
The Academic Faculty

by

Ana Luisa Stringari de Castro

In Partial Fulfillment
of the Requirements for the Degree
Doctor of Philosophy in the
School of Chemical and Biomolecular Engineering

Georgia Institute of Technology
May 2021

ENGINEERING MULTIVALENT VIRAL VACCINES

Approved by:

Dr. Ravi Kane, Advisor
School of Chemical and Biomolecular Engineering
Georgia Institute of Technology

Dr. Manu O. Platt
School of Biomedical Engineering
Georgia Institute of Technology

Dr. Julie Champion
School of Chemical and Biomolecular Engineering
Georgia Institute of Technology

Dr. Mark Prausnitz
School of Chemical and Biomolecular Engineering
Georgia Institute of Technology

Dr. Anant Paravastu
School of Chemical and Biomolecular Engineering
Georgia Institute of Technology

Date Approved: December 11th, 2020

To my Nono. I know that if you were here to see this, you would proudly pinch my cheeks and call me “minha estimada”.

ACKNOWLEDGEMENTS

This thesis and all the work from the last 5 years would not have been possible if it wasn't for the unconditional love and support from my family. Mom, I don't know how I will ever be able to show you my gratitude. Not only for your financial support along the way, but for always offering me a shoulder to cry on after a bad day, or words of advice that only a mother can offer, or even just telling me it's going to be okay when we both know that's a lie. You are my everything. Dad, I know things have been rocky between us, but you, somehow, always knew the right thing to say. You kept me grounded and always reminded me of how much I accomplished and how proud you are of me, even in moments when nothing seemed to be going my way. And to the rest of my family, gosh, I miss you all. You are amazing and I feel so lucky for being born into a family that has so much love to give.

On a less emotional note, I would obviously like to thank my advisor, Dr. Ravi Kane, for providing me with guidance (and money) during my PhD. I admire how invested you are in every single project, and how you always have some solution or word of advice to whatever problem I was facing. Also, I'm sorry. I'm sure I cost you a few strands of hair due to DIII-related stress. I swear I did everything I could, the project was just really really hard.

I would also like to thank my committee members, Dr. Champion, Dr. Prausnitz, Dr. Paravastu, and Dr. Platt for all the helpful feedback throughout this

process and for always being so approachable. Another thanks to our collaborators in the Krammer lab: Dr. Florian Krammer, Jim Duehr, and Juan Manuel.

I also want to thank my awesome lab group. You guys made this experience 10000000x more fun and I will forever cherish my memories from “lab after 5”. Ammar, thank you for teaching me 90% of what I know and for possibly being the only person who gets my sense of humor. Steve, thank you for always letting me take some of your cells whenever I managed to kill mine. Troy, I hope you know I’ll always be here, available to help you with whatever relationship struggles you may have. Mark, Geet, Nicole, Kathryn, Nikki, Abhirup, Chad, and Tania: thank you. Also, a special shout out to the honorary members of the Kane lab: Vivek, Luke, and Shruti. Obviously, I can’t forget about my little army of undergrads: Felix, Ash, Dani, Julia, Kassandra, and Chris. Mentoring you was a pleasure.

Thank you to the CheBesties (ChBesties? Did we ever figure out the proper spelling for this?). I probably wouldn’t have even made it through the first semester of grad school if I hadn’t awkwardly invited myself to hang out with you. I cannot picture going through grad school without you guys. You are all so great and I’m so sure you will accomplish so much in life. And I swear by the spoon in the champagne bottle, it’s like, scientifically proven.

A special thanks to Krysten, the best friend and roommate I could have asked for. Thank you for always being there to eat cake with me when things were rough. And for not letting me eat icing until the point of getting sick. And for being the most emotionally intelligent person I know and always always always saying the

right and compassionate thing (and for siding with me even when I was in the wrong). Also, Nancy, thank you for being such a good friend. And for bringing me a plate of Thanksgiving leftover because you knew I would just work all day. You have such a big heart. I am truly honored to be your friend.

I am not sure if I can do this, but I'm about to be a Doctor, so I'll go ahead anyways: Juno, thank you for being the cutest and fluffiest little cat in the world.

And, saving the best for last, I would like to thank my incredibly supportive boyfriend, James. You were my rock for the last 3 years and I don't know how I would have made it through the last couple of extremely stressful months without your love and encouragement. Thank you for being so understanding. Thank you for hugging me tight and making me feel everything will be okay. Thank you for having dinner ready whenever I got home late. Thank you for not letting me always be so hard on myself. Thank you for being in my life. I can't wait to see where our next adventure will take us.

TABLE OF CONTENTS

LIST OF FIGURES

SUMMARY

The ability to design efficacious vaccines for many diseases has been hindered by existing sequence diversity in pathogen proteins and by newly-acquired mutations that enable escape from adaptive immune responses. To address these limitations, we have developed an approach for nanopatterning protein antigens to focus the immune response on conserved protein regions. This approach combines the site-specific incorporation of non-canonical amino acids into proteins with chemical modification with polyethylene glycol (PEG) or other molecules. We will describe the design of a ZIKV vaccine based on domain III (DIII) of the viral envelope protein (E). By chemically modifying the protein surface, we have demonstrated the ability to refocus the immune response to targeted epitopes on the protein antigen. We also demonstrate the ability to enhance immunogenicity by the multivalent presentation of nanopatterned antigens on scaffolds.

Also in the context of the Zika virus vaccines, it would be advantageous to design a vaccine that promotes the generation of broadly neutralizing antibodies. A promising epitope to target is the Envelope Dimer Epitope (EDE), located at the interface between two E proteins in a dimer, that is highly conserved among Zika and Dengue viruses. To achieve this goal, we will demonstrate an approach that we have developed for stabilizing E dimers on the surface of virus-like particles (VLPs).

Finally, in response to the current pandemic, we will describe the design of vaccines presenting the Receptor Binding Domain (RBD) of the Spike protein of the novel SARS-CoV-2 virus. Furthermore, we will test the ability to use glycans to shield different epitopes on RBD. This approach could be used to design vaccines that generate a more potent SARS-

CoV-2-specific neutralizing antibody response, as well as those that can confer protection against both SARS-CoV and SARS-CoV-2.

CHAPTER 1. INTRODUCTION

In the early 1900s, infectious diseases were widely prevalent in the United States, with smallpox, diphtheria, measles, and pertussis claiming tens of thousands of lives every year [1-3]. Infectious diseases accounted for over 50% of child deaths [4], contributing to a childhood mortality rate of over 20% before the age of 5 [5]. Thanks to the groundbreaking work of Edward Jenner – who demonstrated that cowpox could be used to prevent smallpox [6, 7] – we learned that through medical intervention it was possible to "train" the immune system to recognize and fight pathogens, and thus the idea of a vaccine was created. Due to advancements in the areas of immunology and vaccinology, we can now thank vaccines – and vaccination campaigns – for the eradication of smallpox worldwide and the elimination of polio in the U.S. Such feats have granted vaccines the title of one of the greatest achievements of the last century [8].

Simply put, vaccination stimulates the immune system by mimicking an infection [9, 10]. An infection with a foreign agent first triggers an immediate response by the innate arm of the immune system. Pattern recognition receptors (PRRs) that are presented on the surface of phagocytic cells (such as macrophages, granulocytes, and dendritic cells) can recognize conserved molecular patterns that are shared between viruses, bacteria, and parasites [1-3]. The binding of these PRRs to a compatible pathogen results in the production and release of signaling molecules that recruit other innate cells to the site of infection, and in the opsonization of the pathogen by the phagocytic cell in an attempt to digest it [4, 5]. All components of the innate immune system work together to try to contain the infection and, if possible, eliminate it completely [6].

Another important role of the innate immune system is to initiate the activation of an adaptive immune response, in which T and B lymphocytes play a central role. Unlike the innate immune response, the adaptive immune response is highly specific to each individual pathogen. For instance, naïve T cells become activated when their receptors (TCRs) encounter and bind protein fragments displayed on the surface of phagocytes [7] known as antigen-presenting cells (APCs). APCs present pathogenic peptides on their surface complexed with one of a set of glycoproteins that together form the major histocompatibility complex (MHC), which are divided into two classes (MHC I and MHC II)[8]. The MHC I presents short peptides derived from pathogens that are present in the cytosol of APCs, and engagement between the peptide:MHC I and TCR leads to the differentiation of the T cell into cytotoxic T lymphocytes [9], which aid in the destruction of infected cells. Alternatively, APCs that have engulfed a pathogen and digested it into fragments, present those on the MHC II. The engagement between the TCR and the peptide-displaying MHC II, results in the differentiation of T cells into helper T lymphocytes, which have the role of regulating other components of the immune response [7, 10]. A small portion of the differentiated T lymphocytes develops into long-lived memory T cells [11].

Naïve B lymphocytes, on the other hand, can directly recognize and bind to the soluble pathogen via the interaction between specific pathogenic regions, known as epitopes, and the cell's surface receptors (BCRs) [7, 12, 13]. This engagement results in the pathogen's internalization, digestion, and peptide presentation on MHC II on the surface of B cells [5, 14]. Unlikely other APCs, the goal of antigen-presentation on B cells is not to activate naïve T cells, but to take advantage of T cell's effector functions. The

binding of helper T cells to the peptide-MHC II complex on the surface of a B cell [15] results in the release of cytokines that help trigger B cell activation [5]. This activation is followed by B cell differentiation into short-lived plasma B cells, which produce antibodies that bind and, ideally, neutralize the foreign agent as well as memory B cells, which reside in the lymph nodes [6, 13].

B cells activation can also occur in a T-cell-independent manner, either by the binding of non-specific antigen motifs to different receptors on a B cell surface, or by the crosslinking of BCRs [16, 17]. BCR crosslinking can be achieved by antigens that contain highly repetitive structures and can bind to multiple receptors simultaneously [18, 19]. This results in the phosphorylation of certain receptors and the recruitment of other molecules that will ultimately lead to the activation of the cell [20]. For a long time, it was believed that T-independent B cell activation did not result in the generation of memory B cells. However, recent studies demonstrated that direct antigen activation can generate both long-lasting plasma B cell and memory B cells [19, 21, 22], both of which can undergo somatic hypermutation to generate receptors with enhanced antigen affinity [23].

Vaccination is analogous to the primary exposure to a pathogen (or pathogenic subunits), and would, ideally trigger an immune response that can generate memory lymphocytes. In the case of a secondary exposure to the pathogen, which in this case would be a real infection, the previously generated memory B and T cells quickly start to proliferate, resulting in a more rapid and stronger immune response than the one seen during the primary exposure [1, 24]. Memory B cells and long-lasting plasma B cells, specifically, are able to quickly secrete large amounts of higher-affinity antibodies that

can aid in pathogen neutralization [1]. As a result, the pathogen is eliminated before it has time to infect multiple cells and do damage to the host.

The majority of vaccines that prevent viral or bacterial infections are either live attenuated or inactivated. Live attenuated vaccines are constituted of a weakened form of the pathogen that cannot cause the disease. Such vaccines are often easy to produce and only require one or two doses to generate long-lasting immunity. However, due to the delicate nature of live attenuated vaccines, preservation might be an issue, along with the possibility of the pathogen reverting to its original virulent form. Inactivated vaccines, on the other hand, contain pathogens that have been rendered inactive killed by chemical or physical means, posing no threat of infection, but often resulting in a weaker immune response than what is obtained with live attenuated vaccines [9-12]. Subunit vaccines constitute a third class of vaccines and present only a part of the virus or bacteria, such as a protein or peptide that is required to generate an immune response. Such vaccines are safer, since there is no risk of pathogenicity and also allow us to tackle more challenging diseases, but like inactivated vaccines, they may elicit a weaker immune response than live attenuated vaccines.

Approaches to vaccine design also have to take into account two other factors – immune evasion and immunodominance. Several pathogens can evade the immune system by undergoing mutations, making certain antigens no longer recognizable by memory B and T cells. Fortunately, not all parts of an antigen mutate at the same rate; mutations in some regions (e.g., those that affect interaction with the host cell) could severely hinder the pathogen's infection ability. As a result, proteins often contain regions that are highly conserved and that could, theoretically, be recognized by memory

lymphocytes even after several mutation cycles. Therefore, these regions become a very attractive target in vaccine design. A second factor that one must consider is immunodominance. The adaptive immune response does not target all parts of a protein antigen equally; in fact, in several cases, the immunodominant regions – the ones that elicit the strongest immune response – are not the most conserved regions in the antigen.

A great example of how these factors influence efforts to design effective vaccine is the extensive work that has been done on the design of vaccines based on the Influenza Hemagglutinin (HA) protein, which is composed of a highly variable immunodominant head and a conserved subdominant stalk [25, 26]. Efforts have been made to redirect the immune response to the conserved stalk in order to promote the generation of antibodies that can protect against multiple flu strains [27-29] – i.e., a universal flu vaccine. Refocusing the immune response to selected (usually conserved) epitopes is referred to as immunofocusing [30, 31]. A number of immunofocusing strategies have been developed, including protein truncation, antigen resurfacing, and immunosilencing as recently reviewed [32]. Our focus in this work has been on approaches to engineer protein antigens based on glycan shielding [28, 33-35] and nanopatterning [36].

1.1 Engineering Protein Antigens to Modulate the Immune Response

Glycosylation has been widely used as a tool to modulate the immunogenicity of antigens. Glycans can interfere with epitope recognition [13] and sometimes a single glycosylation site is enough to completely prevent antibody binding [14, 15]. However, a glycosylation-based approach comes with several limitations since post translational modifications might have negative effects in protein folding and oligomerization.

The functionalization of protein antigens with Polyethylene Glycol (PEG) has demonstrated to be an efficient and versatile immunomodulating tool [16, 17]. PEG moieties containing reactive chemical handles allow for their easy and rapid conjugation to amino acids, such as attaching PEG-succinimidyl esters to lysines [18] or PEG-maleimide to free cysteines [19]. Such examples, however, might not allow for specific selection of the PEGylation site since we are limited by the number of lysines and free cysteines on the protein. As an alternative, it is possible to better control PEG conjugation via site-specific incorporation of PEG-reactive unnatural amino acids.

In the past few years, the Kane Lab has worked extensively to apply unnatural amino acid incorporation and protein PEGylation in the context of antigen immunomodulation. Under this premise, the Kane Lab has developed and coined the term nanopatterning, which consists of controlling "on the nanometer scale the chemistry and topography of the protein surface and its accessibility to components of the immune system" [20]. Via protein engineering and PEG conjugation, we were able to shield antigen epitopes and bias the generated immune response upon immunization, redirecting it towards epitopes with neutralizing potential [20]. In this document, we will use protein engineering tools including nanopatterning and glycan shielding to design vaccines against viruses like Zika and SARS-CoV-2.

1.2 Modulating the Immune Response Against Zika Virus and SARS-CoV-2

The Zika Virus (ZIKV) was first isolated in 1947 but it remained dormant for decades until it resurfaced in 2007 on the Yap Islands. Sporadic outbreaks were reported, mainly in the Asian and African continents, until French Polynesia and Brazil were

severely hit in 2013 and 2015, respectively. The increase in the number of ZIKV infections coincided with an increase in the number of registered cases of severe central nervous systems disorders and poor fetal development, suggesting a possible link between them and ZIKV. In 2015, Brazil reported a 20x increase [37] in the number of cases of microcephaly – a fetal neurodevelopmental disorder that results in reduced brain size [38] - with regions recording near 20 cases per 10,000 births [39]. Such data not only strengthens the belief that infections with ZIKV can lead to severe neurological damage, but also that the virus has the ability of crossing the placenta. Additionally, studies [40] involving the analysis of sera of patients diagnosed with Guillain Barré syndrome (GBS), an immune-mediated disease that leads to paralysis [41], during the pandemic period revealed that most patients had ZIKV IgM in their serum. Furthermore, a 14x increase in GBS cases was recorded in French Polynesia that year [40]. Given the severe potential effect of Zika infections, a race for the development of a Zika vaccine began.

This development process is, unfortunately, not as straightforward as one would hope. According to the WHO vaccine roadmap, an ideal Zika vaccine would be efficacious, affordable, and safe to be administered to women of reproductive age, mainly pregnant women. Immunization strategies against Zika should be in place not only for the case of a new pandemic, but also for endemic regions [42, 43]. Although there were originally over 40 vaccine candidates being evaluated in pre-clinical studies [44], a vaccine against the virus is still not available. Sixteen candidates are still undergoing or have completed phase I or II clinical trials, but the main issue comes with the next stage of testing, which involves determining vaccine efficacy. With the decrease in the

incidence of Zika in the last few years, less people are inclined to contract the disease, making it difficult – and costly - to assess whether the vaccine confers protection or not.

As ZIKV infections become less prevalent, the focus of vaccine research shifts to new threats, such as the novel Coronavirus. The Novel Severe Acute Respiratory Syndrome Coronavirus (SARS-CoV-2 or nCoV-19) was first detected in the end of 2019 in the Wuhan province in China and it is on the track to becoming one of United States top killers, with a death count reaching the hundreds of thousands [45, 46]. This virus, which is related to SARS-CoV and MERS-CoV, has spread quickly throughout the globe and great efforts have been spent in the development of a vaccine. Unfortunately, as it is the case with any novel virus, there are a lot of questions surrounding SARS-CoV-2. Unknowns – like the mutation rate of the virus and the nature and duration of elicited antibodies – greatly affect vaccine design. A few cases of reinfections with the virus [47] – that may have already mutated enough to evade pre-existing antibodies – demonstrate the importance of designing a vaccine that will elicit broadly neutralizing antibodies and prevent a similar SARS-CoV-2 pandemic from happening again in the future.

CHAPTER 2. NANOPATTERNING ZIKV DIII TO REFOCUS THE IMMUNE RESPONSE

2.1 Introduction

ZIKV belongs to the Flaviviridae family, which is comprised of over 70 different single-stranded positive sense RNA viruses [48] that are commonly transmitted to humans by arthropods [49]. Due to their means of transmission, diseases caused by flaviviruses are more prominent in tropical regions of the globe, such as Asia and Africa [50]. Some other well-known members of this family are the Yellow Fever, West Nile, and Dengue viruses [51]. Flaviviruses are composed of 3 structural proteins - the precursor membrane (prM), capsid (C) and envelope (E) proteins- and 7 non-structural ones - NS1, NS2A, NS2B, NS3, NS4A, NS4B, and NS5. Among them, the E glycoprotein has shown to be crucial during viral infection since it is responsible for host cell binding and entry [52, 53]. Studies have demonstrated that the E protein is the main target of strongly neutralizing antibodies [49, 54, 55].

Given its role in viral infection, residues of E tend to be conserved [56]. ZIKV and Dengue Virus (DENV) E proteins, for example, have over 50% of sequence homology[57], which results in antibody cross-reactivity between the two. This cross-reactivity, however, does not always correlate with affinity or neutralization potential and anti-ZIKV antibodies might not bind with the same avidity to Dengue virions and vice-versa. In reality, such antibodies have the potential to enhance viral infection in a process known as antibody-dependent enhancement (ADE) [50, 58-60]. ADE is the process in

which pre-existing, cross-reactive, non-neutralizing antibodies can aid viral entry into host cells. In this case, antibodies generated against DENV, for example, might bind ZIKV but not at high enough concentration or avidity to neutralize it. This virus-antibody complex can then be opsonized by myeloid cells via the interaction between the antibody's Fc domain and the cell's Fc receptor [57, 61-63]. Once inside the cell, the virus, which is not neutralized by the antibodies, can proceed with its replication. Myeloid cells do not have the receptors that normally allow for viral entry, so this alternative entry method results in an increased total number of infected cells, which, consequently, leads to increased viremia and more deadly forms of the disease [50]. This infection enhancement has been shown to occur between ZIKV and DENV both through *in vitro* and *in vivo* experiments [50, 58-60] and a schematic of the process is illustrated in Figure 1.

ADE becomes a great concern when we look at ZIKV and DENV endemic regions where a significant portion of the population will encounter one of these two pathogens during their lifetimes and, consequently, have memory cells that target DENV or ZIKV. Therefore, it is of the utmost importance to ensure that any vaccine candidate against one of these viruses elicits an antibody response that will not result in ADE. Such a feat could be achieved by designing a vaccine that will only elicit ZIKV-specific and neutralizing antibodies.

The Envelope protein assembles as dimers that coat the surface of the Zika virion (Figure 2a and Figure 2b) can be subdivided into three domains: DI (yellow), DII (red), and DIII (blue), as shown in Figure 2c. DI acts as a hinge, connecting the other two domains and is the target of most of the serotype-specific antibodies. DII is described as the dimerization domain [64] since it makes contact with itself when E is in its

dimer form, and is the site of the fusion peptide and many cross-reactive epitopes. DIII is believed to be involved in receptor binding and contains epitopes that elicit ZIKV-specific neutralizing antibodies [56, 65-67]. Among the three domains, DIII has the lowest degree of conservation, with only 29% of homology between ZIKV and DENV [67]. The potential of DIII eliciting antibodies that are not cross-reactive, make this protein an attractive antigen in the design of a ZIKV vaccine.

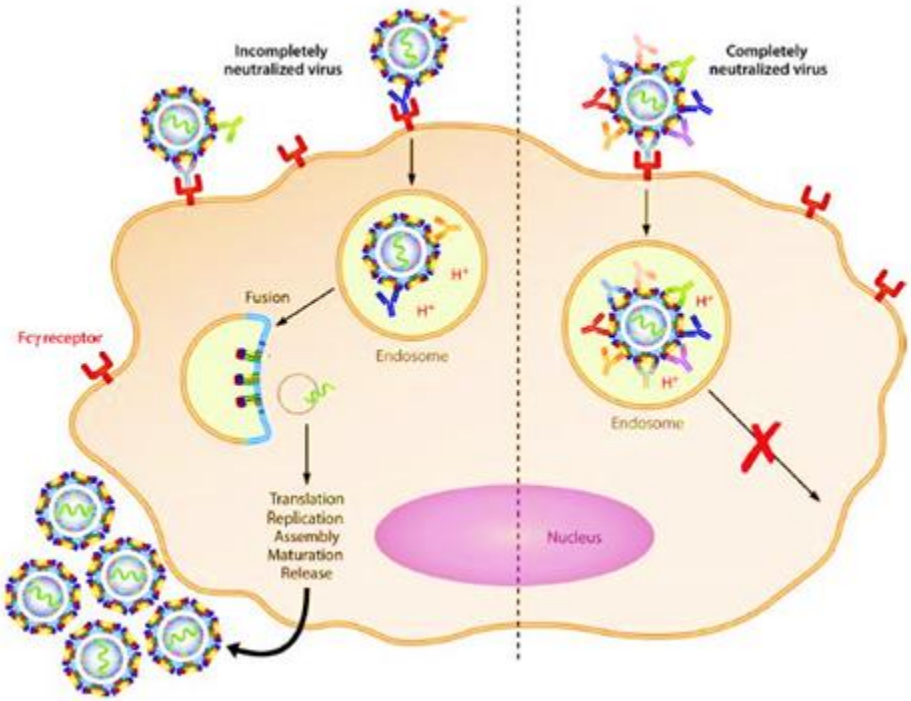

Figure 1. Illustration of the process of antibody dependent enhancement. Cross-reactive and non-neutralizing antibodies bind to the virus and allow for its opsonization by the Fc receptor of immune cells. The non-neutralized virus is able to reproduce when inside the cell. Neutralizing antibodies, on the other hand, prevent viral replication upon opsonization by the cells. Figure adapted from Heinz and Stiasny, 2017 [68].

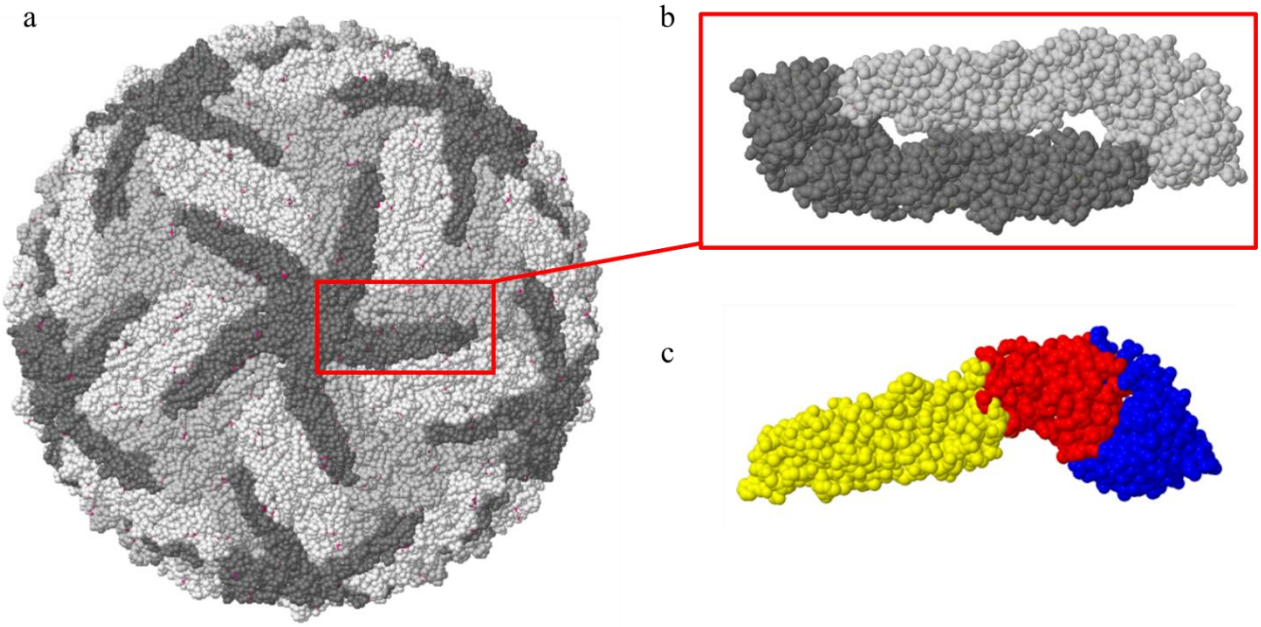

Figure 2. Structure of the Zika Virus. (a) Crystal Structure of the ZIKV virion (PDB 5IRE) with envelope protein monomers shown in light, medium, and dark grey. (b) Two E monomers assemble in a head-to-tail orientation to form E dimers. (c) E monomer with the three domains highlighted: DI (yellow), DII (red), and DIII (blue)

In a recent study, Zhao et al. [69] identified three very distinct epitopes on DIII that are targeted by antibodies with varying degrees of neutralization: the Lateral Ridge (LR), C-C' loop, and ABDE sheet (Figure 3c). The LR epitope is targeted by antibodies that have shown neutralization ability in animal models, such as the antibody ZV-67. The C-C' loop, on the other hand, is targeted by antibodies like ZV-48, which can neutralize some viral strains. This is believed to be due to the dynamic structure of flaviviruses, which are constantly undergoing rearrangement of its surface proteins in a process known as "viral breathing" [70]. Changes in pH and temperature might lead to reorganization of the E protein and affect the spacing between E dimers [70, 71]. Depending on the state of virions and the distance between E proteins, some regions of E might be occluded, and,

as a result, some epitopes might be inaccessible to antibodies, which is likely the case of ZV-48. Lastly, we have the ABDE sheet, which is located on the interface between DIII and DI. This epitope is not easily accessible in the context of the full virion (Figure 3a) and antibodies that target it, such as ZV-2, are poorly neutralizing and have shown no protection in animal models [69]. Given the potential of certain anti-DIII antibodies such as ZV-48 and ZV-67 to neutralize the virus, it would be advantageous to develop a vaccine that would promote the generation of these types of antibodies.

In this chapter, we will demonstrate that it is possible to engineer DIII in order to refocus the immune response towards neutralizing epitopes using our previously developed nanopatterning tool [36]. We selected residues on all three DIII epitopes that are crucial for antibody binding, and through a combination of non-canonical amino acid incorporation and click-chemistry we were able to functionalize DIII with PEG chains. More specifically, we synthesized and characterized two different nanopatterned DIII antigens: Sample DIII*, which has been conjugated to two PEG molecules on the ABDE sheet epitope, blocking binding of ZV-2-like antibodies; and Control-DIII*, which contains one PEG in the LR epitope and a second PEG on the C-C' loop epitope, resulting in inhibition of ZV-67 and ZV-48 binding, respectively.

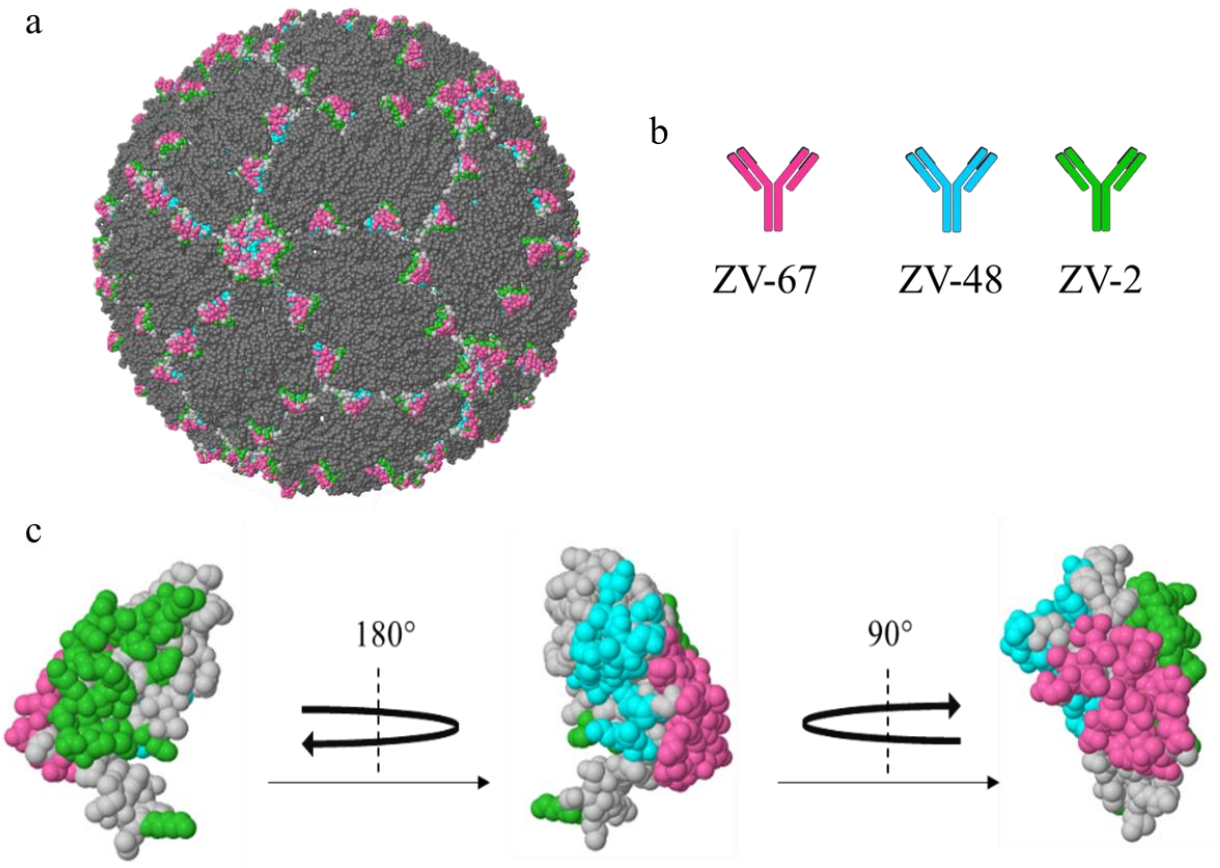

Figure 3. Three distinct epitopes found on ZIKV E protein DIII. (a) Crystal structure of Zika virion with LR (pink), C-C' loop (blue), and ABDE sheet (green) epitopes highlighted. (b) ZV-67, ZV-48, and ZV-2 bind LR, C-C' loop, and ABDE sheet epitopes, respectively. (c) Crystal structure of ZIKV's DIII (PDB 5KVG). All three epitopes have been highlighted, following the same color scheme as in 3a.

To achieve a more robust immune response, we next conjugated our nanopatterned antigens to multivalent nanoscaffolds such as a Branched-PEG-Scaffold and virus-like particles (VLPs). It is well-known that multivalent interactions – the ones that occur between multiple ligands and multiple receptors – may have an order of magnitude higher avidities than their corresponding monovalent interaction [72, 73]. Multivalency is extremely important in the context of immunology since multivalent antigens have the

ability to cluster B cell receptors (BCRs), triggering B cell activation and resulting in clonal expansion and enhanced antibody production [74, 75].

Nanopatterned DIII antigens were conjugated to these nanoscaffold, characterized, and used for immunization experiments with mice. Analysis of the serum post immunization confirmed our ability to refocus the immune response to targeted DIII epitopes. This result may ultimately help to inform the design of a more effective and safe ZIKV vaccine.

2.2 Materials and Methods

2.2.1 Synthesis and Cloning of DIII and Scaffolds.

The sequence for wild-type (wt) DIII (Uniprot A0A0X8GJ44), fused to a C-terminal GGSGG spacer, a SpyTag (AHIVMVDAYKPTK), and a 6xHis-tag, was codon optimized for expression in *E. coli* and cloned into pET-28b(+) between the XbaI and XhoI sites by General Biosystems, Inc. (Durham, NC). The sequence of SpyCatcher (Uniprot Q8G9G1) was optimized for expression in *E. coli* with a C-terminal 6xHis-tag and an additional N-terminal Streptag® II. Primers to replace the codons corresponding to amino acids T327, T353, P366, and K397 on DIII, and T56 on SpyCatcher with an amber TAG codon were purchased from Integrated DNA Technologies (Coralville, IO). Mutations were done via site-directed mutagenesis (SDM), performed using the Q5-SDM kit (E0554S, New England Biolabs) following manufacturer's instructions, yielding the Sample DIII (327 and 366 mutations), Control DIII (353 and 397), and SpyCatcher-F* constructs. The DNA encoding wt DIII was trasnformed into BL21(DE3) Competent cells (NEB C2527H), according to the manufacturer's recommendations. Plasmids encoding

for Sample DIII, Control DIII, and SpyCatcher-F* was co-transformed with pEVOLpAzFRS.2.t1 (Addgene #73546) into BL21(DE3).

For the conjugation to the streptavidin-coated VLP (VLP-SA), the sequence for the C-terminal SpyTag on DIII was replaced by an AviTag [76](GLNDIFEAQKIEWHE) via SDM. The sequences of two MS2 coat protein monomers (GenBank P03612) were fused together to generate an MS2 dimer [77, 78] and an AviTag was inserted into the AB loop between residues 15 and 16 of the second monomer. The DNA was codon optimized for expression in *E. coli* and synthesized by GenScript USA Inc. (Piscataway, NJ), and cloned into pet28b between Nde1 and XhoI restriction sites. The AviTagged versions of wt DIII, Control DIII, Sample DIII, and MS2 were co-transformed into BL21(DE3) with a plasmid encoding BirA. The plasmid coding for streptavidin, which includes a C-terminal hexa-glutamic acid tag [79], was procured from Addgene (#46367) and also transformed in BL21(DE3) cells.

2.2.2 Protein Expression.

Following transformations, all cells were plated overnight on LB-agar plates containing kanamycin and chloramphenicol. A single colony was picked for a 5 mL starter culture which was further scaled up (after growing for 12-16 hrs) to 1 L of 2xYT media containing kanamycin and chloramphenicol. Cells were grown at 37 °C until the OD_{600} reached 0.6-0.8. The temperature was reduced to 30 °C (for DIII) or 16 °C (for MS2) and isopropyl β-D-1-thiogalactopyranoside (IPTG) was added to a final concentration of 1 mM, in addition to 100 μg of *p*-azido-L-phenylalanine (F*), and 200 μg of L-arabinose. Constructs that were co-transformed with pAcm-BirA had biotin added to a final

concentration of 50 μM during induction as well. Cells were allowed to grow overnight before harvest. Expression of streptavidin was done in a similar manner, except ampicillin was used for antibiotic selection and arabinose and F* were omitted during induction. All cultures were harvested the next day and centrifuged at 7,000 xg for 7 minutes. The cell pellets were kept frozen until further use.

2.2.3 Solubilization, Refolding, and Purification of DIII Inclusion Bodies.

All DIII variants were expressed as insoluble inclusion bodies and refolded. The protocol for inclusion body solubilization is described by Nelson et al. [80]. Following the last wash and centrifugation, the final pellet was weighted and each 1g of pellet was resuspended in 5 mL of TE Buffer (10 mM Tris pH, 1 mM EDTA, pH 8.0). 3.4 mg of guanadinium hydrochloride (GdnHCl) and 4 μL of 14.3 M β-mercaptoethanol (BME) were added per 5 mL of solution to completely unfold the proteins. This was followed by a 1 hr incubation with mixing at room temperature and a subsequent centrifugation at 12,000 xg for 15 min for the removal of any insoluble particles. The supernatant was collected and brought to a final volume of 10 mL by adding TE buffer and an additional 4 μL of BME.

Proteins were refolded in Refolding Buffer (10% Glycerol, 100 mM Tris-HCl, 5.0 mM L-glutathione reduced, 0.5 mM L-glutathione oxidized, 0.5 mM AEBSF, pH 8.6) by rapid dilution. In brief, 2 mL of the unfolded protein solution were added dropwise (at approximately 1 mL/min) to 400 mL of cold Refolding Buffer while stirring rapidly. Each drop was added to the center of the vortex formed by the stirring, as close as possible to

the stir bar. This process was repeated in 1-hr intervals until all the protein mixture had been used. This was followed by an overnight incubation at 4^{o}C.

The Refolding Buffer containing the refolded protein was centrifuged at 7,000 xg for 15 min and filtered through a 0.45 µm membrane. Approximately 1 mL of Ni-NTA resin pre-equilibrated with IMAC Binding Buffer (100 mM Tris, 150 mM NaCl, 20 mM imidazole, pH 8.0) was added to 400 mL of the filtered solution and incubated with stirring at 4°C for 1 hr. The solution was then added to a gravity flow column; the Ni-NTA resin with the bound refolded DIII was retained in the column, while the buffer was allowed to flow through.

The resin was washed with 20 column volumes (CVs) of IMAC Binding Buffer and eluted with 2-3 CVs of IMAC EDTA Buffer (IMAC Binding Buffer with 100 mM EDTA) to strip the resin along with the protein. This was done to decrease the final volume of eluate. The eluate was dialyzed against phosphate buffered saline (PBS). On the following day, the dialysis bag was placed on a bed of solid sucrose to facilitate the removal of the liquid, thus increasing the protein concentration.

2.2.4 Purification of SpyCatcher-F Protein.*

A cell pellet obtained from a 1 L culture was resuspended in 20 mL of IMAC binding buffer. Lysozyme at a final concentration of 0.5 mg/mL, 125 units of Benzonase, and sodium deoxycholate (DOC) at a final concentration of 0.1% were added to the lysate. The dissolved pellet was sonicated for a minimum of 30 min with pulses on for 3 sec and off for 3 sec. Once the pellet was completely dissolved, the lysate was spun down at 27,000 xg for 30 min. The pellet was discarded while the supernatant was poured

over Ni-NTA resin that had been equilibrated with 10 CVs of IMAC Binding Buffer. The resin was washed thoroughly with IMAC Binding Buffer (approximately 20 CVs) and eluted with 5 CVs of IMAC Elution Buffer (100 mM Tris, 150 mM NaCl, 400 mM imidazole, pH 8.0). The eluate was dialyzed overnight against StrepTrap Binding Buffer (100 mM Tris, 150 mM NaCl, 1 mM EDTA). The SpyCatcher-F* was then purified using a pre-packed 5 mL StrepTrap column (Cytiva) following the manufacturer's recommendations. The eluate was buffer exchanged and concentrated using spin filters. Purity was determined by sodium dodecyl sulfate polyacrylamide gel electrophoresis (SDS-PAGE).

2.2.5 Refolding and Purification of Streptavidin.

Streptavidin was expressed, purified, and refolded from bacterial inclusion bodies as described in [79]. The cell pellet from a 1 L culture was resuspended in 25 mL of Pellet Suspension Buffer (50 mM Tris, 100 mM NaCl, pH 8.0) containing 250 units of Benzonase and 25 mg of lysozyme by vortex mixing. The resuspended cells were incubated at 4°C with stirring for 30 min to 1 hr and were then homogenized for 30 sec. This was followed by a 3-min sonication with 3 sec on/ off pulses. Once the pellet was completely dispersed, the mixture was centrifuged at 27,000 xg for 15 min. The supernatant was discarded, and the cell pellet was resuspended in another 25 mL of Pellet Suspension Buffer with 25 mg of Lysozyme and the steps above were repeated.

Following the second centrifugation, the pellets were resuspended in 50 mL of Wash Buffer 1 (50 mM Tris, 100 mM NaCl, 10 mM EDTA, 0.5% v/v Triton-X), homogenized for 30 sec, and sonicated for 30 sec. The solution was centrifuged at 27,000

xg for 15 min and the supernatant was discarded. This process was repeated 2-3 more times, after which the same steps were repeated with Wash Buffer 2 (50 mM Tris, 10 mM EDTA).

The final pellet was then suspended in 5 mL of Pellet Suspension Buffer and 3.4 g of GdnHCl were added to the mixture to unfold the proteins. This solution was incubated with stirring for at least 1 hr, after which it was centrifuged at 12,000 xg for 10 min to remove any insoluble particles.

Proteins present in the GdnHCl mixture were then refolded by rapid dilution. 500 mL of chilled PBS were placed on a stir plate and mixed rapidly until a vortex was formed. The GdnHCl solution was added dropwise to the center of the vortex. This was followed by an overnight incubation at 4°C.

The solution was centrifuged at 7,000 xg for 15 min and filtered through a 0.45 µm membrane to remove insoluble particles. Ammonium sulfate was added slowly to a final concentration of 1.67 M (approximately 40% saturation of ammonium sulfate) and the mixture was incubated for 3 hr at 4 °C with mixing. The solution was once again centrifuged for 7,000 xg for 15 min. Unwanted proteins precipitated at this step while streptavidin remained in solution. Additional ammonium sulfate was added slowly with stirring until a saturation of approximately 82% was reached (amounts of ammonium sulfate were experimentally determined). This was followed by an overnight incubation at 4 °C. The solution was then centrifuged at 17,000 xg for 15 min to precipitate the streptavidin. The supernatant was discarded and the formed pellet was resuspended in 25 mL of IBAC Binding Buffer (50 mM Sodium Borate, 300 mM NaCl, pH 11). This solution

was centrifuged for 10 minutes at 12,000 xg and transferred to a new tube for column purification.

5 mL of Iminobiotin-Sepharose affinity column (Affiland, S.A.) resin were poured onto a gravity flow column and pre-equilibrated with 5 CVs of IBAC Binding Buffer. The streptavidin solution was then poured over the resin, which was then washed with 10 CVs of IBAC Binding Buffer. The protein of interest was eluted with 4 CVs of IBAC Elution Buffer (20 mM KH_2PO_4, pH 2.2). The eluate was collected and dialyzed against PBS for long-term storage.

2.2.6 VLP Purification.

The cell pellet from a 1 L culture was resuspended in 100 mL of CaptoCore Equilibration Buffer (20 mM Tris, pH 9) along with 125 units of Benzonase, 50 mg of lysozyme, and 1 tablet of a SigmaFast EDTA-free protease inhibitor cocktail. The solution was incubated for approximately 20 min and DOC was added at a final concentration of 0.1 g/mL. The solution was sonicated for a total of 15 min with 3 sec on/ 3 sec off pulses and centrifuged for 20 min at 27,000 xg for the removal of cell debris. Four HiScreen CaptoCore 700 (GE) columns were connected in series, equilibrated with 10 CVs of CaptoCore Equilibration Buffer, and loaded with 25 mL of the MS2 solution. The columns were washed with 11 CVs of Equilibration Buffer with 1.8 mL fractions being collected during this wash. The column was cleaned according to the manufacturer's recommendations and equilibrated with 10 CVs of CaptoCore Equilibration Buffer. The loading and washing process was repeated three more times until all the MS2 had been purified. Early fractions (5 through 15) were characterized by SDS-PAGE and further

purified with a Superdex 200 Increase 10/300 GL column (GE). Purified MS2 was further characterized by dynamic light scattering (DLS).

2.2.7 Protein PEGylation and Biotinylaion.

5k mPEG-DBCO (Nanocs Inc., Boston, MA) was added to concentrated DIII to a final concentration of 10 mg/mL and incubated at 4°C overnight with mixing. The reaction was purified with a HiLoad 16/600 Superdex 200 pg (GE) column for product isolation. 1 mL fractions were collected and characterized by SDS-PAGE; fractions containing the target product were pooled, transferred to a dialysis bag, and concentrated by being placed on a bed a solid sucrose.

Large amounts of purified SpyCatcher were allowed to react with a 4-arm-PEG-DBCO (5 kDa per arm) commercially obtained from Nanocs Inc. (Boston, MA). Reagents were mixed at a 1.7x molar ratio of SpyCatcher per DBCO molecule and allowed to react overnight at 4 °C with mixing. The reaction was purified with a HiLoad 16/600 Superdex 200 pg column. 2 mL fractions containing a mixture PEG conjugated to 2, 3, and 4 SpyCatcher -F* proteins were collected, combined, and purified again. This process was repeated until we were able to isolate the 4- and 3-arm products.

For *in vitro* biotinylation, a biotinyation kit (Avidity, LLC, #BirA500) was used according to the manufacturer's recommendations. Biotinylated DIII was purified by IMAC following the previously described protocol. The eluate was concentrated and buffer exchanged to PBS via spin filtration. Biotinylated MS2 was isolated by SEC with a Superdex 200 Increase 10/300 GL column.

2.2.8 Conjugation of DIII to Branched PEG Scaffold.

Small scale reactions were set up to determine the stoichiometry that resulted in complete consumption of the Branched PEG Scaffold. Reactions were characterized by SDS-PAGE and disappearance of the scaffold was monitored. Reactions were then scaled up, incubated overnight at 4 ℃, and purified with a 1 mL StrepTrap column (GE), according to the manufacturer's specifications. The eluate was concentrated on a bed of solid sucrose and dialyzed against PBS.

2.2.9 Conjugation of Streptavidin and DIII to VLPs.

The concentrations of biotinylated MS2 and streptavidin were estimated by BCA and protein amounts were calculated based on the total mass of VLP available for the reaction. A 20x molar ratio of streptavidin was transferred to a small glass vial and stirred rapidly. MS2 was added to the vial in 2.5 µL increments (pipet tips were change before each addition) until all the MS2 had been used. The reaction was allowed to proceed for 10 minutes before being injected into a Superdex 200 Increase 10/300 GL column for purification. Fractions containing the reaction product were pooled together, concentrated, and quantified. For the reaction with biotinylated DIII, the VLP-SA was added at a 1.25x molar excess to DIII. DIII consumption was monitored by SDS-PAGE.

2.2.10 Expression of Anti-DIII Antibodies.

DNA encoding the light and heavy chain variable regions of ZV-2 (PDB ID: 5KVD), ZV-48 (PDB ID: 5KVE), and ZV-67 (PDB ID: 5KVG) were optimized for

mammalian expression and synthesized and cloned in the TGEX-LC and TGEX-HC vectors by Gene Universal Inc. (Newark, DE).

HEK 293F cells were transfected with the constructs using an ExpiFectamine Transfection Kit (ThermoFisher Scientific) following the manufacturer's instructions. Cells were incubated at 37°C with shaking and harvested between day 5 and 7. Cell cultures were centrifuged for 5 min at 4,000 xg. The supernatant was collected and purified using a HiTrap MabSelect SuRe column (GE) following the manufacturer's protocol.

2.2.11 ELISA

Proper folding and correct shielding of wt DIII and DIII mutants were confirmed by enzyme-linked immunosorbent assay (ELISA). 96-well plates were coated with 50 µL of DIII at 4 µg/mL and incubated at room temperature for 1 hr. This was followed by a 2-hr incubation with 100 µL of 5% bovine serum albumin (BSA) in PBST buffer (PBS and 0.2% Tween-20). Plates were washed three times with 100 µL PBST and incubated with 50 µL of primary antibodies (ZV-2, ZV-48, and ZV-67) diluted to 1 µg/mL with 1% BSA in PBST for an additional hour. The plates were once again washed three times with PBST and incubated for 1 hr with 50 µL of Horseradish Peroxidase (HRP)-conjugated anti-human antibodies diluted in 1% BSA in PBST. Following incubation, plates were washed three times with PBST and 50 µL of TMB solution were added. 5 to 10 minutes after TMB addition, 50 µL of Stop Solution (160 mM sulfuric acid) were added and the absorbance at 450 nm was measured.

2.2.12 Immunizations

For immunization with DIII mutants on the Branched PEG Scaffold, 1 µg of the DIII antigen was brought up to a final volume of 50 µL with PBS. Prior to immunization, an additional 50 µL of Addavax adjuvant was added to the samples. Mice were immunized at week 0 with 100 µL of the antigen and adjuvant mixture and two boosts were administered at four-week intervals following the first injection. Serum was collected on day 99.

Immunizations with DIII conjugated to VLP-SA were conducted in a similar manner. 2 µg of antigen were delivered in combination with Addavax adjuvant in a prime injection, followed by two boosts six and four weeks apart, respectively. Serum from individual animals was collected three weeks after the second boost and pooled.

2.2.13 Serum Antibody Titers

Antibody titers were determined by ELISA. A 96-well plate was coated, blocked with 5% BSA and washed as previously described. 1 µL of serum from individual animals was diluted in 99 µL of PBST containing 1% BSA, and serially diluted 11 times. 50 µL of each dilution were then added to the wells. Wells were incubated, washed, and developed following the previously described ELISA protocol. Titers were determined to be the last dilution before absorbance dropped below the cutoff value. Cutoff was calculated as the average absorbance of the control wells (no primary antibody added to wells) plus three times the standard deviation.

2.2.14 Immunodepletions

For depletions with PEGylated DIII constructs, 720 µL of Ni-NTA beads were washed with IMAC Binding Buffer containing 1% BSA and incubated with 250 µg or 66 µg of Sample DIII* and Control DIII*, respectively. Both amounts were estimated to be in large excess relative to the amount of serum anti-DIII antibodies. The antigen was allowed to bind to resin for at least 1 hr at 4 °C. The resin was washed with 10 CVs of 1% BSA in IMAC Binding Buffer and resuspended in 1 CV of the same buffer forming a resin slurry. Sera from all four groups were diluted 1,000 times with 1% BSA in IMAC Binding Buffer. Between 30 and 40 µL of resin slurry were added to the diluted sera and incubated for 1 hr at 4°C with mixing. Incubation was followed by a 5 min centrifugation at 2,000 xg which resulted in the precipitation of the resin. The supernatants were transferred to a new tube and mixed with 30 to 40 µL of fresh DIII-conjugated resin slurry. This process was repeated 5-7 times. After the final incubation, the sera were centrifuged several times for the removal of any traces of resin. The depleted sera were tested against wt DIII by ELISA.

Depletions using streptavidin-shielded DIII were performed in a similar manner. A DIII variant with a point mutation allowing for F* incorporation on amino acid 327 (DIII-327*) was expressed, refolded, and purified as described previously. DIII-327* was reacted with a large excess of DBCO-biotin reagent and purified by IMAC, resulting in DIII-327-b. Streptavidin agarose beads were washed with 1% BSA in PBS and in incubated with 100 µg of DIII-327-b. 1 µL of serum from each group was diluted in 500 µL of 1% BSA in PBS and incubated with the DIII-327-b-conjugated beads for multiple centrifugation and incubation cycles. ELISAs were performed to probe binding of the depleted sera against wt DIII.

2.3 Results and Discussion

2.3.1 Engineering and Synthesizing Multivalent Nanopatterned DIII Antigens

Our goal was to demonstrate that the bio-orthogonal coupling of PEG chains to selected epitopes of protein antigens can result in epitope shielding and, consequently, a refocused immune response upon immunization. This method, which we termed as "nanopatterning", was successfully employed to an engineered domain III of Zika's E protein. Upon a careful analysis of the footprint of three distinct anti-DIII antibodies, we selected solvent accessible amino acids that were crucial for antibody binding to DIII. The codons for the chosen residues were then mutated to an Amber codon (TAG), which has low usage in E. coli (7%) and rarely terminates essential genes [81] . The synthesis of orthogonal tRNAs that have the ability to suppress the Amber codon and insert an amino acid in its place was first reported by Kleina et al. [82]. These orthogonal tRNAs were further modified to allow for the incorporation of amino acids that are not part of the genetic code and that can extend the functionality of proteins [83]. In this context, Chin et al. [84] designed a synthetase for the incorporation of p-azido-L-phenylalanine (F*) – a phenylalanine analogue that contains a reactive azide group [85]- in response to an Amber codon. This tRNA and F* pair was used for the synthesis of our mutants, giving them additional properties due to the presence of the azide group.

DIII's structure was initially found to be extremely sensitive to mutations and the incorporation of F* often resulted in misfolded protein. Therefore, several mutation sites were screened and their effect on folding was analyzed. Initially, amino acids 311, 313, 327, 333, 396, 353, 375, 394, 396, and 397 were mutated to Amber codons. All DIII

constructs were co-transformed with the pEvol-pAcFRS.2.t1 [86] plasmid in *E. coli* cells and expressed in the presence of F*.

Two cysteines in the DIII sequence form a disulfide bond, which is crucial for proper protein folding. Although we originally attempted expressing DIII in *E. coli* cells that have the capacity to refold proteins with multiple disulfide bonds [87], the addition of mutations in the protein sequence resulted in large amounts of misfolded DIII. As a result, DIII mutants had to be expressed as inclusion bodies, solubilized, and refolded *in vitro*. ELISAs were performed following each DIII synthesis to ensure that the refolding protocol was successful, and that folding was not compromised by the insertion of the unnatural amino acid. Mutants T327F*/P366F* and T353F*/T397F* showed the best yield and correct conformation and were thus selected as Sample DIII and Control DIII, respectively.

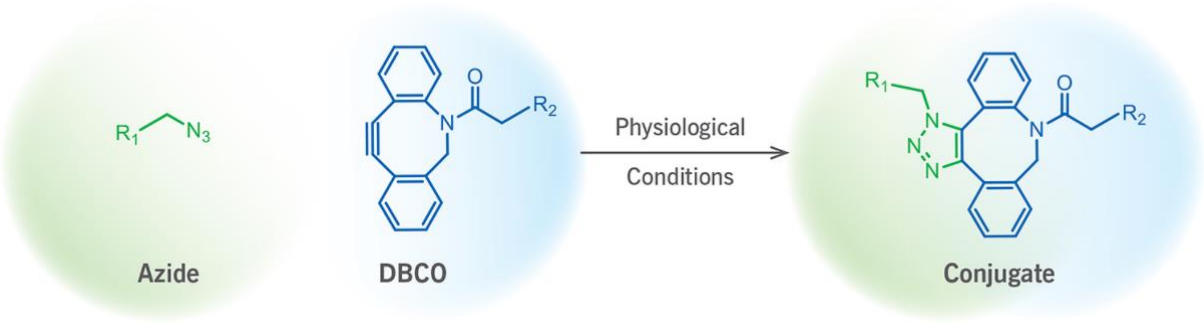

Figure 4. Schematic of Click chemistry reaction between azide and DBCO. Figure retrieved from [88].

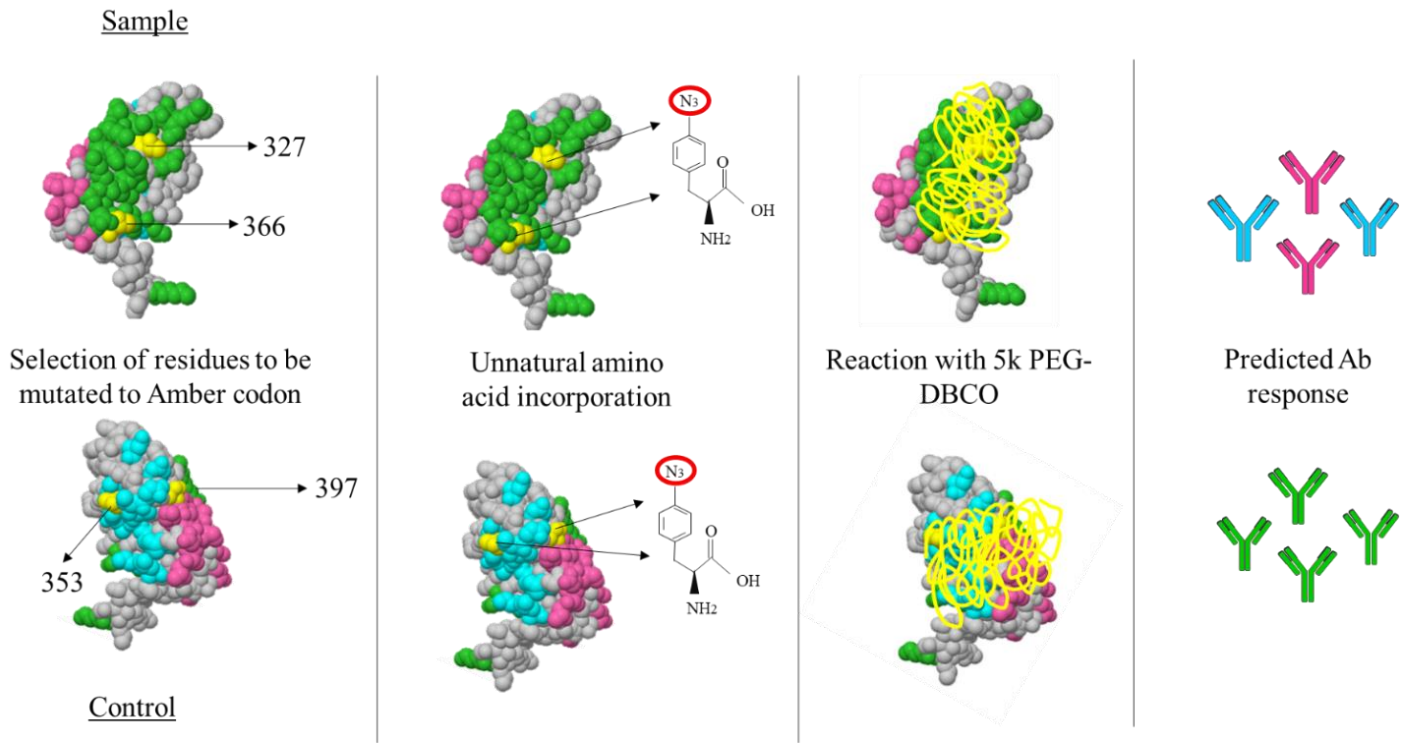

Figure 5. Synthesis of Sample and Control DIII*. Two residues (yellow) on the ZV-2-binding epitope were mutated to an Amber codon and replaced by F*. The mutant was conjugated to 5kDa PEG-DBCO chains, resulting in the Sample DIII* antigen. Due to the shielding of the ZV-2-binding epitope, we expect the immune response to be made up mostly of ZV-67 and ZV-48 antibodies. Similarly, residues on ZV-48 and ZV-67-binding epitopes were also replaced by F* and conjugated to PEG, resulting in the Control DIII* antigen. As a result, we predict only ZV-2 antibodies to be generated.

Cyclooctynes are very unstable and react readily with azides without the presence of catalysts [89]. The cycloaddition reaction between the two groups is part of a class termed "Click chemistry" reactions, which have played a crucial role in the development of polymer therapeutics [89, 90] once they allow for an easy conjugation of functionalized polymers to proteins (Figure 4). In our case, the reactivity between the azide found in F* allowed for the conjugation of the DIII mutants to a Dibenzocyclooctyne (DBCO)-functionalized 5 kDa (5k) PEG chain, resulting in

antigens Sample DIII* and Control DIII* (Figure 5). All constructs were purified and characterized by SDS-PAGE, as shown in Figure 6.

We next synthesized a multivalent version of our DIII antigens with the goal of enhancing the generated immune response during immunization. The DIII constructs were conjugated to a novel "Branched-PEG-Scaffold", which made use of the SpyCatcher protein and the SpyTag peptide pair originally developed by the Howarth lab [91]. A domain of the bacterium *Streptococcus pyogenes* was split into a peptide – the SpyTag – and a protein – the SpyCatcher – fragment, which, when reacted together, form a stable isopeptide bond that is resistant to heat and most proteases (Figure 7a).

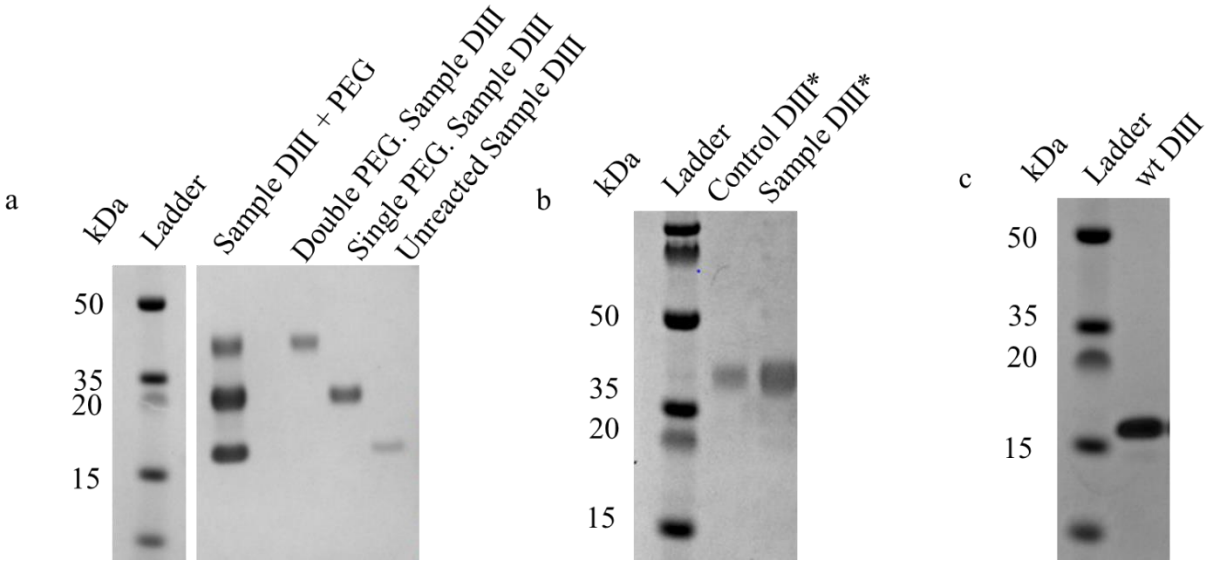

Figure 6. Characterization of DIII Antigens by SDS-PAGE. (a) Sample DIII* was reacted with PEG and purified by SEC. (b) Purified Control and Sample DIII*. (c) Purified wild-type (wt) protein.

We modified the sequence for the SpyCatcher protein to allow for the incorporation of F* upon expression (SpyCatcher-F*), and a 4-arm PEG-DBCO polymer (5kDa PEG in each arm) was purchased and allowed to react with SpyCatcher-F*, generating our multivalent Branched-PEG-Scaffold (Figure 7b). The reaction between the SpyCatcher-F* and the 4-arm PEG did not reach a yield of 100%, resulting in a mixture of 1, 2, 3, and 4 SpyCatchers proteins per branched PEG molecule (Figure 8). As a result, several rounds of SEC were required to isolate the desired product. SEC fractions containing a mixture of the trimer and tetramer products were used for our experiments.

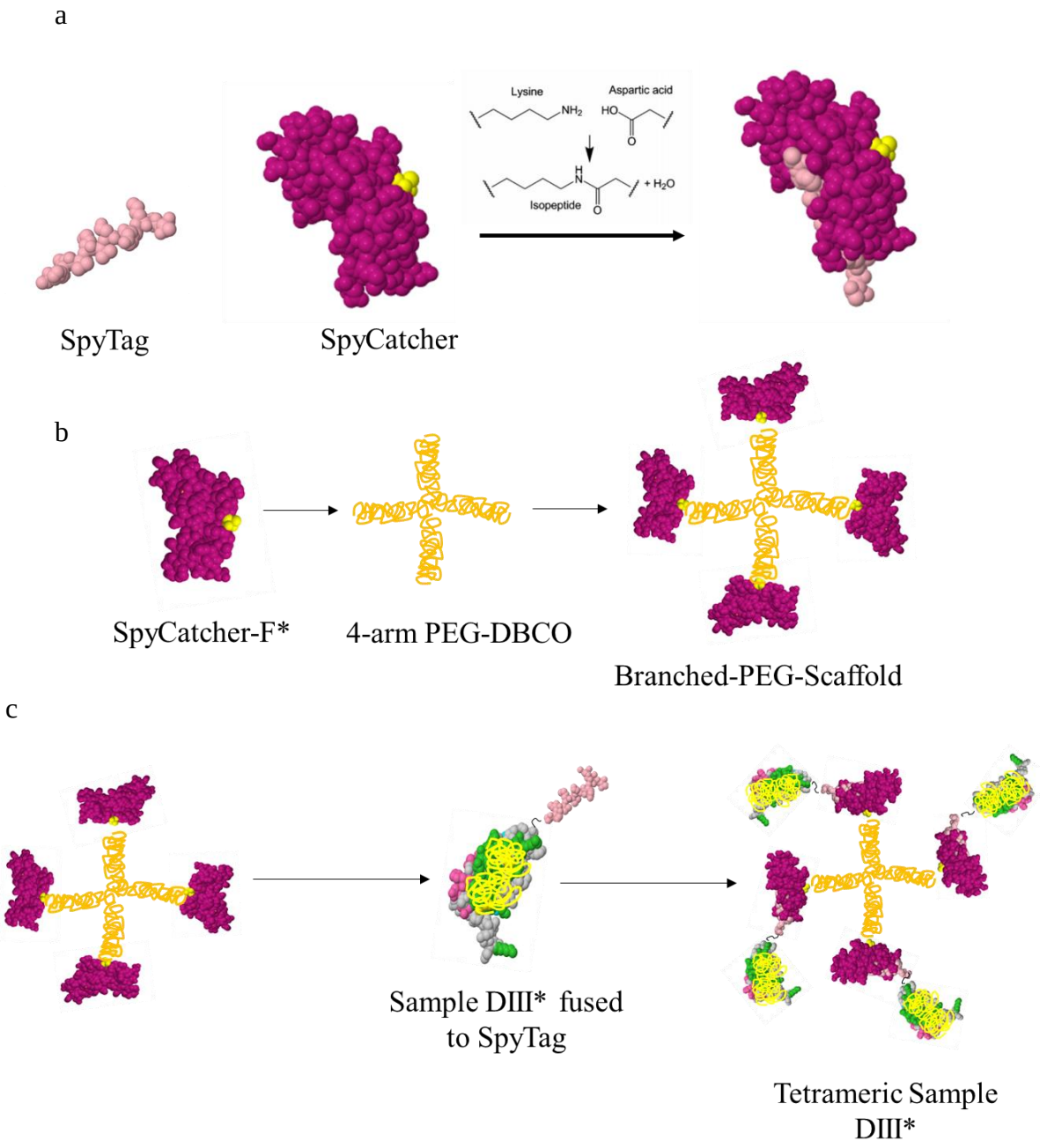

Figure 7. Schematic of the Synthesis of Multivalent Sample DIII* Antigens. (a) The SpyCatcher protein (purple) and the peptide SpyTag form an isopeptide bond when reacted together. (b) The SpyCatcher protein was mutated to allow for the incorporation of the unnatural amino acid F* and conjugation to a 4-arm PEG-DBCO molecule, yielding the Branched-PEG-Scaffold. (c) A C-terminal SpyTag was incorporated to the sequence of DIII. The bond formed between the SpyTag and SpyCatcher allowed for DIII conjugation to the Branched-PEG-Scaffold, generating a multivalent DIII antigen.

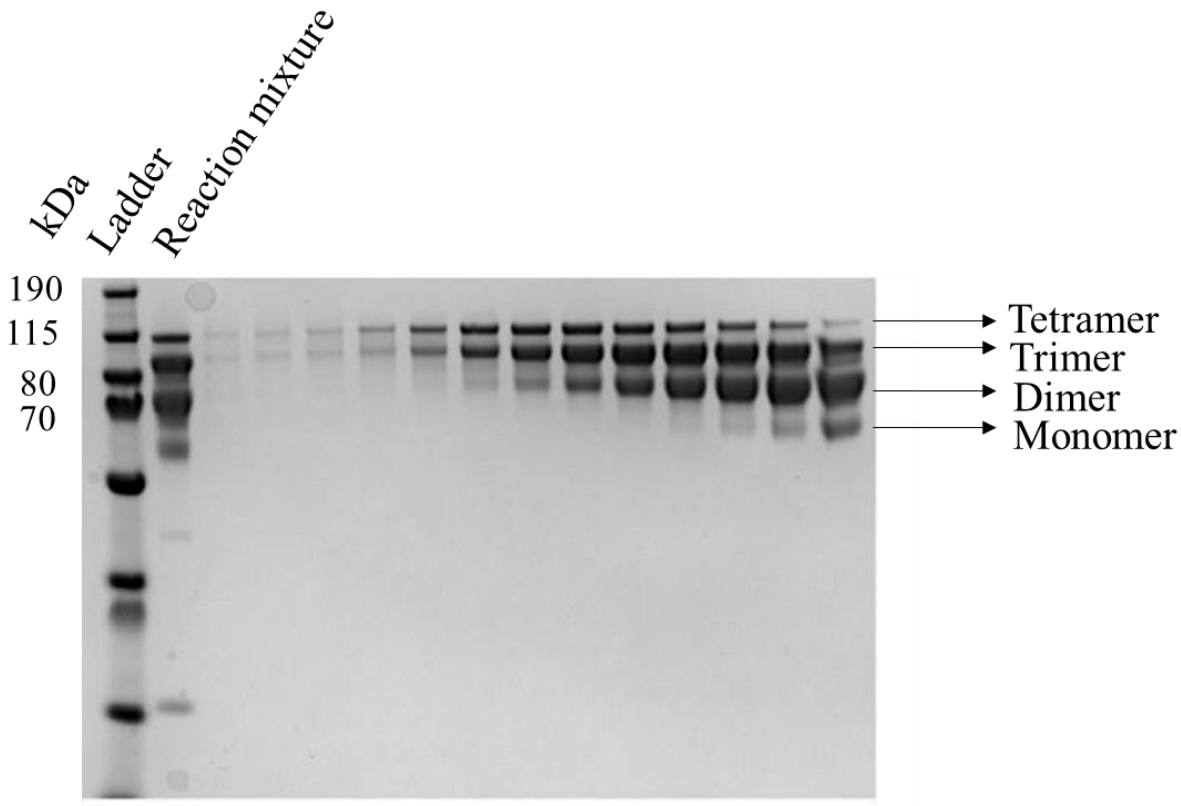

Figure 8. Purification of Branched PEG Scaffold by SEC. Fractions collected from SEC were analyzed by SDS-PAGE. Often a mixture of 1, 2, 3, and 4 SpyCatcher proteins per Branched PEG were seen. Fractions containing mostly the trimer and tetramer product were combined and used for DIII conjugation

The sequence for the SpyTag peptide was inserted at the C-terminus of DIII to allow for the conjugation of the proteins to the Branched-PEG-Scaffold (Figure 7c). To optimize the reaction conditions, the SpyCatcher scaffold was allowed to react with the DIII antigens at different ratios and unreacted scaffold disappearance was monitored by SDS-PAGE. Once the optimal stoichiometry was determined, reactions were scaled up and purified. Sample purity was confirmed by SDS-PAGE (Figure 9a) and binding of ZV-2, ZV-48, and ZV-67 was probed by ELISA (Figure 9b). The results confirmed shielding

of the PEG-conjugated epitopes: while all three antibodies bound to wt DIII, the ZV-2 antibody did not bind to Sample DIII*, and both ZV-48 and ZV-67 antibodies did not bind Control DIII*. None of the three antibodies showed significant binding to bovine serum albumin (control).

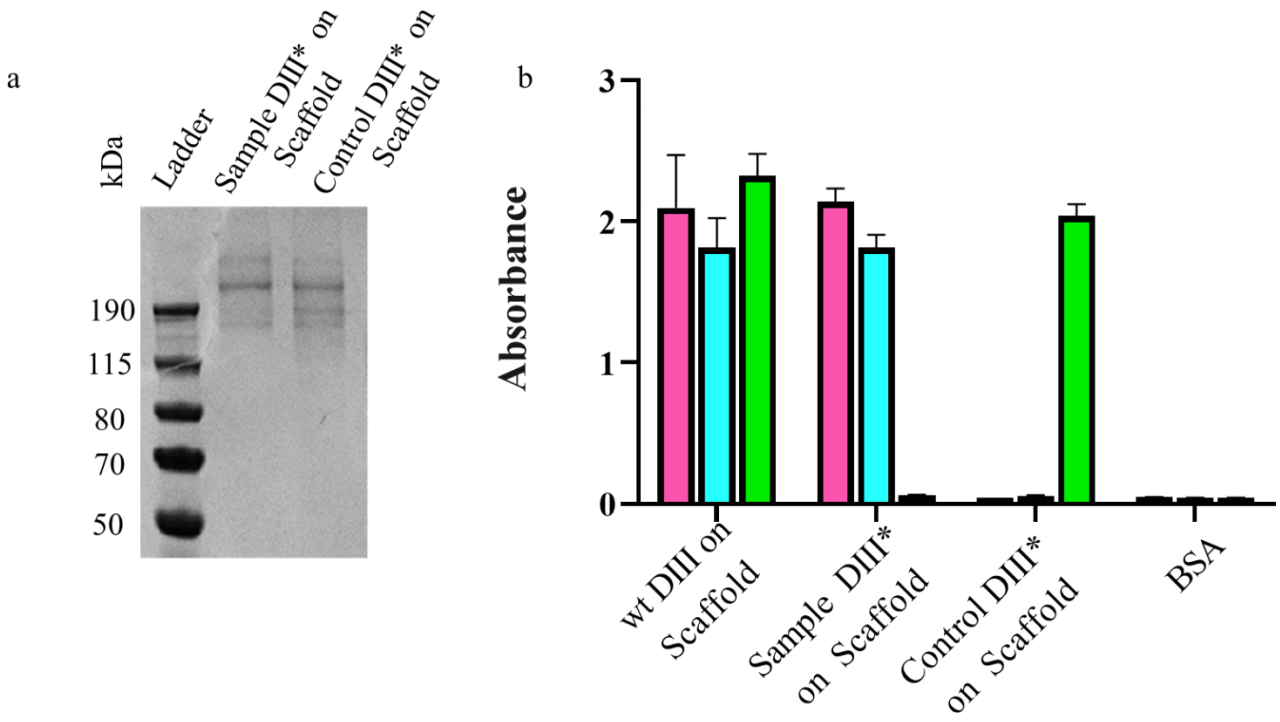

Figure 9 Characterization of Multivalent DIII Antigens. (a) SDS-PAGE image of Branched-PEG-Scaffold alone and Branched-PEG-Scaffold conjugated to Sample DIII* and Control DIII*. (b) Binding of multivalent wt, Sample, and Control DIII* to ZV-67 (pink bars), ZV-48 (cyan bars), and ZV-2 (green bars) antibodies by ELISA.

Having demonstrated the ability of nanopatterning to modulate the recognition of DIII antigens by anti-DIII antibodies *in vitro*, we next tested the antibody response to these antigens *in vivo*. In brief, three groups of five BALB/c mice were immunized with 1 μg

of wt DIII, Sample DIII*, or Control DIII* conjugated to the Branched-PEG-Scaffold. A prime injection was followed by two boosts four weeks apart. Serum was collected on day 99 and further analyzed.

To determine antibody titers, serial dilutions of pooled sera from each group were tested against wt DIII by ELISA. Antibody titers are expressed as the area under the curve (AUC) and are shown in Figure 10. The results demonstrate that all DIII constructs elicited anti-DIII antibodies. However, the group immunized with Sample DIII* had the lowest titers among the three DIII-immunized groups, with almost one order of magnitude difference between the AUC values obtained for Sample DIII* versus Control DIII*-immunized animals. Given the low antibody titers, further characterization of sera from Sample-DIII*-inoculated animals was not possible at this point.

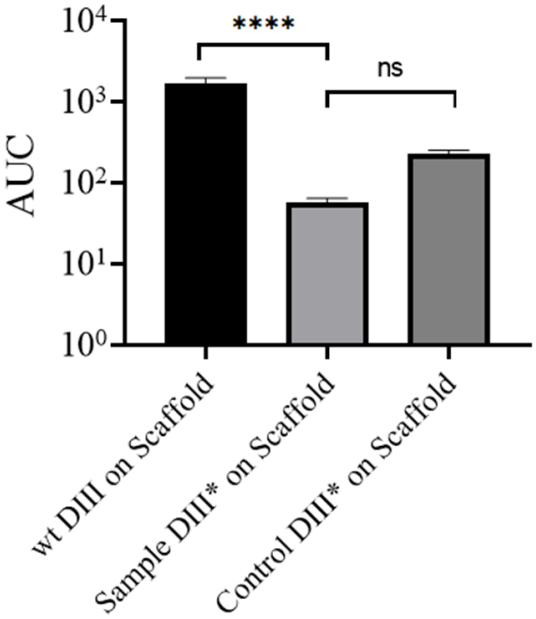

Figure 10. Antibody Titers Following Immunization with DIII Antigens on Branched-PEG-Scaffold. Serum collected on day 99 of the experiment was serially diluted and tested against wt DIII. End-point titers are expressed as Area Under the Curve (AUC)

and were determined to be the last dilution above the cutoff value (mean of baseline signal + 3 SD). **-p<0.0001, ns-not significant.**

Such a surprising result could possibly be associated to a low dose and low valency of the antigens. Given the complexity of the multivalent DIII synthesis scheme, our antigen yields were extremely poor, which forced us to perform immunization with a lower dose than what has been suggested in literature [92, 93]. In addition, our constructs had a valency of three or four, which might have not been high enough to promote optimal BCR clustering and yield an enhanced antibody response. To overcome such issues and to enhance the immunogenicity of the nanopatterned antigens, we next explored the effects of using a nanoscaffold that for the display of more copies of the protein antigen on its surface, such as the virus-like particles (VLPs).

2.3.2 Synthesis of Nanopatterned DIII Antigens Displayed on VLPs

The capsid protein of many viruses can spontaneously assemble into nanoparticles of 20-150 nm in diameter. Although these nanoparticles mimic the organization and structure of real viruses, they lack viral genetic material, which makes them non-infections. The presence of repetitive subunits allows for the conjugation of several copies of antigenic proteins to a single particle, promoting the crosslinking of multiple B cell receptors at once [94-96].

MS2 is an *E. coli*-infecting bacteriophage that has been widely studied and used for vaccine development with high success. Upon expression, 180 copies of the MS2 coat protein organize into stable noncovalent dimers, which further assemble into an

icosahedral shell, resulting in a VLP of 22-29 nm radius [78, 97]. Out of the 90 coat protein dimer copies present on the MS2 surface, 30 of them form symmetric C/C dimer, while the other 60 form asymmetric pairs referred to as A/B dimers [98-100]. Amino acid sequences of the coat protein have been previously mutated to incorporate new peptides and epitopes without compromising the overall VLP structure [77, 78]. The AB-loop in particular, has shown to be an attractive site for peptide incorporation, since it "protrudes prominently from the VLP surface" [78].

We genetically modified the MS2 coat protein sequence to allow for its expression as a single-chain dimer [78] and introduced an AviTag peptide (GLNDIFEAQKIEWHE) [76] in the AB loop of the second monomer. By co-transforming plasmids coding for the engineered MS2 and the enzyme BirA[76] into *E. coli* cells and expressing them in the presence of biotin, we were able the obtain high yields of MS2 that had been partially biotinylated. A commercially available kit was used to fully biotinylate the VLPs *in vitro*. DLS measurements showed that the synthesized MS2 VLP had an average radius of 16 nm (Figure 11a).

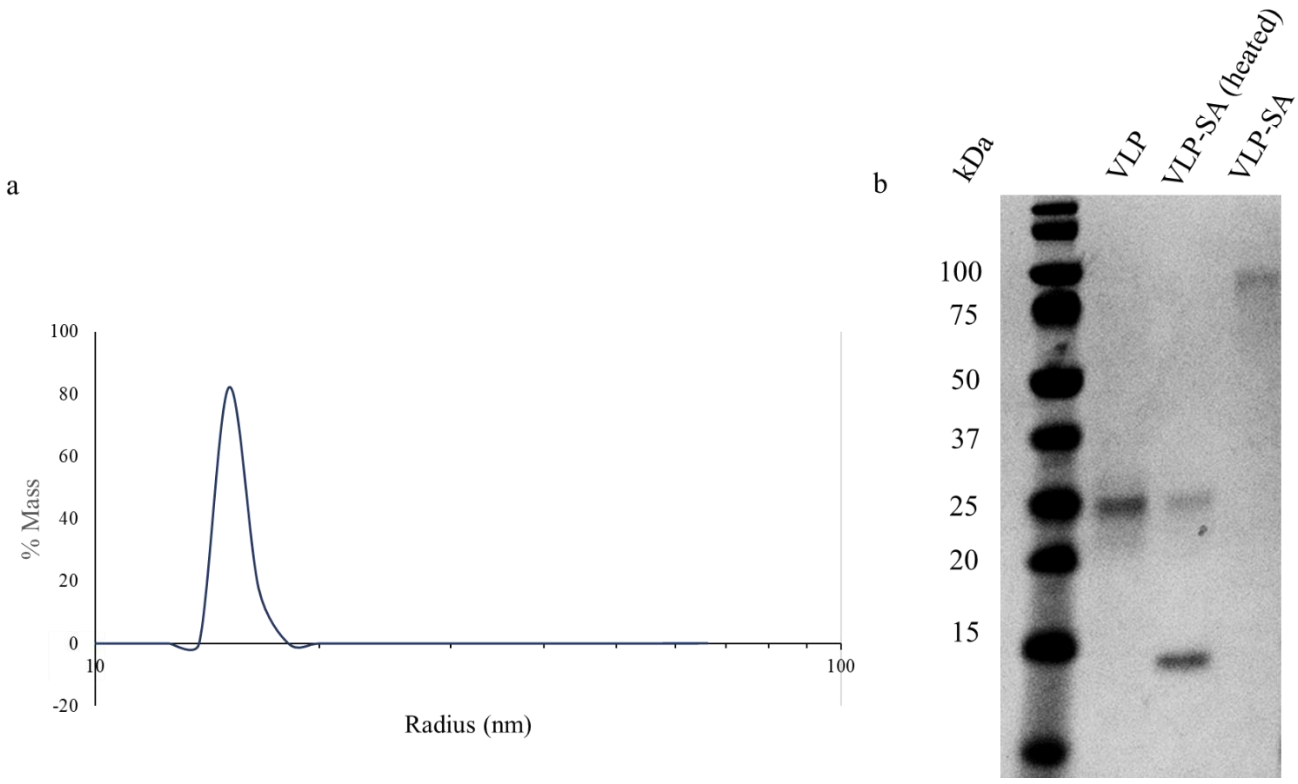

Figure 11. Characterization of VLPs. (a) Radius of VLP as measured by DLS. (b) Characterization of MS2 VLP before and after conjugation to streptavidin by SDS-PAGE.

Next, we expressed and refolded SA – which had been modified to incorporate a purification tag – and reacted it with our biotinylated VLPs [79]. After a short incubation, we were able to see 100% reaction yields, as shown by SDS-PAGE (Figure 11b). The excess SA was easily removed by SEC and the final product – a VLP-streptavidin (VLP-SA) conjugate – was ready to be coupled to additional biotinylated molecules through the remaining SA's free biotin binding sites.

An AviTag was inserted on the C-terminal of DIII as a replacement for the SpyTag without compromising protein folding or expression. The plasmid encoding the enzyme

BirA [76] was transfected along with the plasmid encoding for the DIII mutants, and biotin was added to the media during induction. This allowed for partial biotinylation of the expressed DIII. Once expressed, DIII was refolded and PEGylated following the method described in the previous section. Purified PEGylated proteins were further biotinylated *in vitro* to bring biotinylation yields close to 100%. Excess biotin was removed by IMAC and the biotinylated DIII constructs were dialyzed and concentrated. The VLP-SA was then reacted with DIII at a 1.25 molar excess to ensure complete DIII consumption. This process is illustrated in Figure 12a. Epitope shielding of DIII antigens conjugated to VLP-SA was confirmed by ELISA. Figure 12b shows shielding of ZV-2 antibody to Sample DIII* on VLP-SA while no antibody binding is seen for VLP-SA alone. Conjugation of Sample DIII* to VLP-SA is demonstrated by SEC shift (Figure 12c) and SDS-PAGE (Figure 12d).

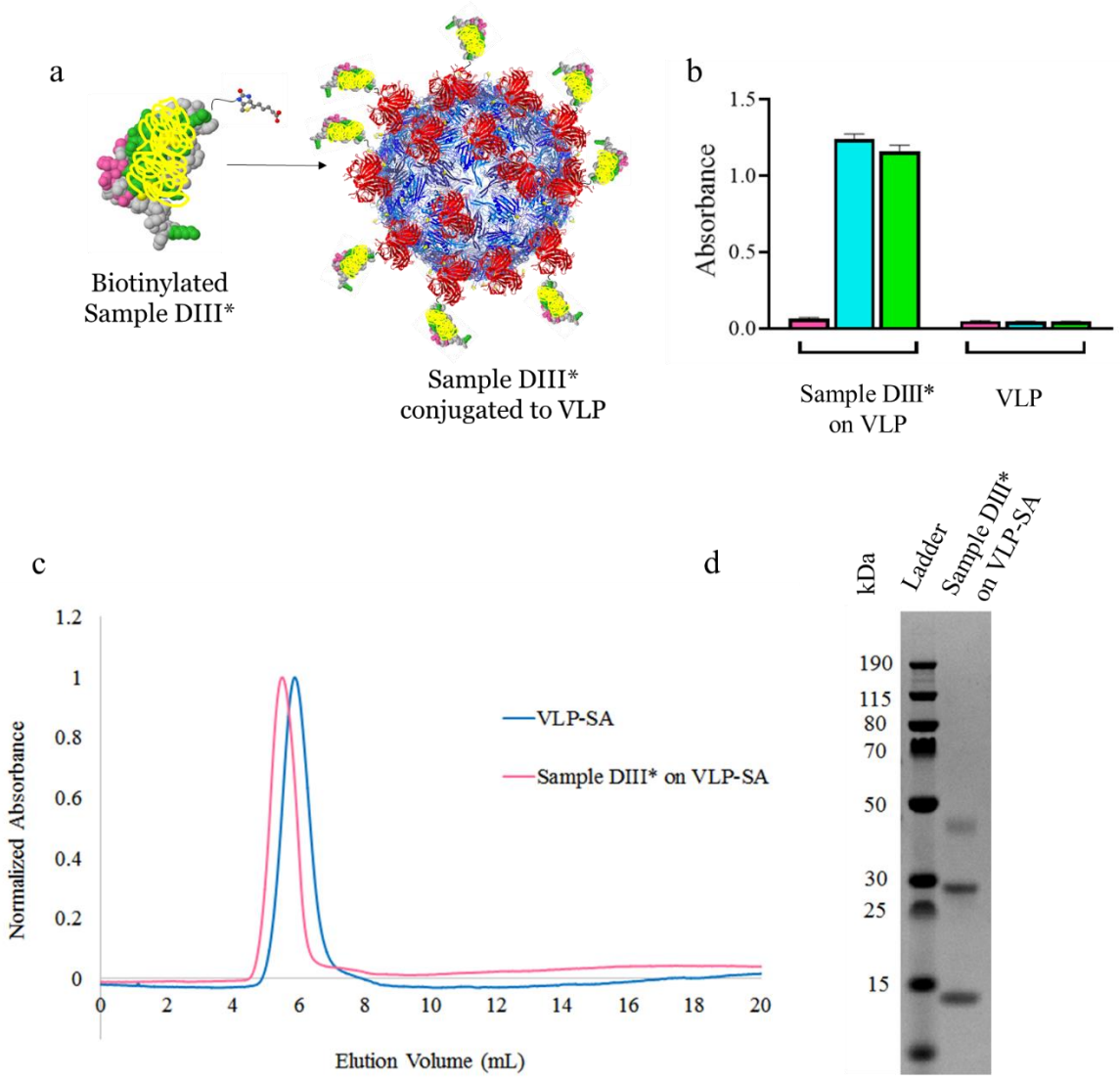

Figure 12. Design and characterization of DIII antigens conjugated to Virus-like Particles. (a) Representative scheme, illustrating the generation of Sample DIII*-VLP-SA. An Avitag was inserted on the C-terminus of the DIII constructs to allow for the incorporation of a biotin molecule. The biotinylated DIII antigens were conjugated to the VLP-SA. (d) Characterization of the binding of ZV-2 (green), ZV-48 (cyan), and ZV-67 (pink) antibodies to Sample DIII* on VLPs and streptavidin-coated VLPs alone by ELISA (mean ± SD, n = 3). (c) SEC chromatogram of VLP-SA in comparison to Sample DIII* on VLP-SA. The decrease in the elution volume suggest proper conjugation of the DIII antigen to the scaffold. (d) Reaction between biotinylated Sample DIII* and VLP-SA as shown by SDS-PAGE. The sample was heated prior to analysis, allowing us to visualize Sample DIII* (top band), MS2 dimer (middle band), and Streptavidin monomers (bottom band).

Following characterization, antigens were used for a new immunization experiment. Inoculations consisted of a prime injection followed by two boosts six and four weeks apart, respectively. A 2 µg dose of DIII was used in combination with the Addavax adjuvant. Mice were bled three weeks after the second boost; sera of animals from the same group were pooled and analyzed.

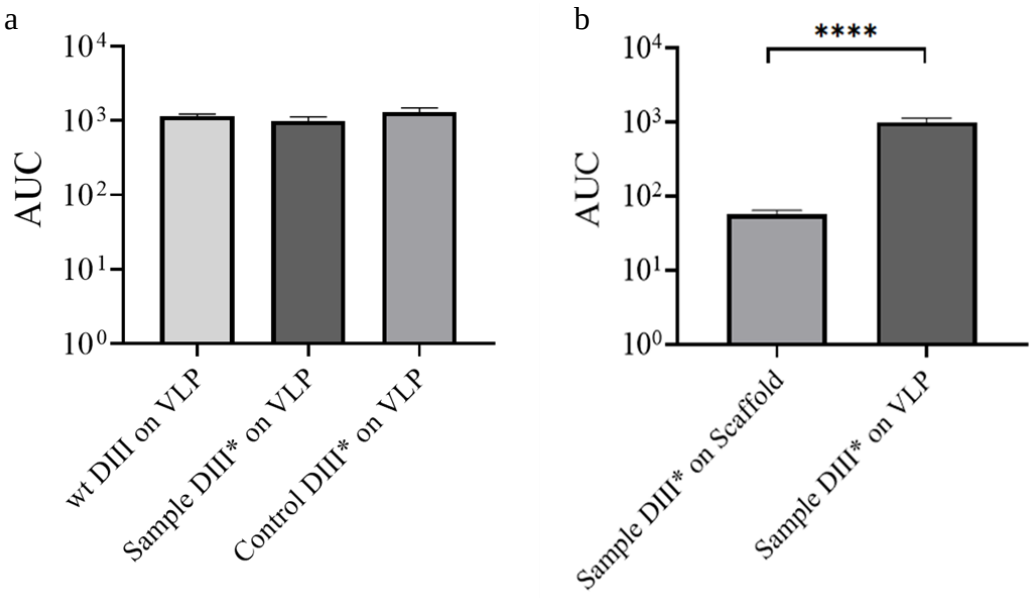

Figure 13. Endpoint Antibody Titers Following Immunizations with DIII Antigens on VLPs. (a) Titers (shown as AUC values) for wt, Sample, and Control DIII*. (b) Comparison between endpoint titers obtained from immunizations with Sample DIII* on Branched-PEG-Scaffold vs. Sample DIII* presented multivalently on VLPs. (**-p<0.0001).**

Antibody titers were determined by probing the binding of serial dilutions of sera to wt DIII by ELISA. As shown in Figure 13, there was a noticeable increase in the antibody titers for the Sample DIII*-immunized group when this antigen was presented from VLP-SA. Titers for the Sample DIII* on VLP-SA were comparable to the titers

obtained for the wt DIII and Control DIII* groups (Figure 13a). Additionally, titers for animals immunized with the Sample DIII* on VLP-SA were one order of magnitude higher than the titers seen after immunizations with Sample DIII* on the Branched PEG Scaffold (Figure 13b).

Immunodepletions were performed to assess whether there was a difference in the types of anti-DIII antibodies generated in the Sample DIII*-immunized group versus the Control DIII*-immunized group and whether refocusing of the antibody response had occurred. Sample DIII* and Control DIII* were immobilized on Ni-NTA beads and incubated with pooled sera. Large excesses of both nanopatterned DIII proteins were used to ensure complete antibody depletion from the sera. 96-well plates were coated with wt DIII and the binding of the depleted sera was probed. Figure 14a and Figure 14b show a schematic of the expected results of depletion with Sample DIII*. Animals immunized with Sample DIII* were predicted to produce only ZV-48 and ZV-67-like antibodies; therefore, depletion with the Sample DIII* antigen should lead to the removal of the majority of antibodies in the sera. As a result, low binding to wt DIII should be observed. Immunizations with Control DIII* are expected to elicit mostly ZV-2-like antibodies, which should not be depleted by Sample DIII*, resulting in higher binding of the depleted sera to wt DIII. Figure 15b shows the predicted trend following antibody depletion with Control DIII*. Most antibodies present in the sera of the Sample DIII*-immunized animals should remain in the solution, while the majority of antibodies in the sera of mice inoculated with Control DIII* should get removed. As a result, depleted sera from the Sample DIII* group should show a higher binding to wt DIII by ELISA in comparison to the depleted sera from the Control DIII* group.

As seen in Figure 14c and Figure 15c, the results are consistent with our predictions. Depletion with Sample DIII* resulted in baseline levels of wt DIII-binding for the Sample DIII* sera, suggesting removal of the majority of antibodies. Significantly higher binding was seen for the Control DIII* sera, implying the presence of antibodies in the serum following a depletion with Sample DIII*. For the depletions with the Control DIII* antigen, the opposite trend was seen: binding to wt DIII was high for the Sample DIII* group and near baseline for the Control DIII* group, leading us to conclude that successful depletion only occurred with the Control DIII* sera.

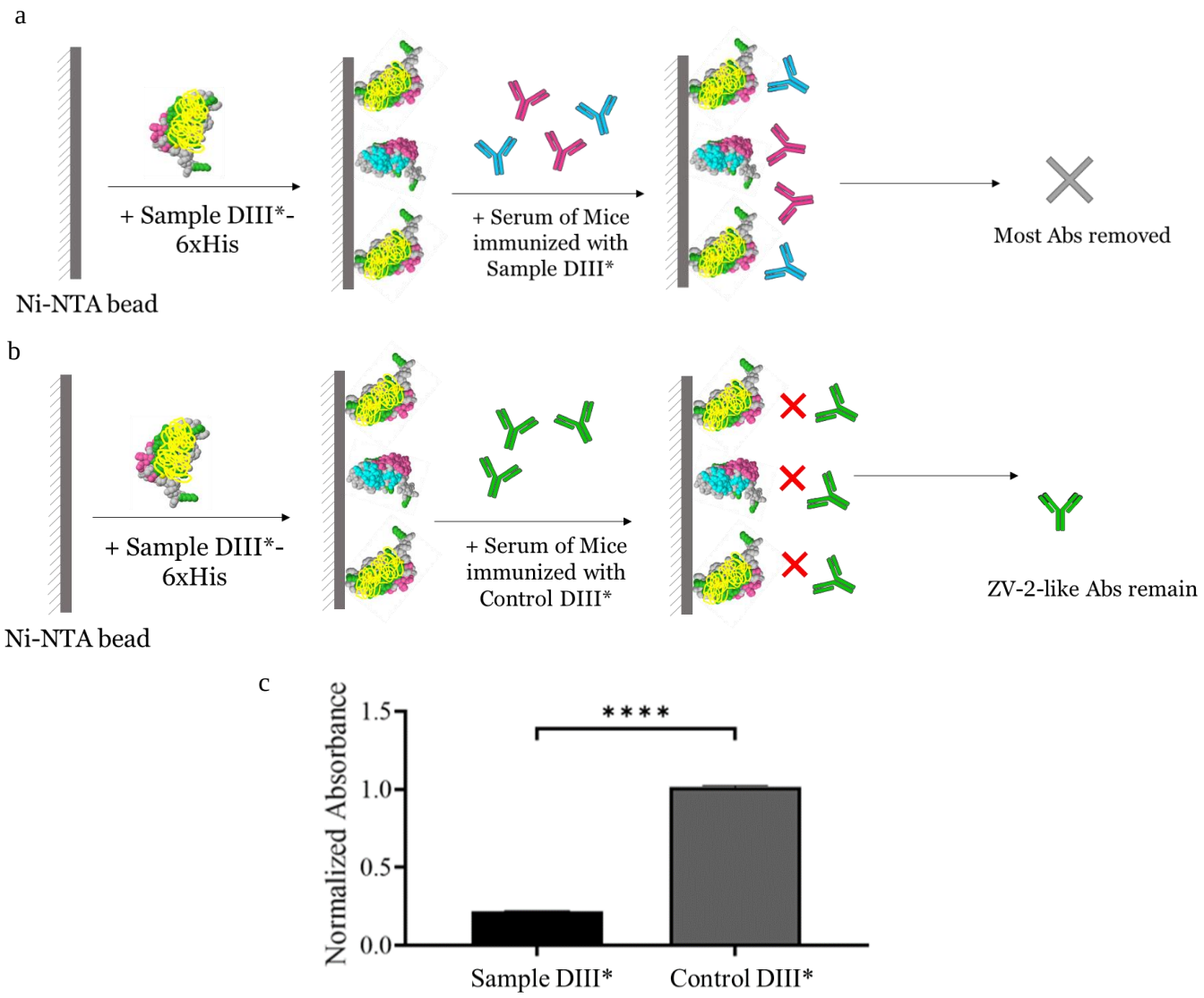

Figure 14. Depletion of Sera with Sample DIII*. (a) Sample DIII* was immobilized on Ni-NTA beads and incubated with serum from Sample DIII*-immunized animals. The beads should lead to the depletion of ZV-48 and ZV-67-like antibodies, resulting in the removal of majority of antibodies in the sample. (b) Sample DIII*-immobilized beads should not be able to deplete antibodies from sera of animal immunized with Control DIII*. ZV-2-like antibodies should remain in the sample. (c) Binding of depleted sera against wt DIII by ELISA. **** p<0.0001 determined by Sidak's multiple comparison test, n=3.

a

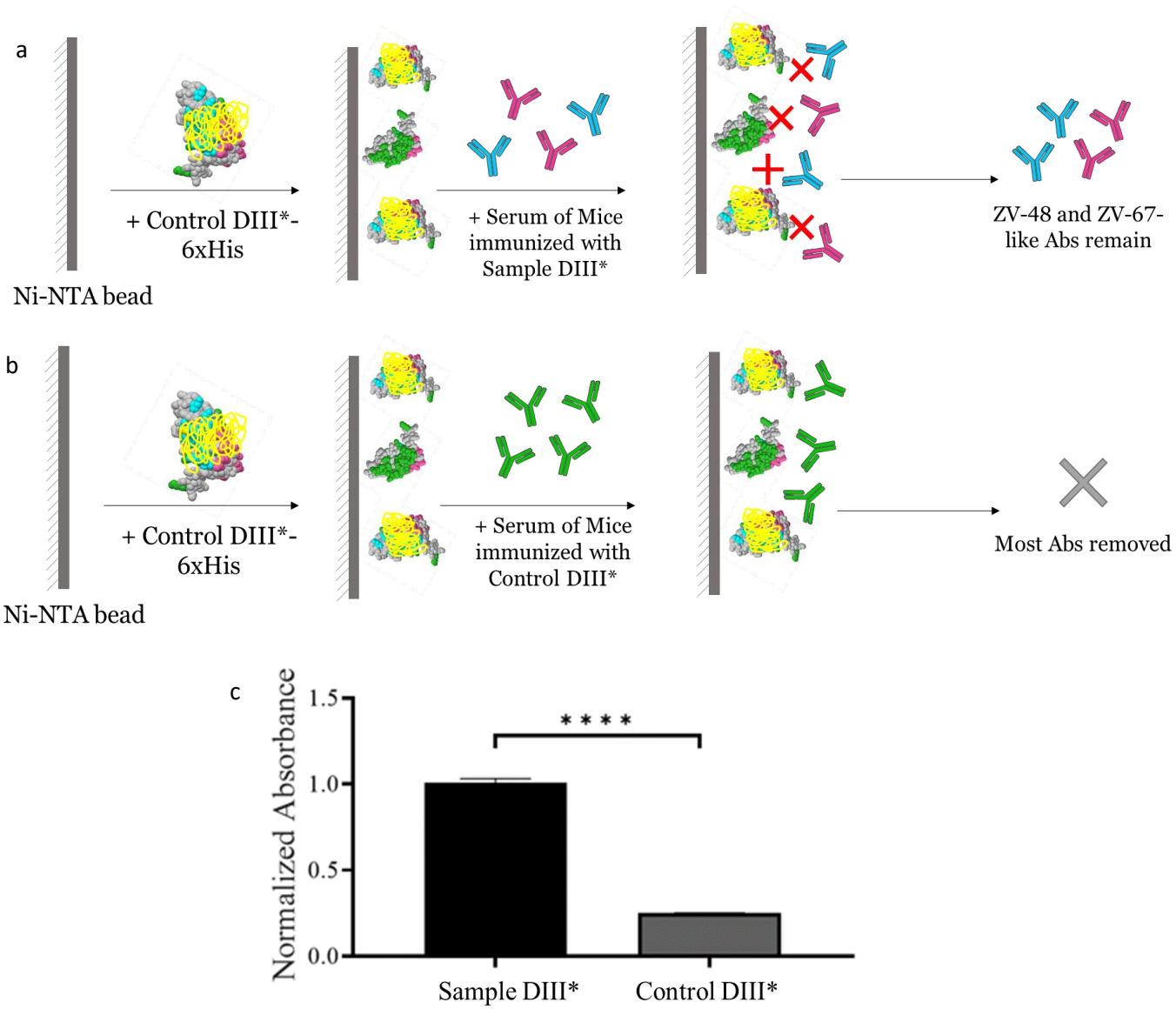

Figure 15. Depletion of Sera with Control DIII*. (a) Control DIII* was immobilized on Ni-NTA beads and incubated with serum from Sample DIII*-immunized animals. ZV-48 and ZV-67-like antibodies should not bind Control DIII* and therefore should not be depleted. (b) Control DIII*-immobilized beads are expected to deplete ZV-2-like antibodies from sera of animals immunized with Control DIII*. As a result, most antibodies should be removed from the sample. (c) Binding of depleted sera against wt DIII by ELISA. **** $p<0.0001$ determined by Sidak's multiple comparison test, n=3.

An alternative depletion experiment was also performed to further validate our findings. We expressed a DIII variant containing a point mutation on the ZV-2 epitope

(T327F*). The mutant was allowed to react with DBCO-biotin to generate DIII 327-b and further conjugated to streptavidin-agarose beads (Figure 16a). We reasoned that the bulky nature of streptavidin would sterically block access of antibodies in the sera to the ZV-2 epitope, allowing the antibodies binding to other parts of the protein to be selectively depleted. Dilutions of sera were incubated with the DIII 327-b-streptavidin beads and the binding of the depleted sera to wt DIII was characterized by ELISA. The depletion schematic and ELISA results are shown in Figure 16b and Figure 16c, respectively. The data are consistent with the findings from the previous depletion experiment. As predicted, depletion with DIII 327-b resulted in removal of the majority of antibodies from the sera of the animals immunized with Sample DIII*, a behavior that was not seen for the group immunized with Control DIII*. These findings further confirm that nanopatterned DIII antigens can refocus the immune response.

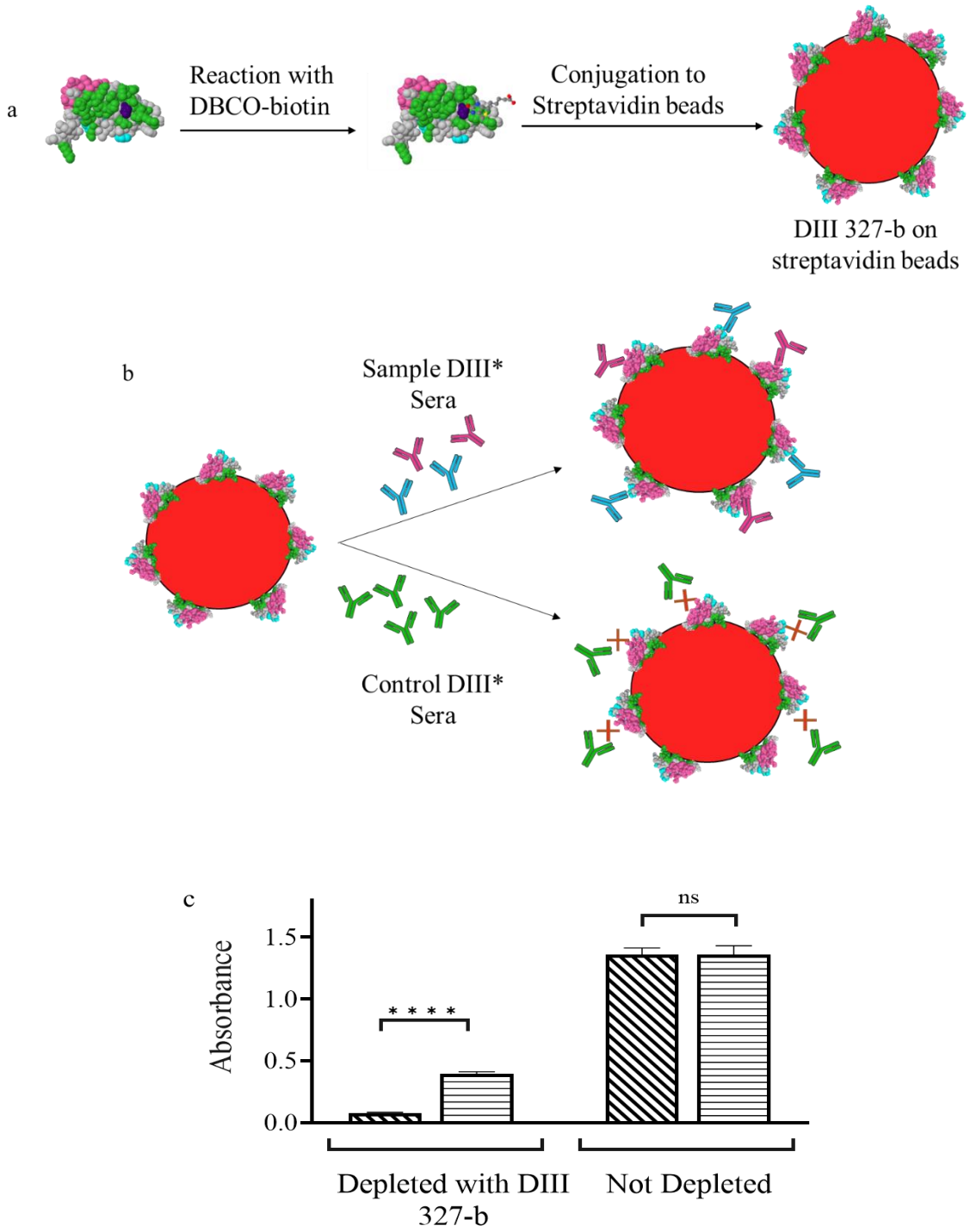

Figure 16. Depletion of sera with sterically shielded DIII confirms refocusing of immune response. (a) Scheme illustrating the strategy used to generate DIII-coated Streptavidin beads. Residue 327 (dark blue) on DIII was replaced by F* and conjugated to DBCO-biotin, resulting in protein DIII 327-b. DIII 327-b was immobilized on streptavidin agarose beads. (b) The DIII 327-b-conjugated streptavidin beads were incubated with

sera from Sample DIII* and Control DIII*-immunized animals. Depletion of sera from mice immunized with VLPs presenting Sample DIII* should result in removal of most antibodies. ZV-2-like antibodies should remain in the sera from mice immunized with VLPs presenting Control DIII* following depletion with DIII 327-b. (c) Binding of depleted and undepleted sera from Sample DIII* (▨) and Control DIII* (▤) groups to wt DIII was determined by ELISA. Higher binding is seen for depleted sera from the Control DIII* group. **** p<0.0001 determined by Sidak's multiple comparison test, n=3.

2.4 Conclusions and Future Directions

The presented data allows us to conclude that immunization with multivalent DIII antigens elicited anti-DIII antibodies in a mouse model. Moreover, nanopatterning of the DIII antigens allowed the antibody response to be refocused to targeted epitopes, and the use of VLPs as a multivalent scaffold resulted in high antibody titers for the nanopatterned antigens. Nonetheless, the potential of Sample DIII* as an efficacious vaccine is yet to be determined. Viral challenges following immunizations with Sample DIII* will help assess the neutralizing potency of the elicited antibodies. If our efforts prove to be successful, this same nanopatterning strategy could be used for the design and synthesis of other novel viral vaccines.

Given the promising results obtained from nanopatterning ZIKV DIII antigens, it would be interesting to assess the ability of our nanopatterning tool to refocus the immune response on different viral antigens. An ideal candidate for this test would be the Dengue virus, which is closely related and has a very similar structure to ZIKV. DENV is endemic in certain regions of the world and according to the WHO there are approximately 390 million cases of Dengue Fever per year [62, 101]. In addition, DENV is subdivided into four serotypes, which means a single person can become infected up to four times. ADE

has been observed to occur after infections with heterologous serotypes, which helps highlight the importance of developing a vaccine against DENV that will elicit a robust immune response made up of neutralizing antibodies.

Similarly to ZIKV, distinct epitopes were identified on Domain III of DENV E protein. In brief, the LR and A strand epitopes are targeted by neutralizing antibodies, while the AB loop and C-C' loop have shown to elicit antibodies with non- or poorly neutralizing ability. Therefore, it would be beneficial to employ our nanopatterning strategy to DENV DIII protein in order to refocus the immune response towards the LR and A strand epitopes. We would follow a similar approach to the one described previously: replace amino acids on the different DIII epitopes with F*, functionalize the DIII mutants with DBCO-PEG, and conjugate them to multivalent nanoscaffolds. The initial stages of this new project have started, and potential mutants have already been selected and expressed. We are confident on the potential of obtaining successful results for the nanopatterning DENV antigens as well.

CHAPTER 3. SYNTHESIZING A ZIKV E PROTEIN DIMER-BASED VACCINE

3.1 Introduction

As discussed in Aim 1, dimers of the envelope (E) protein coat the surface of the Zika virus and play a crucial role in viral infection. In the mature and infectious form of the virus, there are 90 copies of E protein dimers arranged in a head-to-tail orientation [68, 102, 103] (Figure 2b). The E protein is responsible for host cell binding and entry [49] and is the main target of neutralizing antibodies [54, 55, 104]. As a result, vaccine development efforts have focused on the E protein, with several candidates having demonstrated protective efficacy against ZIKV in rodents and non-human primates [105, 106]. However, given the continuing threat posed by DENV and the homology between the E proteins of ZIKV and DENV, a vaccine that could elicit broadly protective antibodies against ZIKV and DENV would be a significant accomplishment.

A class of antibodies that target a quaternary epitope on the dimer interface have demonstrated to be protective against not only multiple ZIKV strains but also against multiple DENV serotypes [107, 108]. These broadly neutralizing antibodies (bnAbs) target a region identified as the Envelope Dimer Epitope (EDE), which is highly conserved among flaviviruses [57, 108]. Figure 17a shows the crystal structure of the DENV E protein dimer bound to the c8 bnAb, which binds to the EDE [63]. The antibody footprint on both ZIKV and DENV dimers is highlighted on Figure 17b, and we can see that this footprint is made up of residues located on both E monomers. This region is the binding

site of the viral precursor membrane (prM) protein, which prevents premature exposure of the fusion loop (FL) – a short peptide on E that becomes exposed during host and viral membrane fusion [106] – during viral assembly. PrM locks the dimer in place and hinders conformational changes that can expose the FL, preventing premature membrane fusion [109, 110] . Given the importance of this mechanism, binding of E to prM is crucial and results in the high conservation of the amino acids located in this region [68].

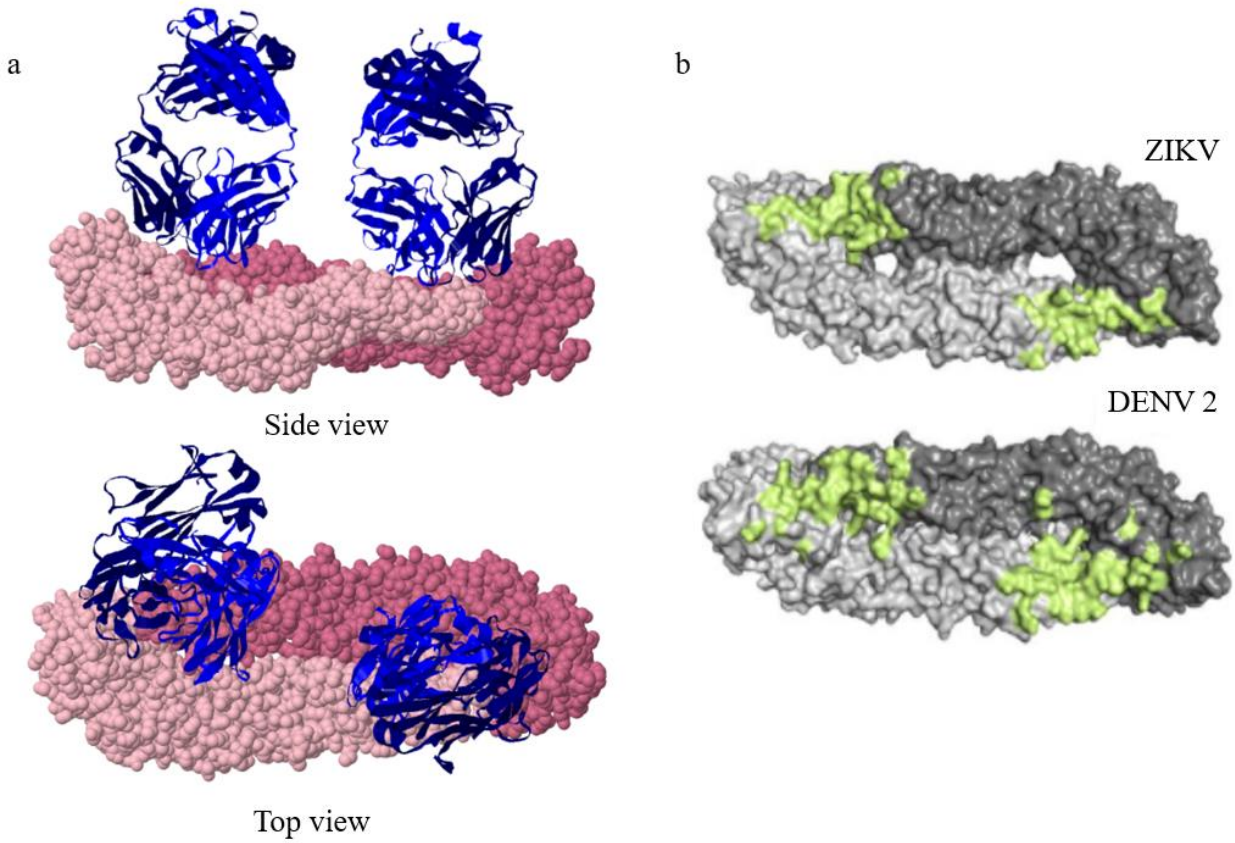

Figure 17. c8 antibody binds to an epitope on the E dimer interface. (a) DENV E dimers (pink) bound to c8 antibody (blue), side view and top view. (b) Dimers of DENV E and ZIKV E protein (grey) with the footprint of c8 highlighted in light green. Figure adapted from [68].

Antibodies bound to the EDE epitope play a similar role as prM – they crosslink the dimer in place and prevent rearrangement and exposure of the FL [54], resulting in viral neutralization. Considering the potential of E dimers to elicit bnAbs, they serve as a viable and attractive alternative to using E monomers for immunization. In contrast to the approach described in Aim 1, where we aim to synthesize vaccines that elicit Zika-specific neutralizing antibodies, Aim 2 consists of designing and synthesizing a vaccine that has the potential to protect against Zika and Dengue viruses. We hypothesize that by delivering ZIKV E dimer conjugated to a multivalent scaffold we can elicit bnAbs that target ZIKV and DENV.

Stabilization of the E dimers, however, is a major challenge. Even though E is found as dimers on the viral surface, recombinant E proteins exist in an equilibrium between the dimer and monomer forms [111]. Although crystallization experiments suggest that at high enough concentrations the dimer is the dominant state of the protein [112], this equilibrium shifts towards the monomer if the concentration is decreased or if the sample is brought to physiological temperatures [112, 113]. This clearly becomes a problem in a vaccine context, since inside the body these dimers could potentially disassemble into monomers, preventing the elicitation of broadly neutralizing anti-EDE antibodies.

Several strategies have been employed to synthesize stable E dimers and yielded promising results [64, 111, 114]. However, some of them pose severe limitations for vaccine design. Metz et al.[111], for example, described the synthesis of E dimers via the immobilization of 6xHis-Tagged E proteins on Ni^{2+}-coated plates to mimic E display on the ZIKV surface and promote dimer formation. Although efficient in forming dimers,

this technology could not be easily translated into a vaccine. Conversely, Slon-Camposet al. [114] and Yang et al. [64] demonstrated the ability to synthesize covalently cross-linked E dimers, which generated EDE-binding and neutralizing antibodies in *in vivo* studies. While their results were promising, their immunizations were performed with monovalent E dimers, allowing for the exposure of the dimer's "underside", a highly conserved [115] but inaccessible region in the context of the virion (Figure 18). Therefore, presenting E dimers on the surface of a nanoscaffold could potentially shield the underside and hinder the generation of antibodies targeting it [115].

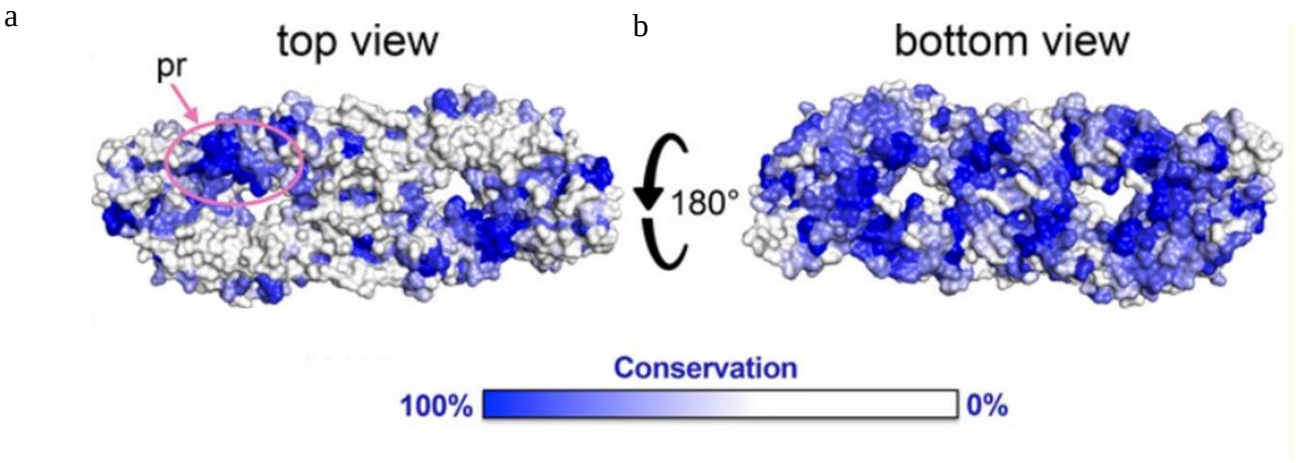

Figure 18. Amino acid conservation among E proteins of several Flaviviruses. Adapted from [115]. Left: Top view of E dimer. The highly conserved prM binding site is circled in pink. Right: The dimer underside shows high amino acid conservation.

Given those considerations, we designed and synthesized a VLP scaffold that when conjugated to E proteins promotes dimer assembly. This novel strategy could,

simultaneously, expose the EDE, block the dimer underside, and present a multivalent version of the antigen to enhance BCR crosslinking and immunogenicity.

3.2 Early Attempts of Dimerizing E Proteins

We pursued a series of different methods to synthesize stable dimers of E, which showed to be unsuccessful or extremely problematic. Our original approach consisted of selecting residues on the E monomer, mutating them to cysteines, and allowing the cysteines to react with maleimide-containing bifunctional cross-linkers. This could be done in two different ways: either by mutating residues on DII and joining two monomers by a very short linker, or by inserting cysteines at the C-terminus of the E monomer and using a long flexible cross-linker that would allow the two monomers to form a dimer in a head-to-tail orientation. We originally replaced amino acid L267 on Domain II with a cysteine and reacted the E mutants with bifunctional bismaleimide-activated PEG linkers (BM(PEG)2 and BM(PEG)3). Cysteines and maleimide molecules can be coupled together by thiosuccinimide bonds in a very specific and efficient reaction [116, 117], thus, we hypothesized that this reaction would bring two monomers close together and promote spontaneous dimer formation. A schematic of this process is shown in Figure 19a. The second strategy consisted of introducing a C-terminal cysteine to the E protein and reacting it with a 10kDa maleimide-PEG-maleimide linker. The cysteine-maleimide coupling would join the extremities of two E monomers together, while the long linker would allow the monomers to arrange in the head-to-tail conformation. The schematic for this approach is also shown in Figure 19b.

The E protein has been reported to have low expression yields [118], and the additional mutations to the protein structure resulted in poor expression across several different cell lines. Furthermore, the insertion of an extra cysteine – in addition to the other six naturally occurring cysteines on E – caused the formation of incorrectly crosslinked monomers. While we were optimizing the process, Rouvinski et al. [119] used a similar approach to form dimers of DENV E proteins, thus, we decided to explore other approaches for stabilizing ZIKV E dimers.

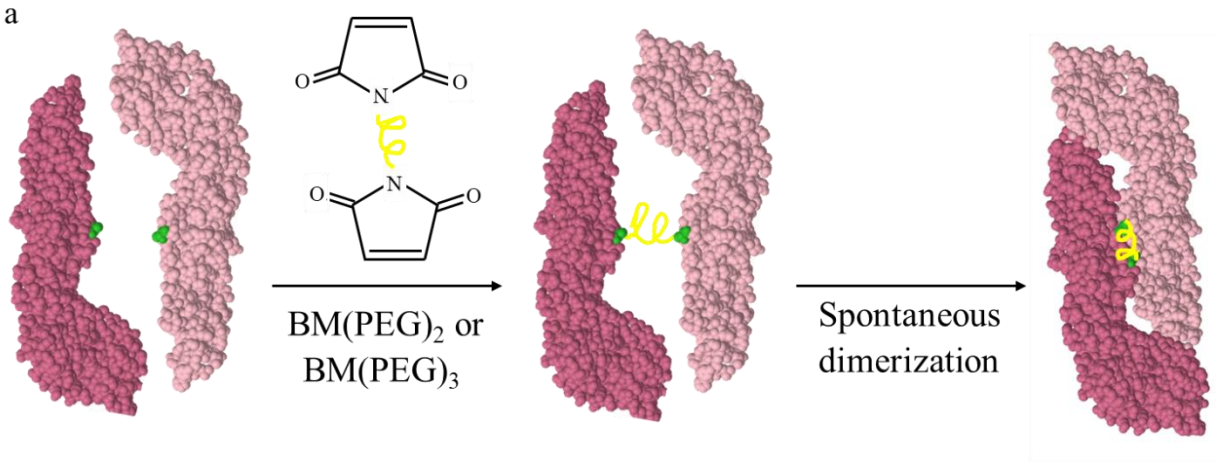

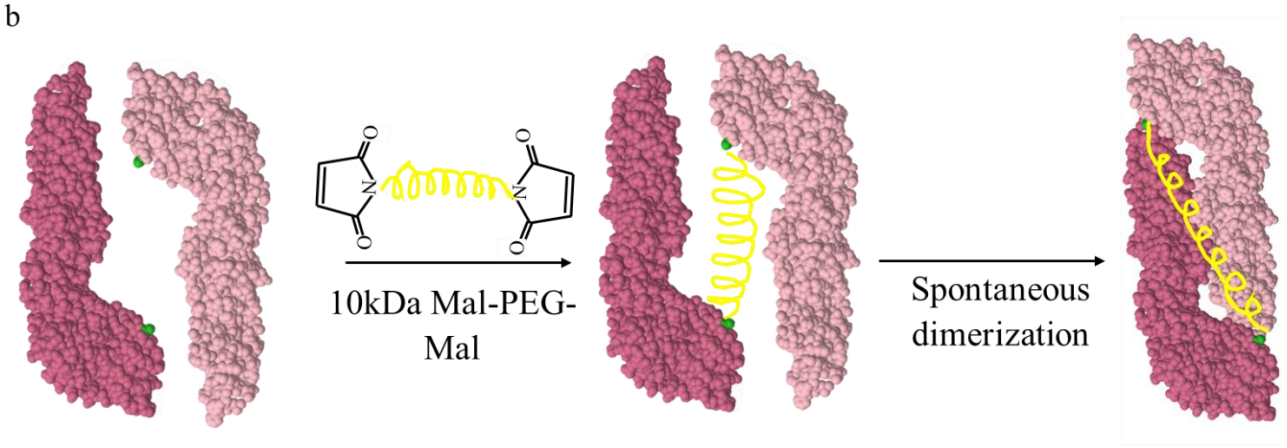

Figure 19. Proposed approaches to promote the dimerization of E protein by cross-linking E monomers. (a) Amino acid 267 (green) was mutated to a cysteine to allow for conjugation of E with a short mal-PEG-mal linker. This linker would bring the monomers together and promote dimer formation. (b) A C-terminal cysteine (green) was incorporated to the sequence of the E protein. This cysteine would be reacted with a 10kDa mal-PEG-mal. The longer linker would allow the monomers to rearrange in the head-to-tail conformation.

We next explored a dimerization approach that would bring two E monomers together by attaching them to a SnoopCatcher homodimer. The SnoopCatcher and SnoopTag pair [120] is analogous to the SpyCatcher/SpyTag pair described in section 2.3.1; when mixed, the SnoopCatcher protein and SnoopTag peptide form an isopeptide bond resistant to heat and proteases. To form the SnoopCatcher homodimer, we incorporated an F* at its C-terminus. This modified SnoopCatcher was then allowed to react with a 5k DBCO-PEG-DBCO molecule via copper-free azide-alkyne cycloaddition. By fusing a SnoopTag to the C-terminus of E and allowing this protein to react with the SnoopCatcher homodimers, we were expecting to bring together two individual E proteins to form anti-parallel dimers. A schematic of the process is shown in Figure 20.

Although we were able to synthesize the SnoopCatcher homodimers in small amounts and react them with E proteins, the low yields did not allow us to move forward with this synthesis approach. As a result, we developed an alternative dimer synthesis method that allowed us to generate multivalent scaffolds presenting E dimers more rapidly and with better yields. This strategy will be described in more detail in the next section.

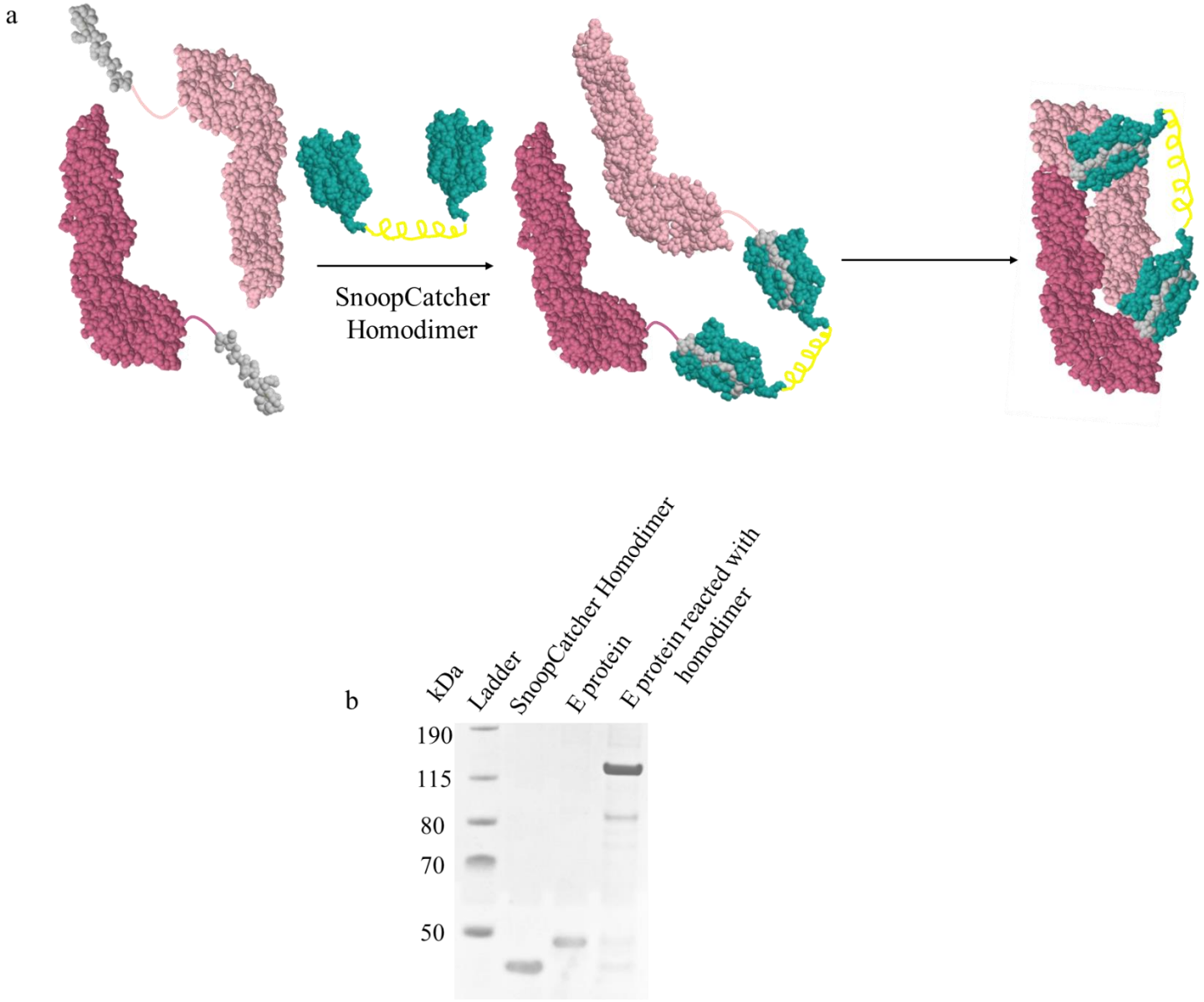

Figure 20. Schematic for a novel synthesis of E protein dimer using the SnoopCatcher and SnoopTag pair. A SnoopTag (grey) was fused to the C-terminus of E (pink). This allowed for coupling of E to a SnoopCatcher (green) homodimer, linked by a PEG chain (yellow). The homodimer was expected to bring the E monomers together to promote spontaneous dimer formation.

3.3 Synthesis of E Dimers Conjugated to VLPs

Given the influence of E protein concentration on dimer formation, we hypothesized that by immobilizing multiple copies of the antigen on a fixed surface we could achieve a high local concentration of E, thereby promoting spontaneous dimerization. As a result, this strategy would not be affected by sample dilutions or changes in temperature. Additionally, we rationalized that by optimizing the distance between each E monomer, we could bring them close together while ensuring that they had enough space and flexibility to assemble in the required head-to-tail orientation. Furthermore, the conjugation of E to a multivalent nanoscaffold would allow us to present multiple copies of the antigen from a single scaffold, enhancing the immunogenicity, while simultaneously blocking the underside of the protein that is inaccessible in the context of the virion.

Given these objectives, we chose an approach that consists of attaching E monomers to VLPs via a series of linkers in order to bring the E proteins together to form dimers. More specifically, we conjugated SnoopTagged E proteins to an engineered SnoopCatcher protein that had been functionalized with a PEG-biotin, allowing for the attachment of this E-Catcher pair to the VLP-streptavidin scaffold described in Section 2.3.2. We hypothesized that the VLP would provide enough binding sites for E to achieve a high local concentration of E monomers, while the protein linkers in combination with the PEG chain would offer flexibility and allow the two E monomers to assemble in an anti-parallel/ head-to-tail format.

The process of synthesizing MS2 VLPs and conjugating them to streptavidin molecules was described previously. We expressed in *E. coli* a variant of SnoopCatcher with an F* incorporated at the C-terminus (SnoopCatcher-F*). SnoopCatcher-F* was next allowed to react with a 2k DBCO-PEG-biotin, resulting in the SnoopCatcher-2k-bio protein. A SnoopTag was fused to the C-terminus of the E protein to enable its attachment to the SnoopCatcher-2k-bio via the SnoopTag-SnoopCatcher reaction. This pair, named E-Sncat-2k-bio, was then conjugated to the VLP-SA. A schematic of this process is shown in Figure 21.

The MS2 VLP is made of up 90 copies of MS2 coat protein dimers, which means, ultimately, 90 potential sites for E attachment. To determine the local E concentration, we assumed that all 90 biotin-binding sites of the VLP were conjugated to one E monomer and divided that by the volume of our system. Based on DLS measurements we estimated the radius of the MS2 VLP to be roughly 16 nm. Using the crystal structure of Streptavidin (PDB 3RY2), we determined the average end-to-end length of the protein to be approximately 2.8 nm. Considering that biotin occupies "pockets" within the structure of streptavidin, it is safe to assume that Streptavidin molecules will be bound tightly to the VLP surface, allowing for little movement and flexibility. The streptavidin-conjugated VLPs, therefore, constitute our "core" particle, with a fixed radius of 19 nm (Figure 22a)

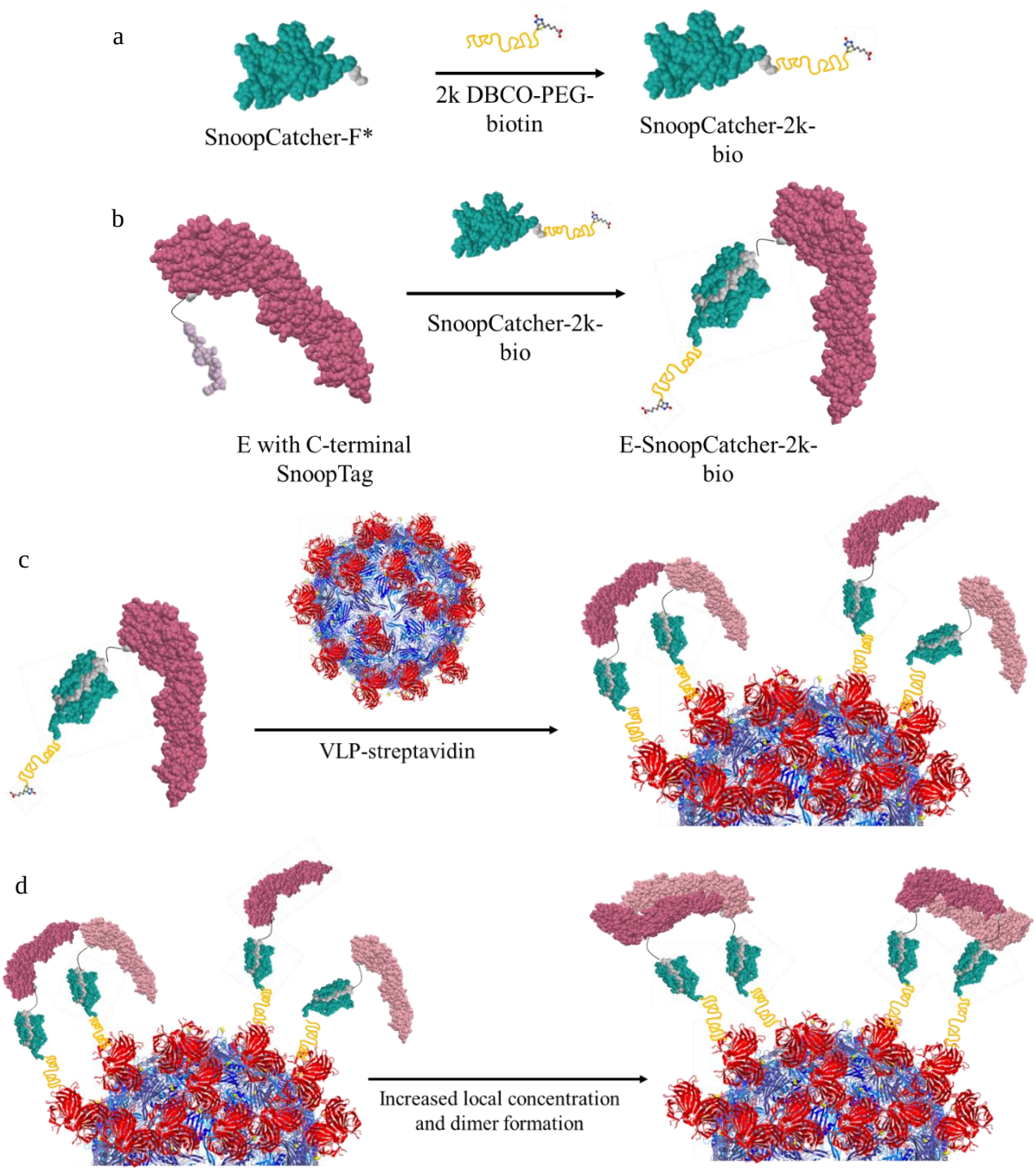

Figure 21. Schematic of synthesis of E protein dimer via VLP conjugation. (a) Mutant SnoopCatcher-F* was functionalized with a 2kDa DBCO-PEG-biotin, generating SnoopCatcher-2k-bio. (b) A SnoopTag was inserted on the C-terminal of E to allow for its conjugation to the SnoopCatcher-2k-bio. (c) The E + SnoopCatcher-2k-bio pair was conjugated to the VLP-streptavidin via the biotin-streptavidin interaction. (d) The high

concentration of E on the surface of the VLP would shift the equilibrium towards the formation of E dimer.

Using crystal structures, we estimated the approximate length of the SnoopCatcher and the E proteins to be 5.3 nm and 11.2 nm, respectively (Figure 22b). Unlike the "core" particle, these have either short linkers or purification tags within their sequences, resulting in an E-SnoopCatcher pair that displays more flexibility than the "core" particle. Hence, the E-SnoopCatcher pair, in combination with the PEG linker, make up the "flexible" portion of the particle (Figure 22c). We estimated the root mean square (RMS) end-to-end distance for the PEG chain in solution [121] – to be ~ 3.9 nm. The PEG, SnoopCatcher, and E protein combined have a total length of ~21 nm, resulting in a total particle radius of 40 nm.

To obtain an estimate of the volume accessible to the E monomers, we subtracted the volume of the 19 nm-radius VLP-SA "core" from the volume of the 40 nm-radius particles. This resulted in a volume of roughly 239,270 nm^3. Assuming that each of the 90 sites of MS2 are occupied by one E monomer, we end up with 90 E monomers, or 1.5 x 10^{-22} mol of E monomers, in a volume of 239,270 nm^3, corresponding to a local E concentration of approximately 627 μM, which is much greater than the reported dissociation constant (K_d) for E dimerization of 2.1 μM at 23 °C [112]. Studies have demonstrated that for DENV E monomer, the K_d value can be 50 times higher at physiological temperatures. [112] Even if we assume the K_d for ZIKV E dimers to behave the same way, our local concentration of E will still be high enough to promote dimerization.

Although the E protein is 11.2 nm long, the region of contact between the two monomers within the dimer spans a distance of ~9.2 nm. Therefore, when conjugating our E proteins to the VLP, we want to keep them approximately 9 nm apart. We believe that a distance much shorter than this could result in crowding of E proteins, preventing them from rearranging in a head-to-tail orientation. A distance much longer than that would keep the monomers too far apart, impeding dimer formation as well. This rationale consolidated our choice of using the 2 kDa PEG-biotin linker. We believe its root mean square end-to-end length of 3.9 nm would provide enough space between E protein monomers, while still maintaining them at close proximity for dimer assembly. In addition, the flexibility of the PEG chains would allow the monomers to get closer or farther apart if necessary.

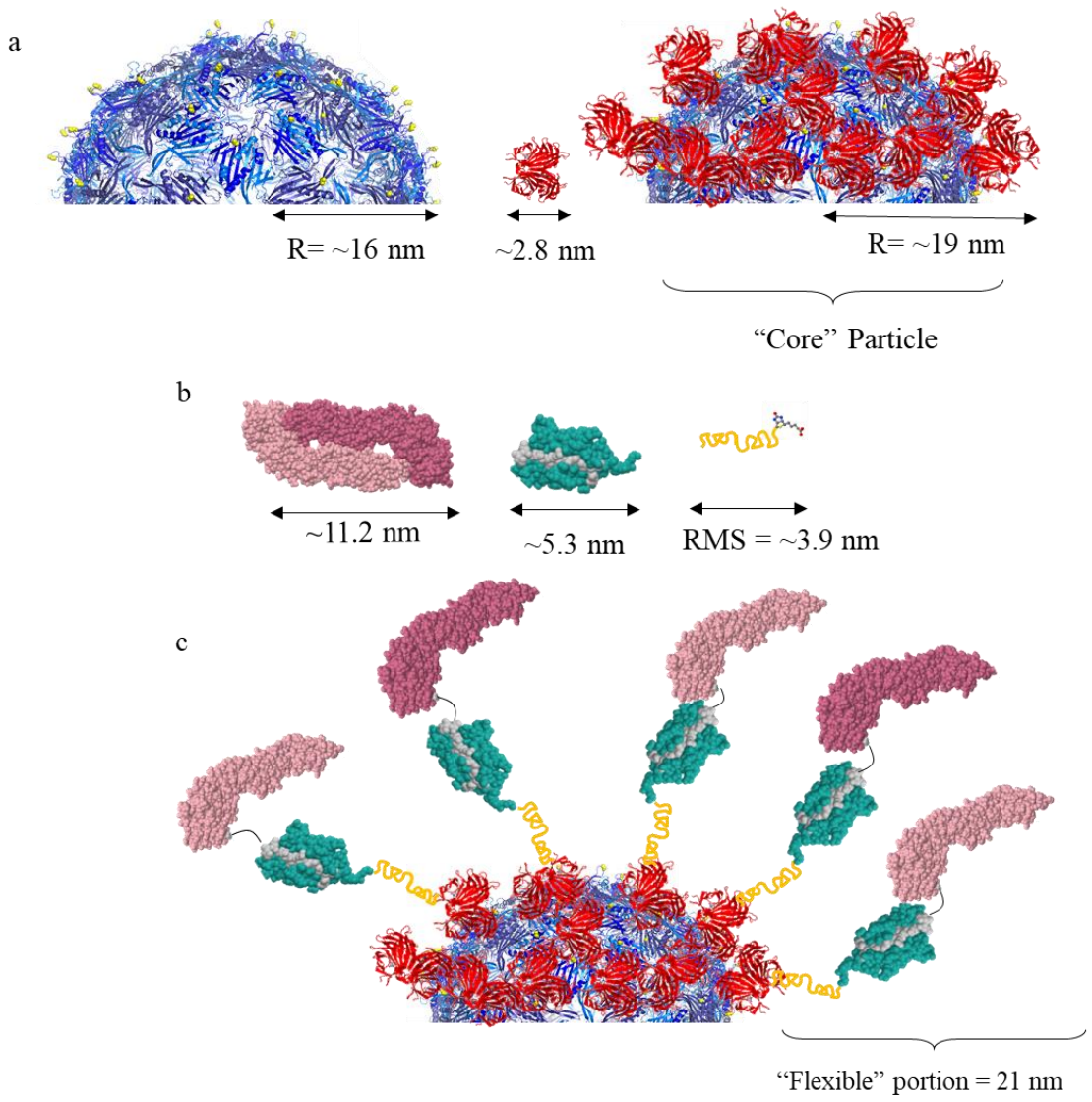

Figure 22. Estimating the local concentration of E protein on the VLP surface. (a) Radius of VLP and length of streptavidin. When combined they result in the "core" particle. (b) Lengths of E protein, SnoopCatcher, and 2k DBCO-PEG-bio. (c) When conjugated to the VLP, the PEG, SnoopCatcher, and E protein make up the "flexible" portion of the particle.

3.4 Materials and Methods

3.4.1 Cloning of E Protein, SnoopCatcher, and VLP.

The process for synthesizing the MS2 and streptavidin proteins is the same as described in section 2.2. Based on the entire genetic sequence of the Zika virus (GenBank ANO46313.1), we designed construct 19C-prM-E-ZIKV, which encoded for the last 19 C-terminal amino acids of the capsid protein, the prM, and the E protein sequences [122]. The sequence corresponding to wo C-terminal GGSGG repeats, followed by a SnoopTag and a StII purification tag were also added to the sequence. The DNA was codon-optimized for expression in insect cells and cloned into the PIEX vector by Gene Universal. Using this DNA as a template, our collaborators in the Krammer lab (Icahn School of Medicine, Mount Sinai, NY) synthesized a construct coding for the sequence of E, SnoopTag and a 6xHis tag which was cloned in the pfastBacDuo plasmid.

The wild-type (wt) sequence encoding SnoopCatcher (UniProt A0A0H2UNT6) was codon-optimized for expression in *E. coli* and cloned into pET28b with a C-terminal 6xHis-tag by Integrated DNA Technologies Inc. (Coralville, IO). Through site-directed mutagenesis, we inserted an Amber codon, as well as sequences encoding a GGSGG spacer, and a SpyTag between the SnoopCatcher and 6xHis-tag sequences.

3.4.2 *Expression and Purification of E protein.*

The initial baculovirus stock carrying the genetic material for E protein expression were kindly shared with us by Krammer lab. Baculovirus stocks were amplified as needed by infecting fresh Sf9 cells. Sf9 cells were seeded in large T175 flasks at a density of 2 x 10^5 cells/cm^2 and allowed to settle for 20 min to adhere to the flask surface. The supernatant was aspirated and replaced by 50 mL of TNM-FH medium (ThermoFisher

Scientific) with 3% of fetal bovine serum (FBS). 400 µL of the original baculovirus stock were added and the flask was swirled to allow even distribution of the baculoviral inoculum. The flask was incubated at 28ºC without CO_2 for 6 days. The media was harvested and centrifuged at 2000 xg for 5 min to yield the amplified baculovirus stock.

For expression of E protein, Hi5 cells were cultured in Express Five Serum-Free Medium supplemented with 16 mM of L-Glutamine (E5SFM medium) at 28ºC. $60x10^6$ cells were centrifuged at 100 xg for 7 minutes and the supernatant was aspirated. The cell pellet was resuspended with 1-2 mL of the baculovirus stock and incubated for 20 minutes at room temperature. Infected cells were transferred to a 250-mL shaker flask containing 98 mL of fresh E5SFM media and allowed to grow at 28ºC for 3 to 4 days.

Cells were harvested and spun down at 4,000 xg for 5 minutes. Prior to IMAC, the supernatant had to be dialyzed for the removal of medium additives that damage the Ni-NTA resin. The cell medium was dialyzed against 4 L of IMAC Binding Buffer. The dialysis buffer was replaced twice over the course of 2 days. The dialyzed solution was then filtered through a 0.45 µm membrane for the removal of precipitated salts and poured over 1 mL of pre-equilibrated Ni-NTA resin in a gravity-flow column. The wash and elution steps for the resin were followed as previously described.

3.4.3 Expression and Purification of SnoopCatcher.

The DNA encoding the SnoopCatcher mutant was co-transformed with pEVOLpAzFRS.2.t1 (Addgene) into BL21(DE3) competent cells and plated overnight on LB-agar plates containing kanamycin and chloramphenicol. A single colony was picked for a 5 mL starter culture which was further scaled up (after growing for 12-16hrs) to 1 L

of 2xYT media containing kanamycin and chloramphenicol. Cells were grown at 37˚C until the OD reached 0.6-0.8. IPTG, L-arabinose, and *p*-azido-L-phenylalanine were added to a final concentration of 1 mM, 13.3 mM and 0.5 mM respectively, and the temperature was reduced to 30^{o}C. Cells were allowed to grow overnight before harvesting. Harvesting and lysis of cells follow the same protocol described for the SpyCatcher protein in section 2.2.

Purification of the SnoopCatcher was performed at 4°C. The lysate of cells expressing the SnoopCatcher protein was poured into a gravity-flow column containing Ni-NTA resin that had been pre-equilibrated with IMAC Binding Buffer. The resin was thoroughly washed with at least 20 CVs of IMAC Binding Buffer and the protein was eluted with 5 CVs of IMAC Elution Buffer. The eluate was collected and analyzed by SDS-PAGE. If the level of purity of the sample was unsatisfactory, then further purification by SEC was performed using a GE Superdex Increase 75 10/300 GL column. Protein purity was determined by SDS-PAGE.

3.4.4 PEG functionalization of SnoopCatcher proteins

SnoopCatcher concentration was estimated by BCA. For the synthesis of PEG-functionalized SnoopCatcher, purified SnoopCatcher protein was allowed to react with a 5x molar excess of 2k DBCO-PEG-biotin (Nanocs, Boston, MA) and incubated overnight at 4°C with mixing. Reaction yield was determined using SDS-PAGE on the following day. An additional 5x molar excess of PEG was used when the yield was exceptionally low. Excess PEG was removed by IMAC following the standard protocol. Given that the reaction between the SnoopCatcher and PEG did not reach completion, SEC was required

for the isolation of the target product, SnoopCatcher-2k-bio. The reaction mixture was injected into a HiLoad 16/600 Superdex 200 pg (GE) column and 0.5 ml fractions were collected and analyzed by SDS-PAGE. Fractions containing the target protein were combined and concentrated. Complete separation between PEGylated and unPEGylated SnoopCatcher was not possible and small amounts of unreacted protein remained in the purified product.

3.4.5 Synthesis of E Dimers on VLPs.

To determine the optimal E to SnoopCatcher-2k-bio ratio, small scale reactions with different E:SnoopCatcher ratios were set up and allowed to react overnight. The reaction products were analyzed by SDS-PAGE and the disappearance of SnoopCatcher was monitored. The chosen stoichiometric ratio was the one with the smallest amount of E that resulted in consumption of most of the SnoopCatcher-2k-bio.

The Streptavidin-conjugated VLPs were then added to the reaction mixture in an equimolar ratio to the SnoopCatcher. Proteins were allowed to react for approximately 10 minutes at room temperature. Successful conjugation of E-SnoopCatcher (E-Sncat-2k-bio) pairs to the VLPs were confirmed by SDS-PAGE, SEC, and ELISA. SDS-PAGE was performed at 4^{o}C to help preserve the integrity of the streptavidin-biotin bond during the electrophoresis.

3.4.6 ELISA

96-well plates were coated with 50 µL of E-Sncat-2k-bio and VLP mixtures with a final estimated E dimer concentration of 1 µg/mL and incubated at room temperature

for 1 hr. As controls, we also had well with the equivalent amount of E monomers, VLP alone, and SnoopCatcher-2k-bio alone. Plates were blocked with 100 µL 5% BSA in PBST for 2 hrs and washed three times with 100 µL of PBST. 50 µL of EDE-binding antibodies, c8 or c10 (Absolute Antibody, Oxford, UK), at a concentration of 1 µg/ml were added to each well. Binding of monomer-targeting antibodies to the assembled dimers and controls was also tested by incubating the samples with 50 µL of ZV-67 and 4g2 (Absolute Antibody) at 1 µg/mL. This step was followed by a 1-hr incubation and three additional washes with PBST. Wells were then incubated with 50 µL of diluted HRP-conjugated anti-mouse or anti-human secondary antibodies for 1 hr. Incubation was followed by three washes with PBST. Wells were developed and absorbance at 450 nm was measured. The same protocol was also performed at 37 °C to assess the effect of physiological temperatures on dimer assembly.

3.5 Results and Discussion

3.5.1 Expression of E protein and Synthesis of VLP-conjugate

Our collaborators in the Krammer lab provided us with an initial baculovirus stocks, allowing us to express E monomers *in-house*. Hi5 cells were infected with baculoviruses carrying the DNA for E protein, resulting in expressions with modest yields (~ 100 µg/L of culture). The recombinant E was characterized by SDS-PAGE (Figure 23a); the observed molecular weight agreed with the ~47 kDa value expected based on the sequence. We also tested the binding of ZIKV-specific antibodies such as ZV-67, and anti-flaviviral antibodies such as 4g2 to the E protein. The ELISA results are shown in Figure 23b. The binding of both antibodies with no binding to control (BSA) confirms

that we were able to express E protein. Binding of ZV-67 also confirms that the protein is correctly folded.

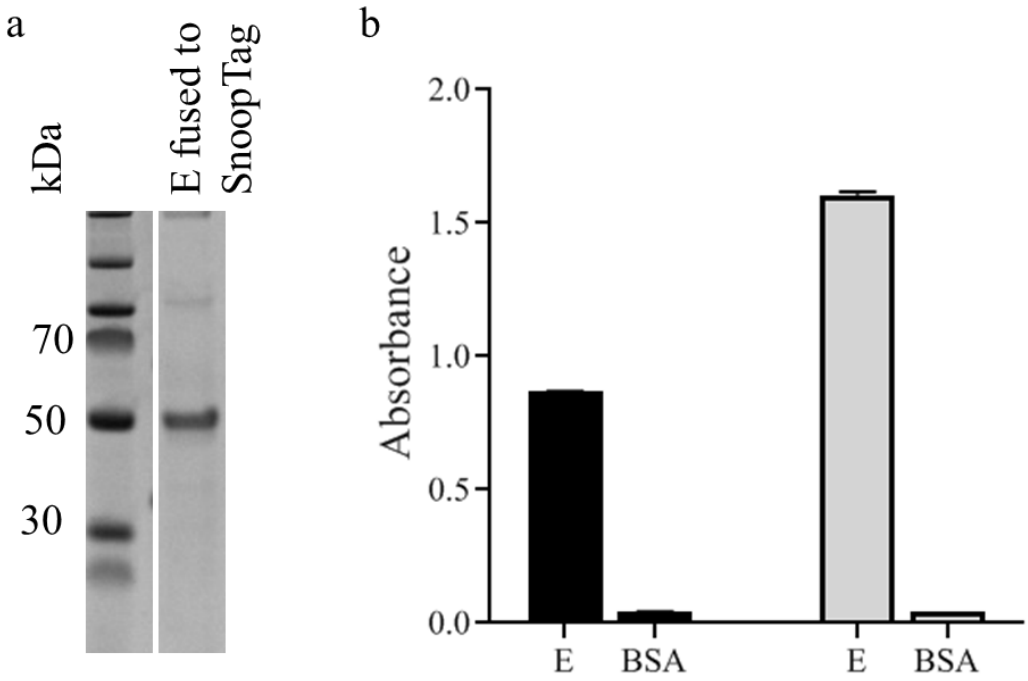

Figure 23. Characterization of E protein and SnoopCatcher functionalized with PEG. (a) Characterization of E protein fused with a C-terminal SnoopTag by SDS-PAGE. (b) Binding of antibodies 4g2 (black bars) and ZV-67 (grey bars) to E and to BSA (negative control).

The engineered SnoopCatcher protein was successfully expressed and allowed to react with a 2k DBCO-PEG-biotin to yield SnoopCatcher-2k-bio (Figure 24a). This construct was then reacted with a molar excess of E protein and the disappearance of SnoopCatcher was monitored by SDS-PAGE (Figure 24b). Our goal was to achieve consumption of the majority of SnoopCatcher-2k-bio to avoid a purification step at this point. In parallel, VLPs conjugated to Streptavidin (VLP-SA) were synthesized as

described in previous sections. An excess of SnoopCatcher-E conjugates was mixed with the VLP-SA for a short time, to allow the formation of E-VLP conjugates. Given the very large size of the E-VLP product, characterization by standard SDS-PAGE was difficult. However, by using a polyacrylamide gel specific for large proteins, we were able to detect some reaction product and monitor the disappearance of E-Sncat-2k-bio after reaction. This is demonstrated in Figure 24c, where we have a side-by-side comparison between the unheated reaction mixture, the heated mixture, and E-sncat-2k-bio alone.

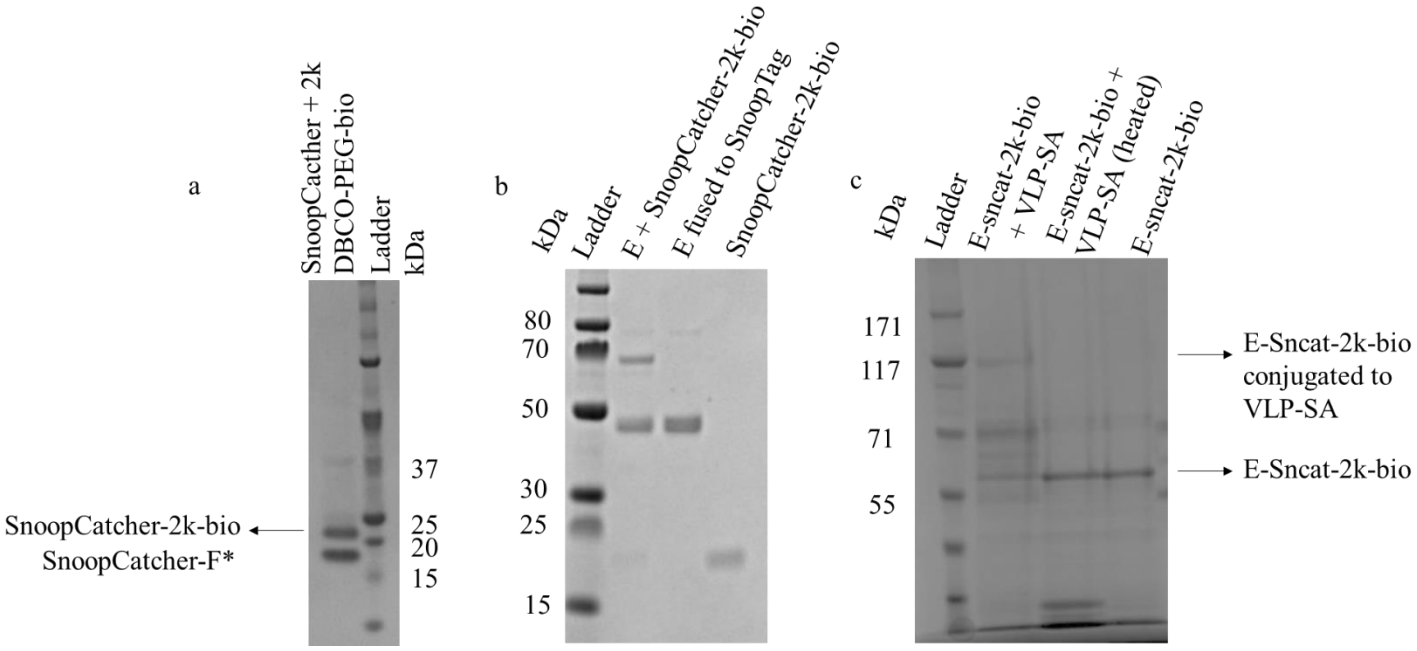

Figure 24. Characterization of reactions involved in the synthesis of E dimers by SDS-PAGE. (a) SnoopCatcher-F* was allowed to react with a 2k DBCO-PEG-bio to yield SnoopCatcher-2k-bio. (b) Product of reaction between E and the PEG-functionalized SnoopCatcher. (c) E-Sncat-2k-bio and VLP-SA reaction mixture compared to the same reaction mixture after heating and E-Sncat-2k-bio alone. We were able to see disappearance of the band corresponding to E conjugated to SnoopCatcher-2k-bio.

3.5.2 Confirming Dimer Formation

Even though we were able to confirm the synthesis of our E-VLP conjugates, we had yet to confirm if stable dimers of E had been formed. Therefore, we tested binding of E-VLPs to two EDE-binding antibodies (c8 and c10) by ELISA. As a negative control, we reacted the VLP-streptavidin conjugate with a large excess of biotin to block all the biotin-binding sites. Therefore, a reaction with the E-SnoopCatcher-2k-bio pair would not result in E conjugation to the VLP and the proteins should remain in solution as monomers. ELISA results are shown in Figure 25 and demonstrate successful binding of both c8 and c10 antibodies to E conjugated to VLP, while no binding is seen for E-SnoopCatcher reacted with the "blocked" VLP, or for E protein alone. There is also no antibody binding to SnoopCatcher-2k-bio, VLP, or BSA. The monomer-binding antibody 4g2 was included in the assay as a control antibody. 4g2 binds to the FLE, which remains accessible in the E dimer conformation and, as a result, all groups containing E bound to the it. These results demonstrate that our strategy yielded correctly assembled dimers of E protein.

We previously mentioned that low concentration tend to shift the dimer-monomer equilibrium towards the monomer. The solutions used to coat the wells prior to the ELISA (Figure 25a) had a final E concentration of 4 μg/mL (0.09 μM), a value that is significantly lower than the dimer dissociation constant (2.1 μM). Binding of anti-EDE antibodies to the immobilized E-VLP conjugates confirms that dilution of the sample does not disrupt the formed dimers, highlighting the effect of the high local concentration of the E monomers when attached to VLPs.

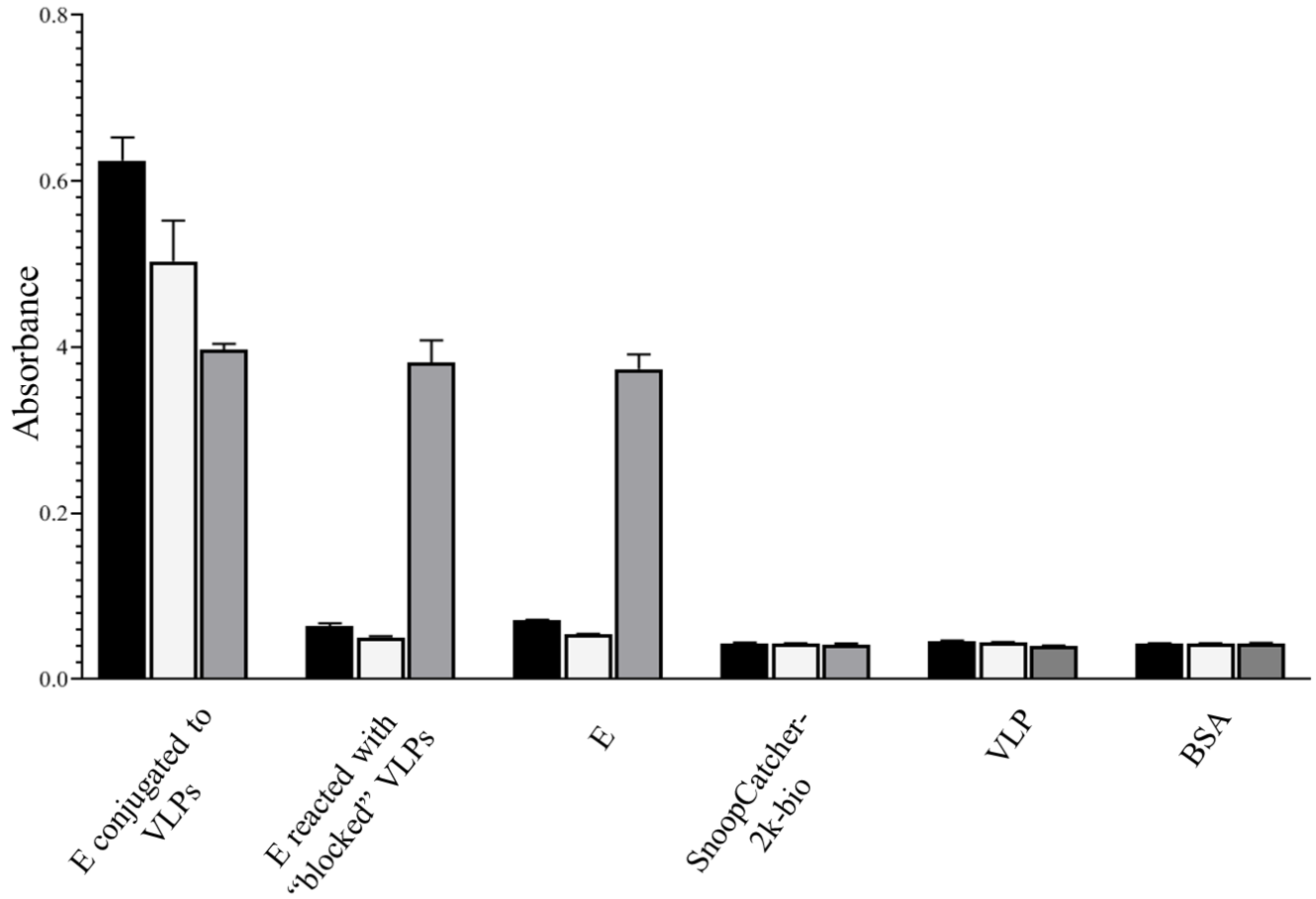

Figure 25. Characterization of antibody binding to E protein conjugated to VLPs by ELISA. (a) ELISA performed at room temperature. EDE-binding antibodies c8 (black bars) and c10 (white bars) showed binding to E conjugated to VLPs. FLE-binding antibody 4g2 (grey) bound to the dimer, to the E on "blocked" VLP, and to the E monomer control. No antibody binding was seen for the SnoopCatcher-2k-bio, VLP, or BSA.

3.6 Conclusions and Future Directions

In this chapter, we were able to demonstrate the successful synthesis of E protein dimers that are stable at high temperatures and low sample concentrations. Furthermore, our dimers are presented multivalently on VLPs, which can promote BCR clustering and enhance the production of antibodies. Unlike previously reported E dimerization approaches, our strategy prevents the exposure of the highly conserved dimer underside, which is not accessible in the Zika virion and has the potential to elicit non-neutralizing antibodies.

Although we are confident in our work, the ability of our E dimers to elicit EDE-targeting antibodies *in vivo* is yet to be tested. The future steps of this project would consist of immunizing mice with the E dimers on VLP along with the E plus "blocked" VLP mixture as a control. An analysis of the serum following immunizations would determine whether there was a difference in the immune response generated by our dimers versus the response generated by the control. We would expect the dimer to elicit the broadly neutralizing EDE-binding antibodies, while the control should elicit E-targeting antibodies that are cross-reactive and poorly neutralizing.

If these results proven to be successful, we would next like to assess whether immunization with the dimer antigen poses any risk of promoting ADE. If the generated immune response is mostly made up of EDE-targeting antibodies, E dimers on VLPs could be used as a vaccine that confers protection against ZIKV and DENV.

However, we must consider the possibility of E dimer antigens still eliciting antibodies that target E monomers, as previous studies have suggested that epitopes such

as the Fusion Loop Epitopes (FLE) are immunodominant and "comprise a significant fraction of the humoral response against flaviviruses" [66, 123, 124]. FLE-targeting Antibodies have been shown to be less potent and promote ADE *in vitro* [123, 125]. Therefore, there is the possibility that immunization with Zika E dimers could still result in the generation on non-neutralizing, ADE-promoting antibodies [53, 57, 126, 127].

Epitope mapping has determined that binding of antibodies to the FLE is greatly reduced by mutations on amino acids W101, G106, L107, and F108 [125]. Therefore, if necessary, we would incorporate some of these mutations into the E protein in order to avoid generation of FLE-binding antibodies. We propose to generate two different mutants as back up antigens, one with the mutation W101A, and another with the mutations W101A and L107R [128, 129]. These mutants would also be reacted with SnoopCatcher-2k-bio and conjugated to VLPs. If dimer formation is still seen, then these constructs could be used for immunization studies and the generated immune response between wild-type E on VLPs and mutant E proteins on VLPs could be compared.

CHAPTER 4. DESIGNING VACCINES TARGETING THE SARS-COV-2 RBD

4.1 Introduction

2020 will likely be remembered as the year the world faced an unprecedented pandemic, which has resulted in catastrophic public health and economic consequences. The Novel Severe Acute Respiratory Syndrome Coronavirus (SARS-CoV-2 or nCov-19), which was first detected in the Wuhan province in China in late 2019, has already infected over 60 million people, and claimed over 1.4 million lives [130]. The number of cases of coronavirus disease 2019 (COVID-19) continues to increase in the United Stated, and the infection is on track to becoming one of country's top killers [45, 46]. Since SARS-CoV-2 was first identified, great efforts and investments have been spent on the rapid development of a vaccine and candidates have demonstrated great efficacy in clinical trials [131-135].

While many patients remain asymptomatic, infections with COVID-19 often result in high fever, cough, myalgia, fatigue, and gastrointestinal symptoms [136, 137]. However, in more severe cases, long-term pulmonary, liver, kidney, and cardiovascular injury may occur [138-141]. Considering the number of lives that have been claimed – and will continue to be claimed – by this coronavirus, along with the potential of life-long organ damage, an efficacious vaccine is of utmost importance.

Unfortunately, as it is the case with any novel virus, there are a lot of questions surrounding SARS-CoV-2 [142]. Unknowns, like the mutation rate of the virus and the

nature and potency of the antibodies that target it, greatly affect vaccine design. A few cases of reinfections with SARS-CoV-2 have already been reported [143, 144], suggesting that the virus may have already mutated enough to evade the previously elicited antibody response and highlighting the importance of focusing on a vaccine that will elicit broadly neutralizing antibodies to prevent a similar SARS-CoV-2 pandemic from occurring again in the future.

SARS-CoV-2 is an enveloped, positive-sense RNA virus [145] that belongs to the genus of *Betacoronaviruses*, which includes SARS-CoV and MERS-CoV [146]. SARS-CoV, became well-known in 2003 after an outbreak resulted in thousands of cases of severe pneumonia and the loss of hundreds of lives [147, 148]. Thankfully, a lot of the research that has been done for SARS-CoV has shown to be useful in understanding SARS-CoV-2 due the similarities between the two viruses. The surface of both SARS-CoV and SARS-CoV-2 is decorated with homotrimers of the Spike (S) glycoprotein protein (Figure 26) which plays a crucial role in viral infection by binding to host cells [149]. A homology of close to 75% is seen between the SARS-CoV and SARS-CoV-2 S protein [150, 151], which results in two very similar modes of infections. Previous studies have shown that binding and entry of SARS-CoV to host cells is done via the angiotensin-converting enzyme 2 (ACE2) [152-154].The receptor-binding domain (RBD) of the S protein interacts with of ACE2 [155], and efficient engagement with this receptor directly correlates with SARS-CoV transmissibility from species to species [152, 153]. Recent experiments demonstrated that, similarly to SARS-CoV, SARS-CoV-2 also uses the ACE2 receptor for host cell entry [154, 156]. Furthermore, the affinity between SARS-

CoV-2 RBD and ACE2 is 10- to 20-fold higher than what has been reported for SARS-CoV RBD [157].

Given its important role in viral infection, the S protein has been identified as the main target of neutralizing antibodies, many of which are directed towards the RBD [151, 158-162]. Several vaccine candidates have focused on using S or the RBD as antigens for immunization against SARS-CoV-2 [158, 163-169]. However, regions of the RBD have shown to be highly variable and immunogenic, and, as a result, the RBD is targeted by a wide variety of antibodies with different degrees of neutralization and cross-reactivity [170].

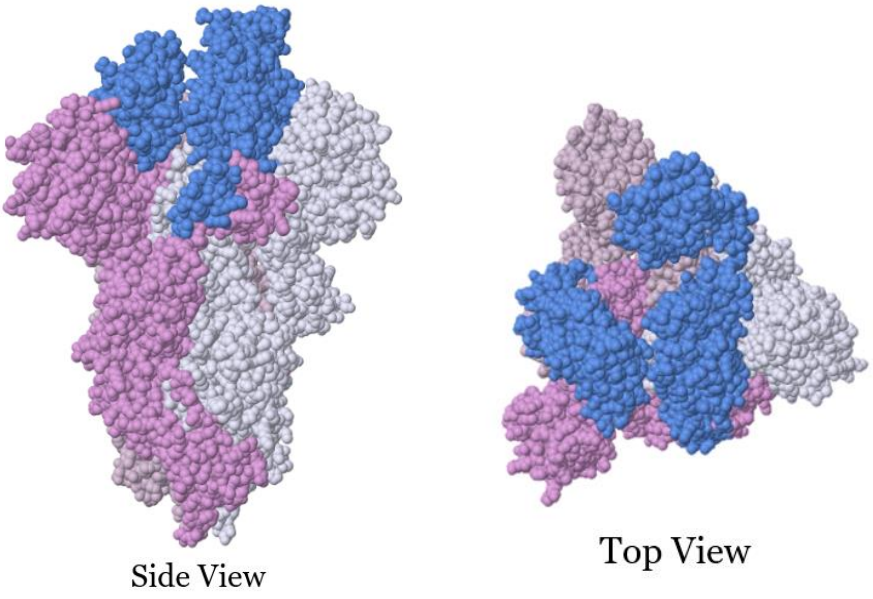

Figure 26. Crystal Structure of SARS-CoV-2 Spike Protein Homotrimers (PDB 6XLU). Individual monomers are shown in different shades of purple. The Receptor Binding Domain is highlighted in blue.

Studies have shown that several antibodies targeting the RBD of SARS-CoV bind weakly and have poor neutralization towards SARS-CoV-2, and vice-versa [157, 171-174]. This difference in neutralization activity can be associated with the degree of conservation of amino acids in different areas of RBD. The region of RBD that is directly involved in the interaction with ACE2, known as the receptor-binding motif (RBM), has shown to be most variable region of RBD, with less than 50% sequence homology between SARS-CoV and SARS-CoV-2 [155, 172]. Although antibodies that target RBM tend to be strongly neutralizing – since they effectively hinder the virus from interacting with the ACE2 receptor – they have shown to be highly specific and demonstrated poor neutralization of closely related viruses [151, 175-177]. The crystal structure of RBD bound to ACE2 is shown in Figure 27a, with the highlighted RBM on the S protein in Figure 27b.

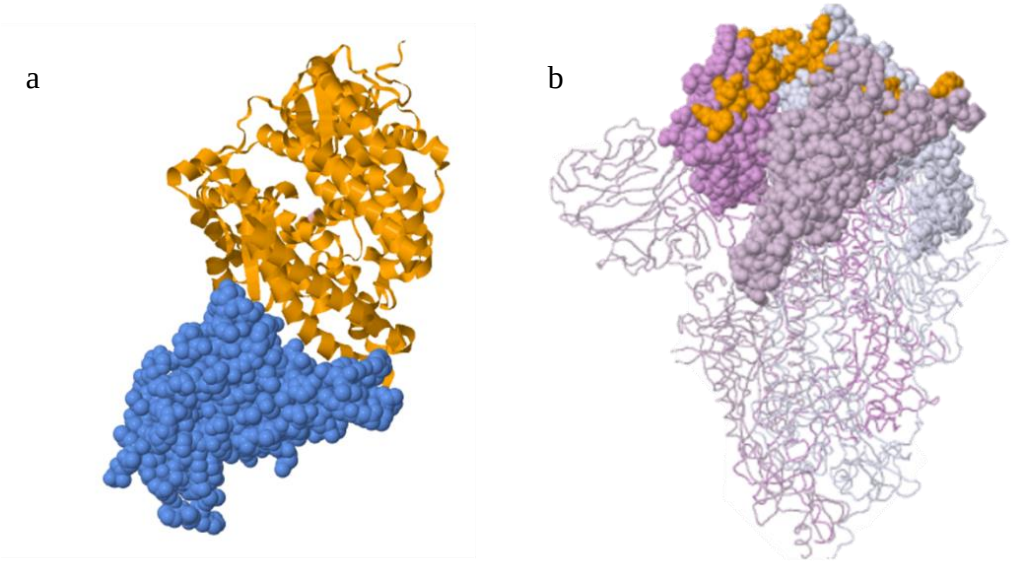

Figure 27. SARS-CoV-2 RBD binds to ACE2 receptor. (a) Crystal structure of RBD (blue) bound to ACE2 (orange), PDB 6M0J (b) ACE2-binding residues on the RBD (orange) are located on top of the trimer (RBD is in spacefill), PDB 6VXX.

A good example of this behavior was demonstrated by studies which explored the neutralization ability of anti-RBM camelid heavy-chain-only antibodies (also known as nanobodies) [171, 178]. While nanobodies H11-D4 and H11-H4 have been shown to completely block attachment of SARS-CoV-2 RBD to ACE2 and to successfully neutralize the virus in *in vitro* assays [171], they did not neutralize SARS-CoV as potently. Such specificity is also seen for the neutralizing S2E12 mAb, another RBM-overlapping antibody that is unable to bind to SARS-CoV [179]. Meanwhile, the opposite behavior – binding or neutralization of SARS-CoV only – is seen for nanobody VHH-72 [178] and mAb362 [159]. All this evidence further demonstrates that the RBM is in attractive site for the generation of potently neutralizing, but highly specific, antibodies.

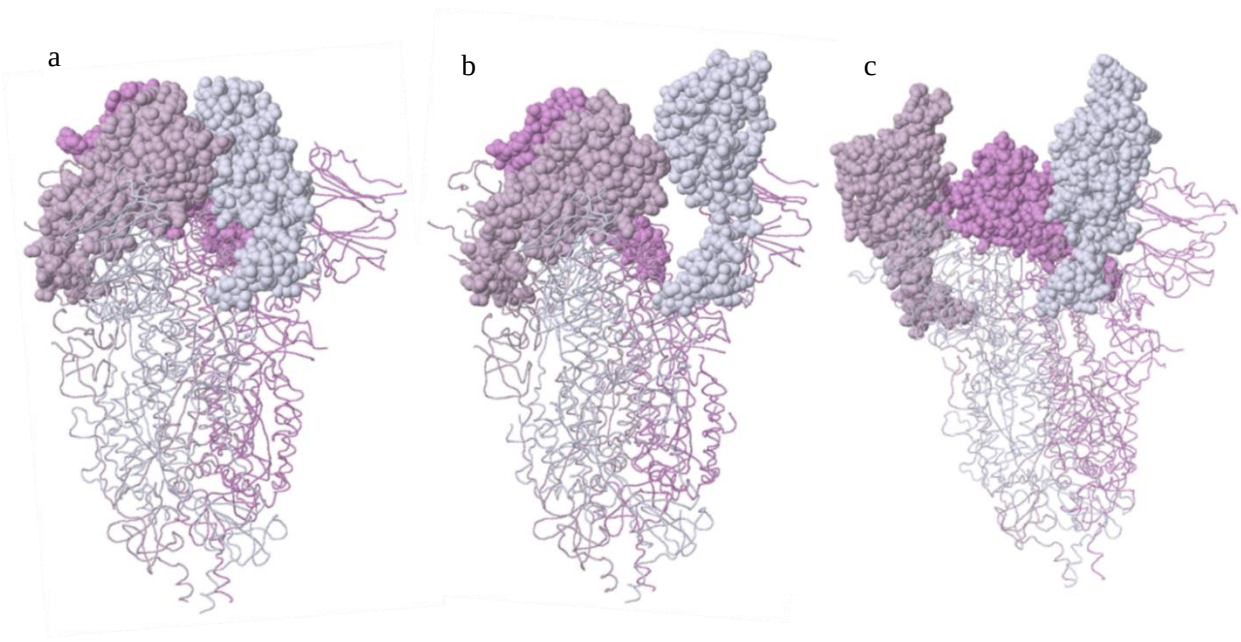

Figure 28. Crystal structure of S homotrimer in different conformational states. (a) Trimer in the closed state. All monomers are pointing down (PDB 6VXX). (b) Two monomers are down, and one monomer is up (purple). PDB 7JV4 (c) Trimer in the open state. All monomers are pointing up (PDB 6VYB).

However, disruption of the RBM-ACE2 interaction is not the only mechanism of viral neutralization. Antibodies that target epitopes outside of the RBM and that have demonstrated some neutralization activity have also been identified. It has been hypothesized that their neutralization mechanism involves destabilization of the S protein trimers [171, 180, 181], given that the latter display an unique dynamic behavior. Cryo-EM structures of S homotrimers showed that they can be found in two different states: open and closed. In the open state, the RBD is pointing “up” and away from S, allowing for the exposure of RBM and, consequently, engagement with ACE2. In the closed state, RBD points “down” and is tightly packed against S, which prevents binding to ACE2 [178, 182]. Figure 28a, 28b, and 28c show the trimer with all three RBDs in the “down” position, two trimers “down” and one “up”, and all three trimers in the “up” position, respectively.

Cryo-EM experiments have found a low abundance of particles that had all three RBDs in the open state, suggesting that this conformation is energetically unstable [157, 178, 183-185]. Antibodies such as CR3022 are believed to rapidly bind to this transient and unfavorable state of trimers, resulting in their irreversible dissociation into S monomers [186]. CR3022 has shown to bind both SARS-CoV and SARS-CoV-2 with high affinity [175, 187], and to potently neutralize SARS-CoV, although its ability to neutralize SARS-CoV-2 is still uncertain and controversial [180, 181, 186]. This can, perhaps, be explained by the cryptic nature of the CR3022-binding epitope, which is only accessible when at least two RBDs in the trimer are in the open position [188]. As a result, a low abundance of SARS-CoV-2 S open trimers could lead to the inability of the antibodies to potently neutralize the virus. Figure 29a shows RBD bound to CR3022,

while the antibody footprint in both closed and open states of the trimer can be seen in Figure 29b and Figure 29c, respectively.

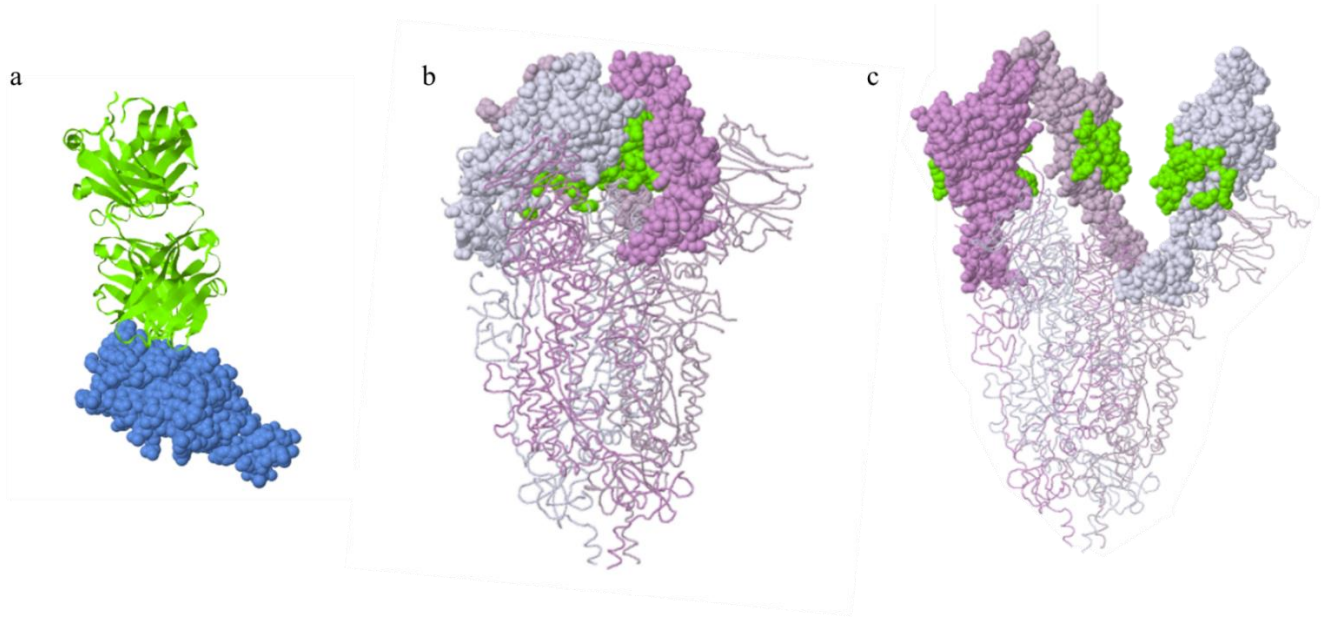

Figure 29. Interaction of RBD with cross-reactive antibody CR3022. (a) RBD (blue) bound to CR3022 (green) (PDB 7JN5). (b) Footprint on CR3022 (green) on S trimers in the closed state. The epitope is not accessible in this conformation (PDB 6VYB). (c) Footprint of CR3022 on open S trimers, showing epitope accessibility (PDB 6VXX).

Other antibodies that do not target the RBM have also been identified. This is the case of the cross-reactive broadly neutralizing mAb S309, which binds SARS-CoV-2 and SARS-CoV RBD with nano- or sub-picomolar affinity, respectively [188, 189]. The S309 epitope is highly conserved – 17 out of its 22 residues are conserved between SARS-CoV and SARS-CoV-2 – and is accessible in both open and closed trimer conformations. In addition, binding of S309 to RBD did not interfere with binding of RBD to ACE2 [188, 189]. RBD complexed to a S309 Fab, along with the S309 footprint on open and closed S trimers are shown in Figure 30a, b, and c, respectively.

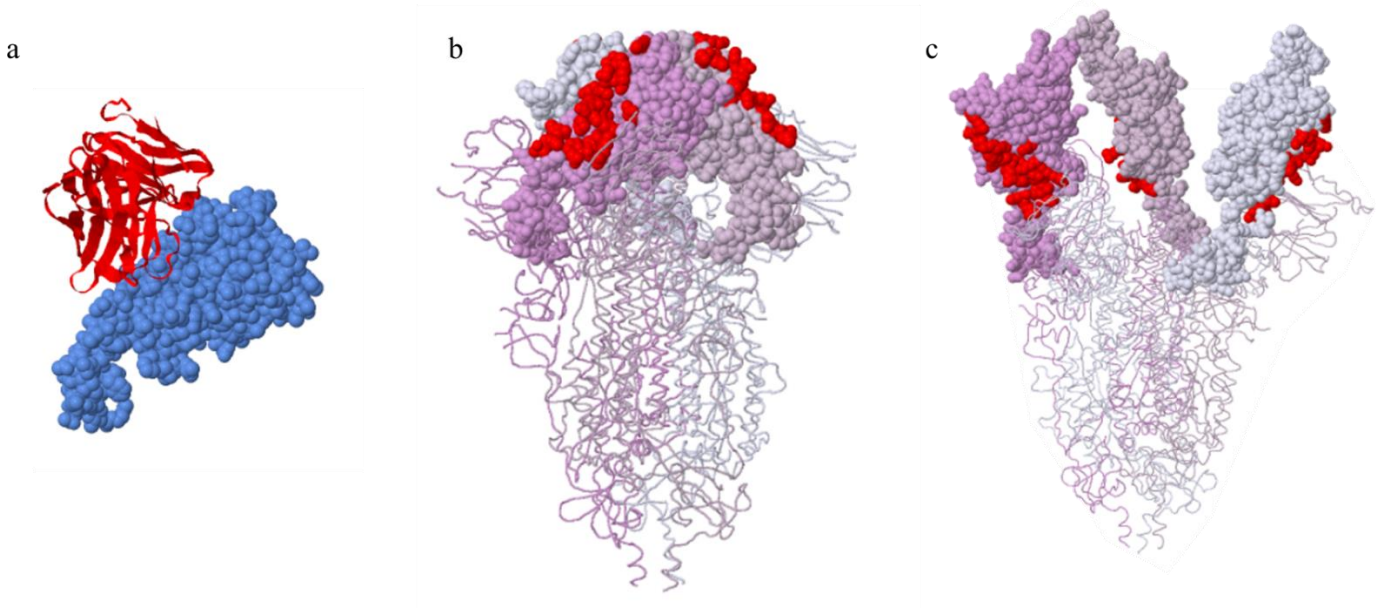

Figure 30. Binding of Antibody S309 to RBD and S trimers. (a) Fab fragment of S309 antibody (red) bound to RBD (blue) (PDB 6WPT). (b) Footprint of S309 on closed S homotrimers (PDB 6VYB). (c) S309 footprint on trimers in the open state. The epitopes is accessible in both conformations (PDB 6VXX).

Given the differences in the nature of the antibodies elicited against different region of SARS-CoV-2 RBD, we hypothesized that engineering the RBD could help refocus the immune response towards targeted epitopes. As a result, the elicited immune response could be designed to be either more potent and SARS-CoV-2-specific, or more broadly neutralizing, offering protection against SARS-CoV and SARS-CoV-2. As a first step towards investigating the influence of refocusing on the neutralizing antibody response to the RBD, we designed two distinct constructs: one that shields the RBM and redirects the immune response towards epitopes targeted by SARS-CoV and SARS-CoV-

2 cross-reactive antibodies; and one that focuses the response on the SARS-CoV-2 RBM by shielding adjacent epitopes on the RBD.

4.2 Shielding SARS-CoV-2 RBD with N-linked Glycans

The refocusing approach employed on RBD is different than what was described in Aim 1, where we used a PEG as a shielding tool. Since the RBD is glycosylated, expressing this protein in *E. coli* for the incorporation of a non-canonical amino acid might affect the structure of the protein. As an alternative, we explored the use of N-linked glycans as successful epitope shielding tools.

Glycosylation is a post-translational modification in which a polysaccharide is linked to an Asparagine (N-linked) or to a Serine/Threonine (O-linked) on the peptide backbone of the protein [190]. The consensus sequence N-X-S/T (where X is any amino acids besides Proline) is a requirement - although not a guarantee - for N-linked glycosylation to occur [191, 192], allowing us to somewhat predict and control potential glycosylation sites. Glycosylation has been successfully used as a strategy for epitope masking in HIV, Influenza, and Respiratory syncytial virus antigens [28, 33, 34]. We, therefore, chose to attach glycans to strategic locations on different regions of RBD to achieve epitope shielding and to refocus the elicited antibody response.

The process of selecting the glycosylation sites was quite complex and required several iterations. This complexity was due to several constraints: we not only had to choose a glycan location that would be optimal for shielding, but also maintain high expression levels, ensure proper protein folding, and a high extent of glycosylation. The selection process consisted of the following steps:

1. Analysis of the crystal structure of RBD conjugated to ACE2, CR3022, and S309 for the selection of solvent accessible residues that were also strategically located on each epitope.
2. Cross-referencing literature data to understand reported effects of mutations on protein yield and antibody/receptor binding [162].
3. Determining glycosylation score – a parameter that indicates how likely the protein is to be glycosylated – using the NGlycPred server (https://bioinformatics.niaid.nih.gov/nglycpred/).

Our aim was to synthesize two different immunogens that have very distinct objectives. The goal of the first immunogen is to induce the production of SARS-CoV-2-specific and neutralizing antibodies, while the second aims to elicit cross-reactive antibodies against both SARS-CoV-2 and SARS-CoV for a more broadly protective vaccine. We here describe the design and synthesis of an antigen with glycans shielding the cryptic CR3022 epitope and the S309 epitope, and a second antigen linked to two glycans covering a large portion of the RBM epitope. Once our antigens were properly characterized, they were conjugated to a multivalent scaffold and used for immunizations.

4.3 Materials and Methods

4.3.1 Selection of RBD mutants

Glycan attachment sites were selected based on a thorough analysis of the crystal structure of SARS-CoV-2 bound to ACE2, CR3022, or S309 (PDBs 6M0J, 6W41, and 6WPS, respectively). Based on the wild-type (wt) sequence of RBD, we identified naturally occurring Asparagine, Threonine, and Serine residues that could be used for the

incorporation of the N-X-S/T motif. In addition to those, other amino acids located on the three epitopes that were solvent accessible were also selected as potential candidates and screened further.

Starr et al. [162] recently published extensive data that demonstrated how amino acid substitutions on RBD affect expression yield and binding to ACE2. This information was extremely useful for the mutant selection process and substitutions that had shown to severely decrease yield were discarded. Additionally, the data demonstrating what amino acids were crucial for ACE2 binding helped us selecting them as potential mutation candidates (when we desired to shield RBM) or to leave them undisturbed (when the goal was to keep the RBM exposed).

The PyMol Software was used to create RBD models reflecting the target mutations. The PDB file of RBD (PDB 6M0J) was uploaded onto PyMoL and mutations were inserted using the software's mutagenesis tool. The new mutated protein model was uploaded to the NGlycPred server, where they were assigned a glycosylation score between 0 and 1. A score of 0 corresponds to a 0% probability of glycosylation happening, while values close to 1 represent a high likelihood of proper glycosylation.

4.3.2 Cloning of RBD, ACE2, CR3022, and mi3-SpyCatcher

Amino acids 319-541 were extracted from the SARS-CoV-2 S protein sequence (UniProt P0DTC2). To this sequence we incorporated genes coding for a C-terminal GGSGG spacer, a SpyTag, and a 6xHis-Tag, resulting in construct 2019-nCoV RBD (319-541)-SpyTag, which was optimized for expression in mammalian cells. Point mutations K356T/S383N/P384K and E484N/F486T/T500N/G502T were inserted to create the

mutants 354/383-RBD and 484/500-RBD. Synthesis and cloning of these constructs were done by Gene Universal Inc. (Newark, DE).

The DNA sequence corresponding to amino acids 1-615 of the ACE2 receptor (UniProt Q9NYF.1) was codon-optimized for expression in mammalian cells and cloned into the pcDNA3.1 vector. For CR3022, the sequences for the light and heavy chains (retrieved from PDB 6W41) were cloned into the TGEX-LC and TGEX-HC vectors, respectively. Codon optimization and DNA synthesis for all three constructs was done by Gene Universal.

DNA encoding the mi3-SpyCatcher fusion protein [193] was cloned into pEt 21a and synthesized by Gene Universal with no additional modifications. All DNA constructs were transformed in BL21(DE3) cells and frozen as glycerol stocks for future use.

4.3.3 Expression and Purification of RBD, ACE2, and CR3022 in mammalian cells

RBD, ACE2, and S309 constructs were expressed in HEK293F suspension cells using the ExpiFectamine™ 293 transfection kit (A14524, Gibco) according to the manufacturer's protocol. Cells expressing the RBD and RBD mutants were harvested 3-4 days after transfection and the supernatant was thoroughly dialyzed against IMAC Binding Buffer and purified by IMAC as previously described. Eluates were further purified by SEC with a Superdex 75 10/300 GL (GE) column for the removal of high molecular weight contaminants.

Cells transfected with ACE2 and CR3022 DNA were harvested 6 days later. Similarly to the RBD proteins, ACE2 was dialyzed against IMAC Binding Buffer and

purified by IMAC. The cell culture medium containing the CR3022 antibodies was directly loaded onto a MabSelect SuRe column (GE) and purified according to the manufacturer's recommendations. All purified proteins were concentrated and stored at 4°C in PBS for future use.

4.3.4 ELISA

96-well plates were coated with 50 µL of wt or mutant RBD at 4 µg/mL and incubated at room temperature for 1 hr. Blocking and washing was performed as previously described. Wells were then incubated with 50 µL of ACE2 and CR3022 antibodies synthesized *in-house*. The plates were washed three more times and incubated with HRP-conjugated anti-human antibodies for an additional hour. Wells were developed with 50 µL of TMB, and the reaction was stopped by adding 50 µL of Stop Solution. Absorbance at 450 nm was measured.

4.3.5 Expression and Purification of mi3-SpyCatcher

BL21 cells transformed with mi3-SpyCatcher were grown at 37^{o}C overnight in 5 mL of 2xYT medium containing Kanamycin. These starter cultures were then diluted into 1 L of 2xYT also supplemented with Kanamycin and allowed to grow at 37^{o}C. Cells were induced with 0.5 mM IPTG when the O.D. reached 0.8 and allowed to grow overnight at 22^{o}C. Cultures were harvested the following day and lyzed according to the protocol described in [193]. In brief, the cell pellet was resuspended in 20 mL of CaptureSelect Equilibration Buffer (25 mM Tris, 150 mM NaCl, pH 8.5) containing 2 µg of lysozyme, 125 units of benzonase, and half of a tablet of SigmaFast EDTA-free protease inhibitor cocktail. The mixture was incubated at room temperature for 1 hr and then sonicated for

5 minutes with 5s on, 5s off pulses. Following sonication, the solution was centrifuged for 30 minutes at 17,000xg, and the supernatant was poured over 5 mL of pre-equilibrated CaptureSelect C-tag Affinity Matrix (ThermoFisher Scientific). The resin was washed with 10 CVs of CaptureSelect Equilibration Buffer and eluted with CaptureSelect Elution Buffer (20 mM Tris, 2 M MgCl2, pH 8.5). All purification steps were performed at 4^{o}C.

The eluate containing the protein of interested was dialyzed against 25 mM Tris, 150 mM NaCl, pH 8.5, overnight with a 50 kDa MWCO dialysis membrane and concentrated by spin filtration with a 50kDa MWCO ViVaspin filters. The concentrated protein was further purified by SEC using a Superdex Increase 200 10/300 GL column. Fractions corresponding to chromatogram peaks were analyzed by DLS and tubes containing large amounts of aggregates were discarded. The remaining fractions were concentrated and stored at 4^{o}C.

4.3.6 Conjugation of RBDs to mi3-SpyCatcher Nanocages

Small scale reactions between the RBD glycans and mi3-SpyCatcher were initially set up to determine optimal stoichiometric ratios. Mixtures were allowed to react overnight and RBD conjugation to the scaffold was determined by SDS-PAGE. Reactions with wt RBD and 354/383-RBD showed a consumption of ~ 90% of RBD. Products of the reaction with 484/500-RBD were further purified using a Superdex 200 column. Sample purity and final RBD concentration were determined by SDS-PAGE.

4.3.7 Immunizations

All immunizations were performed by ProSci Inc. (Poway, CA). Four groups of three mice were immunized with 14 µg of RBD (wt or mutants) conjugated to mi3-SpyCatcher or 16.8 µg of mi3-SpyCatcher mixed with an equal volume of Addavax adjuvant. The prime injection was followed by a boost on day 24. The dose used for the boost was increase to 20 µg of RBD antigen and 24 µg of mi3-SpyCatcher, also mixed with Addavax.

4.4 Results and Discussion

4.4.1 Mutant Selection

One of the main challenges of this project was to select glycosylation sites on RBD that would not only shield the desired epitopes, but also result in decent protein yield, maintain correct protein folding, and show proper glycosylation during expression. The initial step was to analyze the crystal structure of RBD conjugated to ACE2, CR3022, and S309. For the synthesis of the ACE2-blocker, we chose to insert two glycans on the receptor-binding region in order to maximize shielding. We reasoned that the introduction of glycans at residues 484 and 500 would cover a decent portion of the ACE2 binding region and thus selected these as glycosylation sites (Figure 31a). Using the GlyProt server (http://www.glycosciences.de/modeling/glyprot/php/main.php) [194-196], we were able to simulate the conjugation of glycans on residues 484 and 500 of RBD and show how they would interfere with ACE2 binding. Both images are shown in Figure 32. For the shielding of CR3022 and S309, we chose to incorporate glycans on residues 354 (Figure 31b) and 383 (Figure 31c).

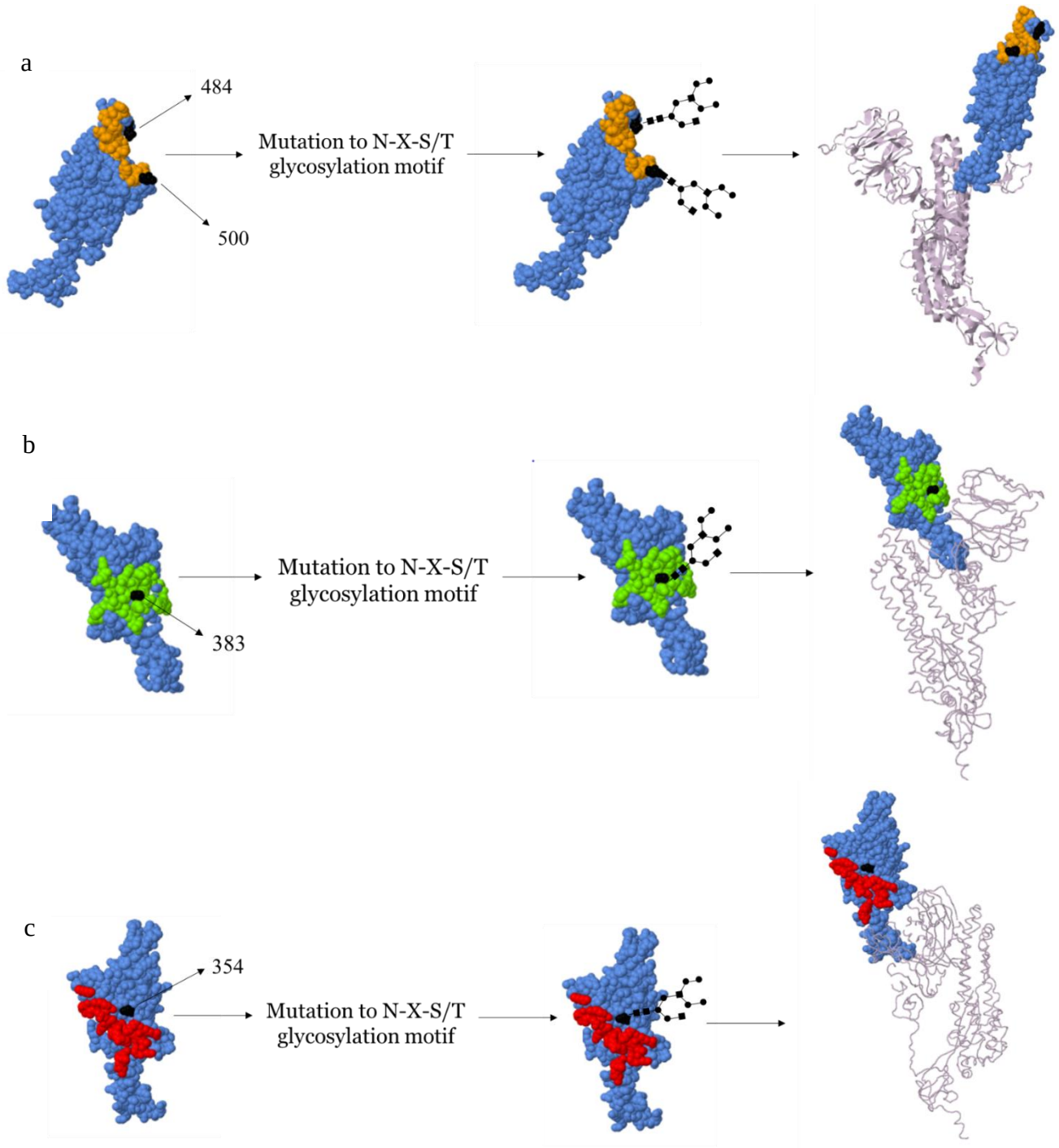

Figure 31. Incorporation of glycosylation sequon for the synthesis of RBD mutants. (a) RBD with N-glycans on residues 484 and 500 (black) for the shielding of ACE2-binding region (orange). (b) RBD with glycosylation motif incorporated for glycan attachment to residue 383 (black) for blocking of CR3022 antibody (epitope shown in green). (c) N-glycan attached to amino acid 354 (black) to shield S309 epitope (red).

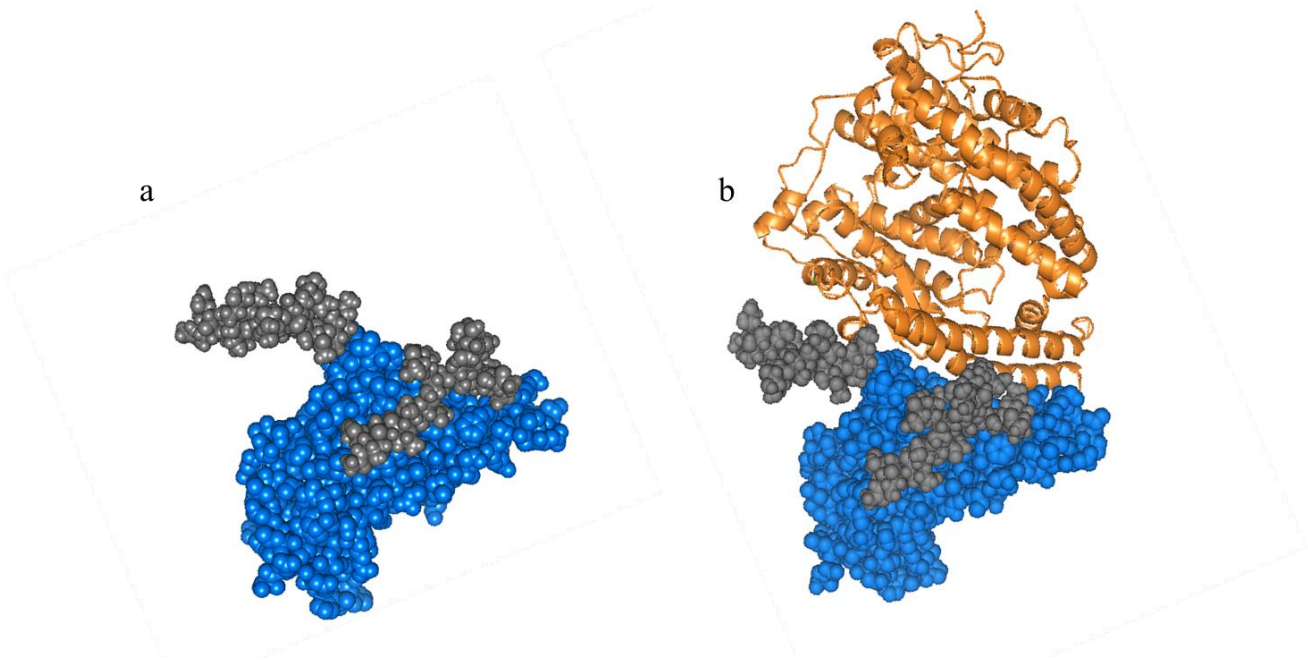

Figure 32. Simulation of glycan attachment to residues 484 and 500 of RBD using the GlyPro Server. (a) Structure of hybrid glycans (grey) attached to RBD (blue). (b) ACE2 (orange) binding to RBD should not be possible due to the presence of the glycans.

Next, we cross-referenced literature data determine possible negative effects of the mutations on protein expression levels. Using a yeast display library, Starr et al. [162] studied substitutions to all RBD amino acids and analyzed their overall effect on protein yield and binding to the ACE2 receptor. The results were recently published and were instrumental for consolidating our mutant choices since low yields would severely hinder our ability to conjugate the antigens to a nanoscaffold. Using the heat map showed in Figure 33a, we concluded that mutations K356T, S383N, P384K, F486T, and G502T

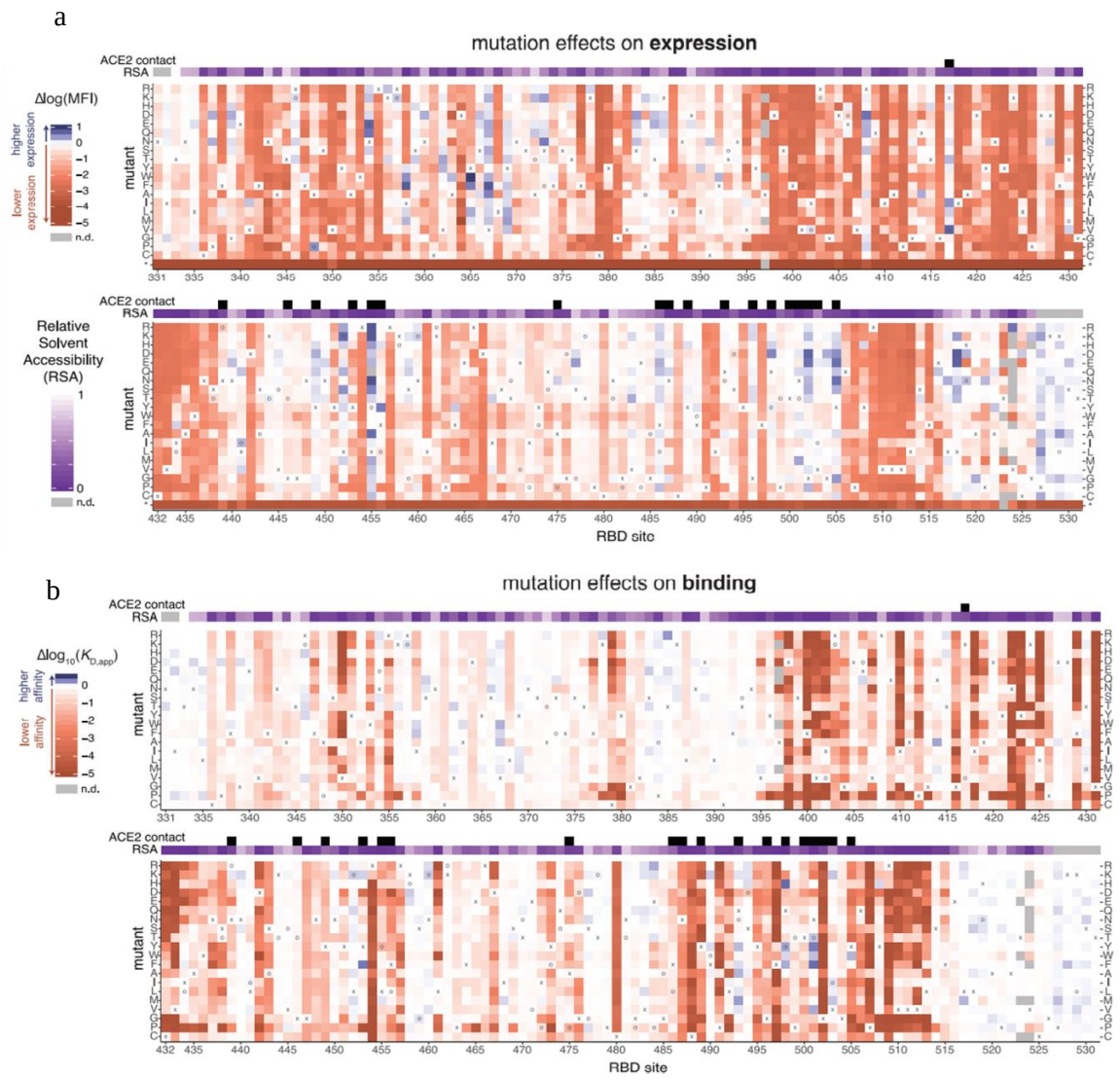

Figure 33. Effects of DNA mutations on RBD expression yields and binding to ACE2. (a) Amino acid substitutions can result in an increase (blue) or decrease (red) or yield. (b) The same substitution can increase (blue) or decrease (red) the affinity of RBD to ACE2. Figures adapted from Starr et al. 2020 *[162]*

would increase yield, while mutations E484N and T500N would have no effect on expression levels. In addition, the heat map in Figure 33b shows which amino acid mutations had an effect on to ACE2 binding. This data was helpful to consolidate our

choice of ACE2-blocker and to ensure that the mutants on the CR3022/S309 blockers would not impact interaction of the antigen with ACE2.

The last step consisted of ensuring that the glycosylation sites would indeed become glycosylated following expression in mammalian cells. Although in theory the N-X-S/T sequon promotes attachment of an oligosaccharide to the Asparagine, not all sequons result in glycosylation since there might be structural constraints [197]. Bioinformatic tools have been developed to help determine the likelihood of glycosylation for a single sequon based on a protein's surface accessibility, secondary structure, local contact order, and residue pattern [198]. The NGlycPred Server allows for the input of any PDB file and, as an output, delivers a score from 0-1, which correlates with the likelihood of successful glycosylation for all glycosylation motifs within the molecule. The scores obtained for all four glycosylation sites were high (above 0.8) and are summarized in Figure 34. This analysis led us to believe that our selected mutants would become glycosylated as predicted.

Residue Number	Glycosylation Score	Glycosylated?
343	0.981	+
354	0.966	+
383	1.00	+
484	0.862	+
500	0.875	+

Figure 34. Glycosylation scores predicted by NGlycPred Server. Scores close to 1 mean a higher likelihood of glycan attachment after expression. Residues number 343 is a naturally occurring N-glycan. PDB file 6M0J was used for the mutations on PyMol.

4.4.2 Expression and Characterization of RBD antigens

The two RBD mutants along with wt RBD were expressed in mammalian cells, purified, and characterized by SDS-PAGE. SDS-PAGE allowed us not only to assess sample purity but also to gauge whether glycosylation was successful or not. Glycans are unable to bind SDS, thus decreasing the net charge-to-mass ratio of the protein-SDS complex. As a result, glycosylated proteins tend to migrate more slowly on a polyacrylamide gel [199, 200]. Even though glycans are often between 1 kDa and 3 kDa [201], this unusual behavior allows us to differentiate between a single or double glycosylated protein. It is important to note that wt RBD contains a naturally occurring N-linked glycan on amino acid 343, which results in an apparent molecular weight higher than the expected 30 kDa. Figure 35a shows the 484/500 and 354/383 mutants right next to wt RBD and the differences in apparent molecular weight are visible.

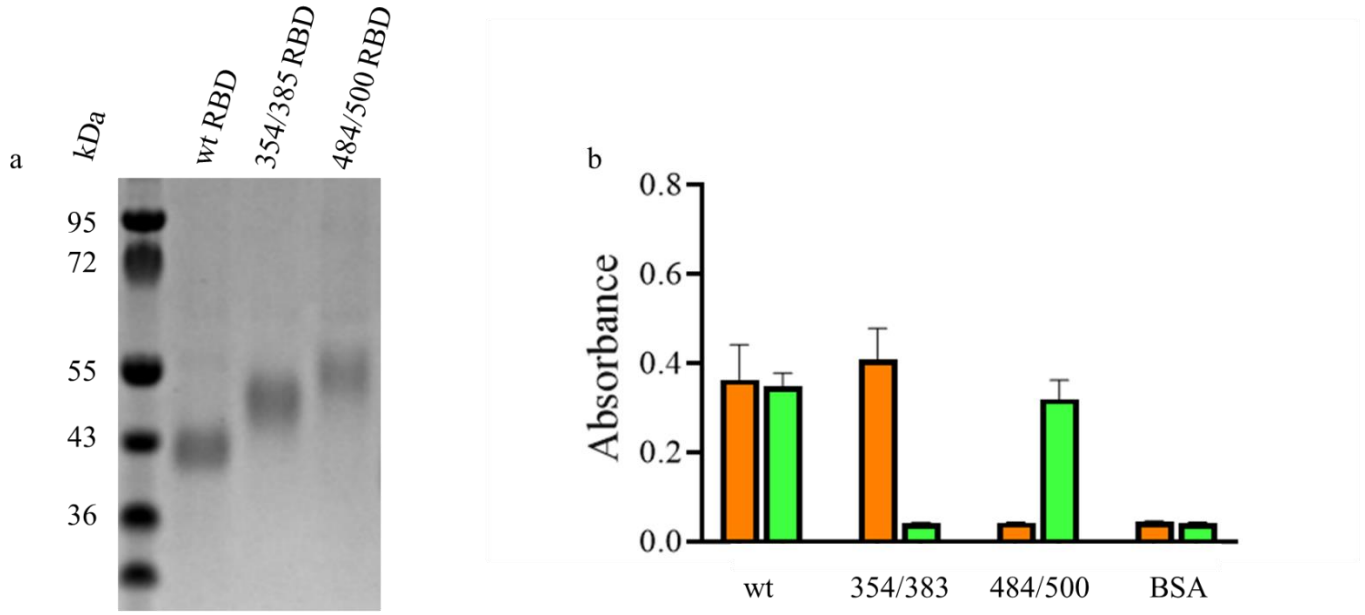

Figure 35. Characterization of RBD antigens. (a) Characterization by SDS-PAGE. (b) Binding of ACE2 (orange bars) and antibody CR3022 (green bars) to wt and mutant RBD by ELISA. BSA was used as a negative control.

It is important to note that, although mutant 354/383 runs lower on a SDS-PAGE in comparison to 484/500, we strongly believe the antigen to have the two predicted glycans. Experiments performed during the screening stage of the project provided evidence that single mutants 354 and 383 were properly glycosylated. Therefore, we believe that when combined, the glycosylation pattern is still maintained. The difference is apparent molecular can likely be explained by different glycans, with different sizes, being attached to each glycosylation site [202].

In order to confirm epitope shielding by the glycans, we tested the binding of wt RBD, 484/500, and 354/383 to CR3022 antibody and recombinant ACE2 by ELISA (Figure 35b). As seen in the figure, both antibodies bound to wt RBD. As expected, ACE2 did not bind significantly to 484/500, whereas CR3022 did not bind to 354/383. This confirms the ability of the glycans to shield targeted epitopes on RBD.

4.4.3 Conjugating RBD antigens to a multivalent nanoscaffold

One of the overarching themes of this thesis is the importance of multivalency for eliciting a robust immune response. Therefore, once again, we designed and synthesized multivalent versions of all of our RBD constructs. We previously described successful conjugation of antigens to a VLP-Streptavidin multivalent platform. Initial experiments expressing the wild-type RBD (wt RBD) fused to an AviTag in mammalian cells, however, resulted in modest yields. Given the additional possibility of losses associated with the *in vitro* biotinylation reaction and the extensive purification required for the isolation of the target product, we chose to use a strategy that allowed us to bypass the biotinylation process and directly conjugate our antigens to nanoscaffolds.

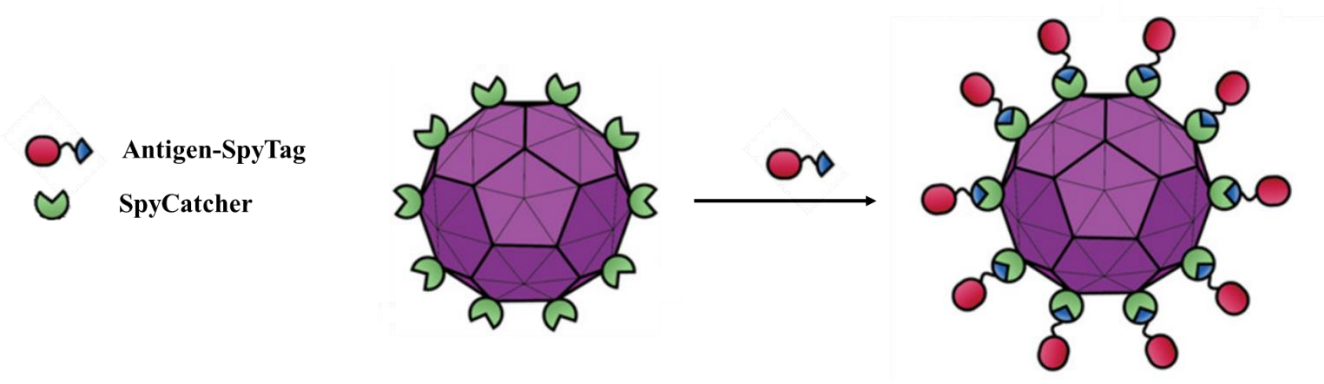

Figure 36. Schematic of mi3-SpyCatcher Scaffold conjugated to a SpyTagged antigen. Adapted from Bruun et al., 2018 [193].

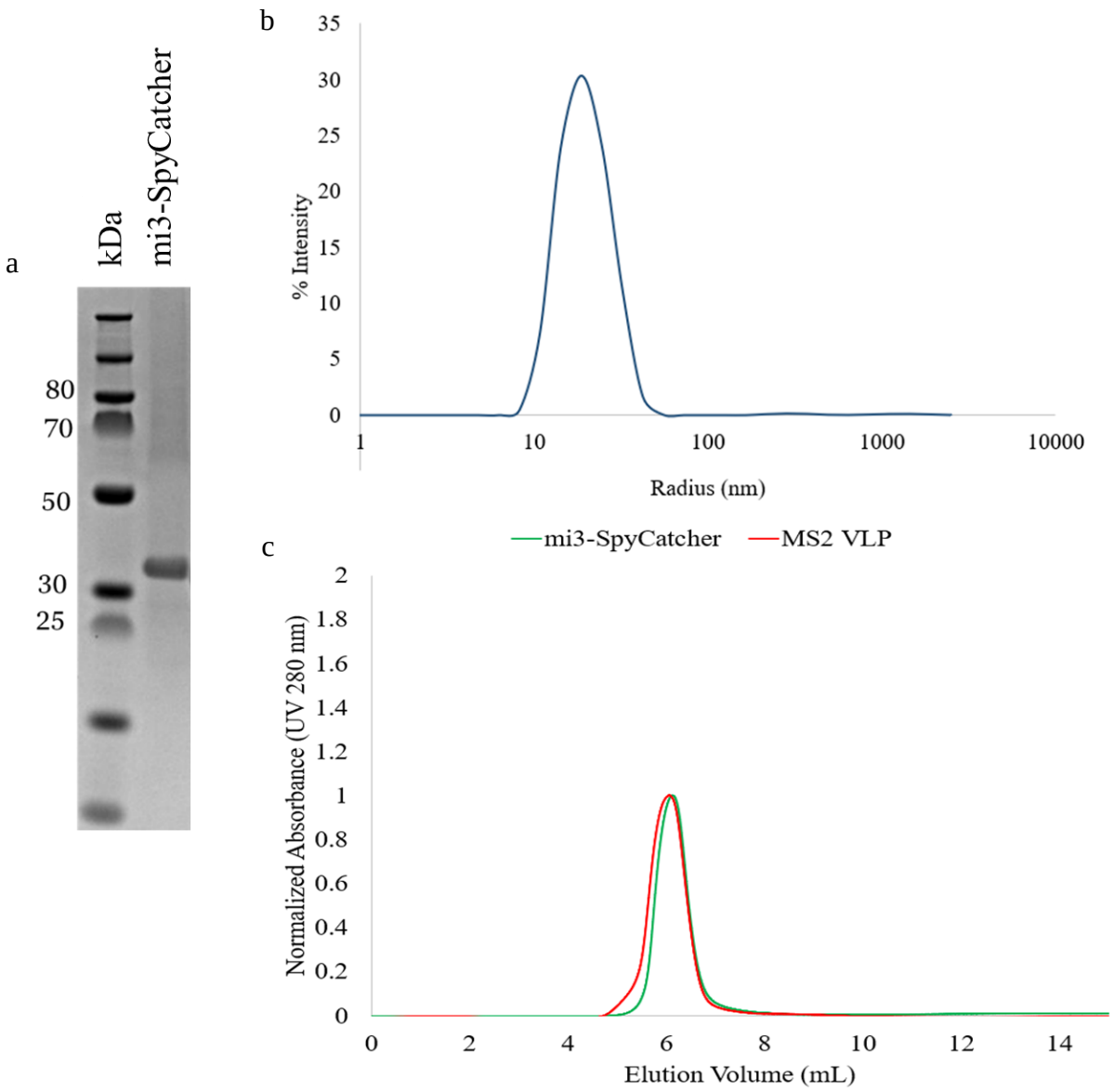

Figure 37. Characterization of mi3-SpyCatcher Nanocages. (a) SDS-PAGE of mi3-SpyCatcher after affinity chromatography and SEC. (b) DLS measurements of purified mi3-SpyCatcher. The measured average particle radius agrees with the literature *[193]* (c) Comparison between SEC elution profiles between MS2 VLP and mi3-SpyCatcher. Both particles have similar sizes, resulting in similar elution volumes.

The Howarth lab had previously reported a platform in which the protein nanocage i301 [203], derived from the bacterium *Thermotoga maritima*, was fused to a

truncated SpyCatcher protein and genetically modified to increase yields and stability [193]. The resulting construct, termed mi3-SpyCatcher, self-assembles into a 60-mer upon expression in *E. coli* and allows for the attachment of SpyTagged proteins. Figure 36 shows a schematic of the conjugation of SpyTagged antigens to the mi3-SpyCatcher. Therefore, replacing the AviTag peptide with a SpyTag allowed us to quickly and easily conjugate our RBD antigens to this new platform.

Following the protocol provided in [193], we were able to successfully synthesize, purify, and characterize mi3-SpyCatcher nanocages, as demonstrated by SDS-PAGE (Figure 37a). mi3-SpyCatcher was expressed in *E. coli* cells, resulting in correctly assembled nanoparticles, as demonstrated by DLS and SEC. DLS measurements showed an average particle radius of 16-18 nm, in agreement with previously reported data [193] (Figure 37). The elution volumes on SEC also suggest the assembly of a large structure. Figure 37c shows the SEC chromatograms of mi3-SpyCatcher in comparison to the MS2 VLP.

After proper characterization of the nanocages, we synthesized multivalent versions of our SpyTagged RBD antigens by allowing them to react with the mi3-SpyCatcher. Small scale reactions were set up to determine the stoichiometric ratio. Excess mi3-SpyCatcher often resulted in near complete (greater than 90%) consumption of the RBD antigen. Furthermore, we determined that an occupation of at least 50% of antigen binding sites on the nanocage would suffice for BCR clustering [204, 205]. Conjugation of the RBD antigens to mi3-SpyCatcher was confirmed by SDS-PAGE, as

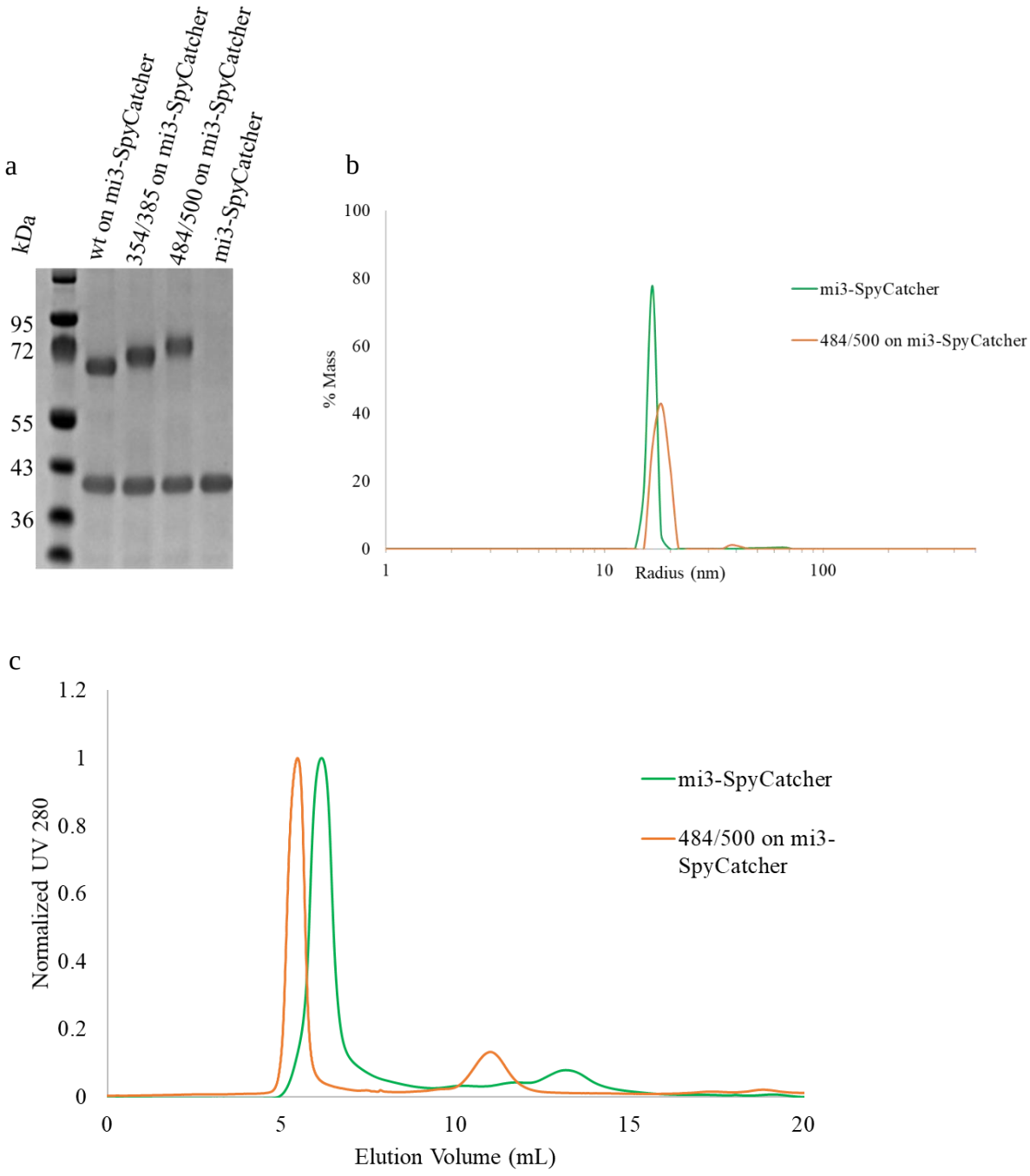

Figure 38. Characterization of RBD antigens conjugated to mi3-SpyCatcher. (a) The reaction product of RBD and mi3-SpyCatcher was analyzed by SDS-PAGE. Higher bands correspond to RBD conjugated to mi3-SpyCatcher while lower bands demonstrate the presence of unreacted mi3-SpyCatcher. (b) Radius of mi3-SpyCatcher vs. 484/500 on mi3-SpyCatcher as measured by DLS. (c) Comparison of SEC elution volumes between mi3-SpyCatcher and 484/500 on mi3-SpyCatcher.

shown in Figure 38a. DLS measurements also showed a difference in particle radius after reaction with RBD, as shown in Figure 38b, as does the difference in elution volumes seen after SEC (Figure 38c).

4.4.4 Immunizations

Given the encouraging results obtained from our antigen characterization, we proceeded to characterize the immunogenicity of the wt and engineered RBD antigens *in vivo*. Animal studies were carried out by ProSci Inc. (Poway, CA). Four groups of three mice were immunized with the multivalent wt RBD, 354/383-RBD, 484/500-RBD, or mi3-SpyCatcher alone. Mice were immunized with 14 µg of antigen mixed with an equal volume of Addavax adjuvant. The prime injection will be followed by a boost 24 days later. Prior to the boost, animals will be bled, and the collected sera will be analyzed. We aim to determine antibody titers to assess whether a robust immune response against RBD was generated.

4.5 Conclusions and Future Directions

We were able to demonstrate the successful synthesis of RBD antigens that had been mutated for the attachment of glycans during expression. Efficient blocking of CR3022 and ACE2 binding to our RBD mutants was demonstrated by ELISA. Furthermore, the antigens were conjugated to a novel nanoscaffold, which has the potential of enhancing the immune response during immunization. This new delivery platform also resulted in high yields, allowing us to perform in vivo experiments with a high dose.

Although the in vivo experiments are yet to be completed, we plan on initially characterizing the animal sera to determine if an immune response was generated towards the RBD antigens. We will test binding of sera to wt RBD in order to estimate the antibody titers for all four groups. A final bleed will take place 2-3 weeks after the boost injection and the nature of the anti-RBD antibodies generated by each group will be assessed. Experiments such as immunodepletions will first help us establish whether refocusing occurred. Viral neutralization experiments (to be performed by collaborators) will then allow us to determine if neutralizing antibodies were generated. In particular, we will compare the ability of the sera from the 354/383 and 484/500-immunized groups to neutralize both SARS-CoV and SARS-CoV-2. If our efforts prove to be successful, we would like to test the ability of the two antigens to protect animals in a viral challenge experiment. These results will ultimately help us determine the efficacy of our novel RBD vaccines.

CHAPTER 5. CONCLUSION AND FUTURE WORK

In the current work, we describe different approaches to engineer viral antigens with the goal of modulating the immune response generated against them. Antigen sequence variability often poses a challenge to vaccine design since antibodies elicited upon immunization might no longer be protective of different (or slightly mutated) strains of the virus. Furthermore, immunodominant regions of protein antigens can cause the immune response to focus on epitopes that are non-neutralizing, making the vaccine ineffective. To overcome some of these challenges, we developed strategies that would allow us to modulate the immune response generated towards proteins of ZIKV and SARS-CoV-2.

Regarding the Zika virus, we applied our nanopatterning tool to Domain III of the ZIKV E protein, an antigen targeted by ZIKV-specific antibodies. We demonstrated how the site-specific attachment of PEG chains to DIII resulted in the successful shielding of selected epitopes on the protein and the refocusing of the immune response towards the exposed epitopes. Furthermore, we demonstrated the effects of multivalency on immunogenicity and explored the use of two different multivalent scaffolds. After comparing the results obtained from immunizations performed with DIII on the Branched PEG Scaffold versus the VLP platform, we concluded that the use of a higher valency scaffold, i.e., the VLP, at a higher dose contributed to an enhanced immune response.

Although we were able to demonstrate that nanopatterning DIII resulted in the refocusing of the immune response, we are yet to determine if our multivalent Sample DIII* could be used as a ZIKV vaccine. Future steps for this project would involve testing

the neutralization potential of the antibodies elicited by our Sample DIII* antigen and assessing its ability to protect mice from a viral challenge. An added benefit of this strategy is that given the specificity of these antibodies towards ZIKV we could potentially prevent ADE from occurring. Therefore, it would be desirable to determine the cross-reactivity of the elicited antibodies and whether they can potentially enhance infections with DENV *in vivo*.

The goal motivating the design of our second ZIKV-based immunogen was to elicit broadly neutralizing antibodies. These would target a quaternary epitope at the E dimer interface, and potentially neutralize both ZIKV and DENV. Although recombinant E protein can exist in both dimeric and monomeric forms, high concentrations shift the equilibrium towards the dimer. Therefore, we conjugated E protein monomers to the surface of a VLP with the goal of increasing the local E concentration and promoting dimerization. We observed the binding of dimer-specific antibodies to our VLP-E conjugates, suggesting the formation of stable E dimers. Future immunization studies will help us determine if these stable dimers can elicit broadly neutralizing antibodies. We propose to immunize separate groups of mice with the E dimers or with a negative control (E monomers mixed with a "blocked" VLP) and compare the types of antibodies elicited in each case. For the dimer group, we hope to see the generation of EDE-binding antibodies, that can potently neutralize both ZIKV and DENV. Ultimately, we would like to determine whether an immunization with our synthesized E dimers can result in the protection of mice from a viral challenge.

However, we must consider the possibility that immunization with our E dimers will generate monomer-binding antibodies (mainly directed towards the FLE) in addition

to EDE-targeting antibodies. If that is the case, we propose to introduce point mutations in the E fusion loop, which should disturb recognition of the epitope by antibodies and help direct the immune response towards EDE. Although several strategies to synthesize E dimers have already been reported, if shown to be successful, our approach would offer a few advantages such as the multivalent presentation of dimers and the blocking of the highly conserved dimer underside.

Lastly, we designed and synthesized a vaccine against SARS-CoV-2, a novel virus that continues to spread and claim thousands of lives every day. The receptor-binding domain (RBD) of the S protein has been identified as the main target of neutralizing antibodies, having epitopes that are targeted by antibodies that are either specific to SARS-CoV-2, or that are cross-reactive between SARS-CoV-2 and SARS-CoV. Hence, we engineered RBD to create two variants of this antigen. The first contained glycans designed to shield SARS-CoV-2-specific epitopes to promote the elicitation of broadly neutralizing antibodies, while the second has glycans designed to focus the antibody response towards neutralizing epitopes in the SARS-CoV-2 receptor-binding motif (RBM). As in Aim 1 and Aim 2, we also conjugated these antigens to a multivalent nanoscaffold, which should contribute to an enhanced immune response. Preliminary results demonstrated successful epitope shielding by the glycans and immunization studies are ongoing.

Once these studies are completed our first goal is to measure the antibody titers against both RBD and S proteins. To determine if there are any differences in the type of antibodies generated by the immunization with 354/383 and 484/500 mutants, we propose to compare the ability of the sera to bind to the SARS-CoV-2 RBD and SARS-CoV RBD.

We would expect to see higher antibody titers against the SARS-CoV RBD for the group immunized with 484/500 than for the group immunized with 354/383, suggesting that a broader protection was generated. It will also be interesting to determine the ability of these anti-RBD antibodies to neutralize SARS-CoV-2 and SARS-CoV. We would ultimately like to test whether our RBD-based vaccines can protect hamsters from a viral challenge.

In summary, this work explored different approaches to modulate the immune response. We described two orthogonal methods of epitope shielding that yielded successful results *in vitro,* and we are excited about assessing their ability to provide protection against the viruses in future *in vivo* studies. In addition, our two alternative ZIKV vaccines may, in two very different ways, eliminate ADE from occurring, thus overcoming one of the main challenges of developing a safe ZIKV vaccine. We also explored the use of different multivalent scaffolds and as per Aim 1 results, we were able to demonstrate the advantages of multivalent antigen presentation. Furthermore, the approaches described here have demonstrated great potential and we look forward to applying them in the design of vaccines against several other pathogens.

REFERENCES

1. Pulendran B, Ahmed R: **Translating Innate Immunity into Immunological Memory: Implications for Vaccine Development**. *Cell* 2006, **124**(4):849-863.

2. Akira S, Uematsu S, Takeuchi O: **Pathogen Recognition and Innate Immunity**. *Cell* 2006, **124**(4):783-801.

3. Medzhitov R, Janeway C: **Innate Immunity**. *New England Journal of Medicine* 2000, **343**(5):338-344.

4. Beutler B: **Innate immunity: an overview**. *Molecular Immunology* 2004, **40**(12):845-859.

5. Janeway CA Jr TP, Walport M, et al.: **Immunobiology: The Immune System in Health and Disease.** In: *Principles of innate and adaptive immunity.* 5th edition edn: Garland Science; 2001.

6. Murphy K: **Basic Concepts in Immunology**. In: *Janeway's Immunobiology.* 8th edition edn: by Garland Science, Taylor & Francis Group, LLC; 2012.

7. Marshall JS, Warrington R, Watson W, Kim HL: **An introduction to immunology and immunopathology**. *Allergy, Asthma & Clinical Immunology* 2018, **14**(2):49.

8. Murphy K: **The major histocompatibility complex and its function**. In: *Janeway's Immunology.* 8th edition edn: Garland Science, Taylor & Francis Group, LLC; 2012.

9. Taniuchi I: **CD4 Helper and CD8 Cytotoxic T Cell Differentiation**. *Annual Review of Immunology* 2018, **36**(1):579-601.

10. Medzhitov R: **Recognition of microorganisms and activation of the immune response**. *Nature* 2007, **449**(7164):819-826.

11. Mahnke YD, Brodie TM, Sallusto F, Roederer M, Lugli E: **The who's who of T-cell differentiation: Human memory T-cell subsets**. *European Journal of Immunology* 2013, **43**(11):2797-2809.

12. Batista FD, Harwood NE: **The who, how and where of antigen presentation to B cells**. *Nature Reviews Immunology* 2009, **9**(1):15-27.

13. Clem AS: **Fundamentals of vaccine immunology**. *J Glob Infect Dis* 2011, **3**(1):73-78.

14. Chen X, Jensen PE: **The role of B lymphocytes as antigen-presenting cells**. *Archivum Immunologiae et Therapiae Experimentalis* 2008, **56**(2):77.

15. Chesnut RW, Grey HM: **Studies on the capacity of B cells to serve as antigen-presenting cells**. *The Journal of Immunology* 1981, **126**(3):1075.

16. Murphy K: **8-cell responses to bacterial polysaccharides do not require**

peptide-specific T-cell help. In: *Janeway's Immunology*. 8th edition edn: Garland Science, Taylor & Francis Group, LLC; 2012.

17. **B-cell activation by T-cell-independent type 2 antigens as an integral part of the humoral immune response to pathogenic microorganisms**. *Immunological Reviews* 2000, **176**(1):154-170.

18. Lesinski GB, Westerink MAJ: **Novel vaccine strategies to T-independent antigens**. *Journal of Microbiological Methods* 2001, **47**(2):135-149.

19. Liao W, Hua Z, Liu C, Lin L, Chen R, Hou B: **Characterization of T-Dependent and T-Independent B Cell Responses to a Virus-like Particle**. *The Journal of Immunology* 2017, **198**(10):3846.

20. Harwood NE, Batista FD: **Early Events in B Cell Activation**. *Annual Review of Immunology* 2010, **28**(1):185-210.

21. Taillardet M, Haffar G, Mondière P, Asensio M-J, Gheit H, Burdin N, Defrance T, Genestier L: **The thymus-independent immunity conferred by a pneumococcal polysaccharide is mediated by long-lived plasma cells**. *Blood* 2009, **114**(20):4432-4440.

22. Obukhanych TV, Nussenzweig MC: **T-independent type II immune responses generate memory B cells**. *J Exp Med* 2006, **203**(2):305-310.

23. Weisel F, Shlomchik M: **Memory B Cells of Mice and Humans**. *Annual Review of Immunology* 2017, **35**(1):255-284.

24. Sallusto F, Lanzavecchia A, Araki K, Ahmed R: **From vaccines to memory and back**. *Immunity* 2010, **33**(4):451-463.

25. Krammer F, Palese P: **Influenza virus hemagglutinin stalk-based antibodies and vaccines**. *Current Opinion in Virology* 2013, **3**(5):521-530.

26. Wang TT, Palese P: **Catching a Moving Target**. *Science* 2011, **333**(6044):834.

27. Krammer F, Pica N, Hai R, Margine I, Palese P: **Chimeric Hemagglutinin Influenza Virus Vaccine Constructs Elicit Broadly Protective Stalk-Specific Antibodies**. *J Virol* 2013, **87**(12):6542.

28. Eggink D, Goff PH, Palese P: **Guiding the Immune Response against Influenza Virus Hemagglutinin toward the Conserved Stalk Domain by Hyperglycosylation of the Globular Head Domain**. *J Virol* 2014, **88**(1):699.

29. Impagliazzo A, Milder F, Kuipers H, Wagner MV, Zhu X, Hoffman RMB, van Meersbergen R, Huizingh J, Wanningen P, Verspuij J *et al*: **A stable trimeric influenza hemagglutinin stem as a broadly protective immunogen**. *Science* 2015, **349**(6254):1301.

30. Kwong PD, Wilson IA: **HIV-1 and influenza antibodies: seeing antigens in new ways**. *Nature immunology* 2009, **10**(6):573-578.

31. Rappuoli R: **The challenge of developing universal vaccines**. *F1000 Med Rep* 2011, **3**:16-16.

32. Arsiwala A: **Engineering Protein Antigens to Refocus the Immune Response**. School of Chemical and Biomolecular Engineering Theses and Dissertations: Georgia Institute of Technology; 2019.

33. Pantophlet R, Wilson IA, Burton DR: **Hyperglycosylated mutants of human immunodeficiency virus (HIV) type 1 monomeric gp120 as novel antigens for HIV vaccine design**. *J Virol* 2003, **77**(10):5889-5901.

34. Frey S, Varner C, Arsiwala A, Currier M, Moore M, Kane R: **The Design of Vaccines Based on the Shielding of Antigenic Site Ø of a Respiratory Syncytial Virus Fusion Protein Immunogen**. *Advanced Healthcare Materials* 2020:2000714.

35. Duan H, Chen X, Boyington JC, Cheng C, Zhang Y, Jafari AJ, Stephens T, Tsybovsky Y, Kalyuzhniy O, Zhao P *et al*: **Glycan Masking Focuses Immune Responses to the HIV-1 CD4-Binding Site and Enhances Elicitation of VRC01-Class Precursor Antibodies**. *Immunity* 2018, **49**(2):301-311.e305.

36. Arsiwala A, Varner C, McCaffery JN, Kell A, Pendyala G, Castro A, Hariharan V, Moreno A, Kane RS: **Nanopatterning protein antigens to refocus the immune response**. *Nanoscale* 2019, **11**(32):15307-15311.

37. Mlakar J, Korva M, Tul N, Popovic M, Poljsak-Prijatelj M, Mraz J, Kolenc M, Resman Rus K, Vesnaver Vipotnik T, Fabjan Vodusek V *et al*: **Zika Virus Associated with Microcephaly**. *N Engl J Med* 2016, **374**(10):951-958.

38. Lancaster MA, Renner M, Martin C-A, Wenzel D, Bicknell LS, Hurles ME, Homfray T, Penninger JM, Jackson AP, Knoblich JA: **Cerebral organoids model human brain development and microcephaly**. *Nature* 2013, **501**(7467):373-379.

39. Schuler-Faccini L RE, Feitosa IM: **Possible Association Between Zika Virus Infection and Microcephaly — Brazil, 2015**. In: *Morbidity and Mortality Weekly Report.* vol. 65. cdc.gov; 2016: 59-62.

40. Cao-Lormeau V-M, Blake A, Mons S, Lastère S, Roche C, Vanhomwegen J, Dub T, Baudouin L, Teissier A, Larre P *et al*: **Guillain-Barré Syndrome outbreak associated with Zika virus infection in French Polynesia: a case-control study**. *The Lancet* 2016, **387**(10027):1531-1539.

41. Hahn AF: **Guillain-Barré syndrome**. *The Lancet* 1998, **352**(9128):635-641.

42. Annelies Wilder-Smith JH, Martin Friede **Zika Vaccine Development Technology Roadmap**. In.: World Health Organization; 2019.

43. Organization WH: **Preferred Product Characteristics for a Zika vaccine for endemic use**. In.; 2019.

44. Vannice KS, Cassetti MC, Eisinger RW, Hombach J, Knezevic I, Marston HD, Wilder-Smith A, Cavaleri M, Krause PR: **Demonstrating vaccine effectiveness during a waning epidemic: A WHO/NIH meeting report on approaches to development and licensure of Zika vaccine candidates**. *Vaccine* 2019, **37**(6):863-868.

45. **Covid-19 "will end up as a Top 10 leading cause of death" in 2020, CDC statisticians tell CNN**

46. Prevention CfDCa: **10 Leading Causes of Death by Age Group, United States-2018**. In. Edited by National Vital Statistics Systems NCfHS, CDC. www.cdc.gov; 2018.

47. Ledford H: **Coronavirus reinfections: three questions scientists are asking**. *Nature* 2020, **585**(7824):168-169.

48. Crill WD, Chang G-JJ: **Localization and Characterization of Flavivirus Envelope Glycoprotein Cross-Reactive Epitopes**. *J Virol* 2004, **78**(24):13975.

49. Lindenbach B, Thiel HJ, Rice CM: **Flaviviridae: The viruses and their replication**. *Fields Virology* 2007:1101-1151.

50. Bardina SV, Bunduc P, Tripathi S, Duehr J, Frere JJ, Brown JA, Nachbagauer R, Foster GA, Krysztof D, Tortorella D *et al*: **Enhancement of Zika virus pathogenesis by preexisting antiflavivirus immunity**. *Science* 2017, **356**(6334):175-180.

51. Vasilakis N, Weaver SC: **Flavivirus transmission focusing on Zika**. *Current Opinion in Virology* 2017, **22**:30-35.

52. Screaton G, Mongkolsapaya J, Yacoub S, Roberts C: **New insights into the immunopathology and control of dengue virus infection**. *Nature Reviews Immunology* 2015, **15**(12):745-759.

53. Dai L, Song J, Lu X, Deng Y-Q, Musyoki Abednego M, Cheng H, Zhang Y, Yuan Y, Song H, Haywood J *et al*: **Structures of the Zika Virus Envelope Protein and Its Complex with a Flavivirus Broadly Protective Antibody**. *Cell Host & Microbe* 2016, **19**(5):696-704.

54. Roehrig J: **Antigenic Structure of Flavivirus Proteins**. *Advances in virus research* 2003, **59**:141-175.

55. Dai L, Wang Q, Qi J, Shi Y, Yan J, Gao GF: **Molecular basis of antibody-mediated neutralization and protection against flavivirus**. *IUBMB Life* 2016, **68**(10):783-791.

56. Crill WD, Roehrig JT: **Monoclonal Antibodies That Bind to Domain III of Dengue Virus E Glycoprotein Are the Most Efficient Blockers of Virus Adsorption to Vero Cells**. *J Virol* 2001, **75**(16):7769.

57. Dejnirattisai W, Supasa P, Wongwiwat W, Rouvinski A, Barba-Spaeth G, Duangchinda T, Sakuntabhai A, Cao-Lormeau V-M, Malasit P, Rey FA *et al*: **Dengue virus sero-cross-reactivity drives antibody-dependent enhancement of infection with zika virus**. *Nature Immunology* 2016, **17**(9):1102-1108.

58. Katzelnick LC, Narvaez C, Arguello S, Lopez Mercado B, Collado D, Ampie O, Elizondo D, Miranda T, Bustos Carillo F, Mercado JC *et al*: **Zika virus infection enhances future risk of severe dengue disease**. *Science* 2020, **369**(6507):1123.

59. Kawiecki AB, Christofferson RC: **Zika Virus-Induced Antibody Response Enhances Dengue Virus Serotype 2 Replication In Vitro**. *J Infect Dis* 2016, **214**(9):1357-1360.

60. George J, Valiant WG, Mattapallil MJ, Walker M, Huang YS, Vanlandingham DL, Misamore J, Greenhouse J, Weiss DE, Verthelyi D *et al*: **Prior Exposure to Zika Virus Significantly Enhances Peak Dengue-2 Viremia in Rhesus Macaques**. *Sci Rep* 2017, **7**(1):10498.

61. Flipse J, Smit JM: **The Complexity of a Dengue Vaccine: A Review of the Human Antibody Response**. *PLOS Neglected Tropical Diseases* 2015, **9**(6):e0003749.

62. Bhatt S, Gething PW, Brady OJ, Messina JP, Farlow AW, Moyes CL, Drake JM, Brownstein JS, Hoen AG, Sankoh O *et al*: **The global distribution and burden of dengue**. *Nature* 2013, **496**(7446):504-507.

63. Rouvinski A, Guardado-Calvo P, Barba-Spaeth G, Duquerroy S, Vaney M-C, Kikuti CM, Navarro Sanchez ME, Dejnirattisai W, Wongwiwat W, Haouz A *et al*: **Recognition determinants of broadly neutralizing human antibodies against dengue viruses**. *Nature* 2015, **520**(7545):109-113.

64. Yang C, Zeng F, Gao X, Zhao S, Li X, Liu S, Li N, Deng C, Zhang B, Gong R: **Characterization of two engineered dimeric Zika virus envelope proteins as immunogens for neutralizing antibody selection and vaccine design**. *J Biol Chem* 2019, **294**(27):10638-10648.

65. Beasley DWC, Barrett ADT: **Identification of Neutralizing Epitopes within Structural Domain III of the West Nile Virus Envelope Protein**. *J Virol* 2002, **76**(24):13097.

66. Oliphant T, Nybakken GE, Austin SK, Xu Q, Bramson J, Loeb M, Throsby M, Fremont DH, Pierson TC, Diamond MS: **Induction of Epitope-Specific Neutralizing Antibodies against West Nile Virus**. *J Virol* 2007, **81**(21):11828.

67. Stettler K, Beltramello M, Espinosa DA, Graham V, Cassotta A, Bianchi S, Vanzetta F, Minola A, Jaconi S, Mele F *et al*: **Specificity, cross-reactivity, and function of antibodies elicited by Zika virus infection**. *Science* 2016, **353**(6301):823-826.

68. Heinz FX, Stiasny K: **The Antigenic Structure of Zika Virus and Its Relation to Other Flaviviruses: Implications for Infection and Immunoprophylaxis**. *Microbiology and Molecular Biology Reviews* 2017, **81**(1):e00055-00016.

69. Zhao H, Fernandez E, Dowd KA, Speer SD, Platt DJ, Gorman MJ, Govero J, Nelson CA, Pierson TC, Diamond MS *et al*: **Structural Basis of Zika Virus-Specific Antibody Protection**. *Cell* 2016, **166**(4):1016-1027.

70. Dowd KA, Pierson TC: **The Many Faces of a Dynamic Virion: Implications of Viral Breathing on Flavivirus Biology and Immunogenicity**. *Annu Rev Virol* 2018, **5**(1):185-207.

71. Zhang X, Sheng J, Plevka P, Kuhn RJ, Diamond MS, Rossmann MG: **Dengue structure differs at the temperatures of its human and mosquito hosts**. *Proc Natl Acad Sci U S A* 2013, **110**(17):6795-6799.

72. Arsiwala A, Castro A, Frey S, Stathos M, Kane RS: **Designing Multivalent Ligands to Control Biological Interactions: From Vaccines and Cellular Effectors to Targeted Drug Delivery**. *Chemistry – An Asian Journal* 2019, **14**(2):244-255.

73. Krishnamurthy VM, Estroff LA, Whitesides GM: **Multivalency in Ligand Design**. *Fragment-based Approaches in Drug Discovery* 2006:11-53.

74. Puffer EB, Pontrello JK, Hollenbeck JJ, Kink JA, Kiessling LL: **Activating B Cell Signaling with Defined Multivalent Ligands**. *ACS Chemical Biology* 2007, **2**(4):252-262.

75. Bennett NR, Zwick DB, Courtney AH, Kiessling LL: **Multivalent Antigens for Promoting B and T Cell Activation**. *ACS Chemical Biology* 2015, **10**(8):1817-1824.

76. Fairhead M, Howarth M: **Site-specific biotinylation of purified proteins using BirA**. *Methods in molecular biology (Clifton, NJ)* 2015, **1266**:171-184.

77. Lino CA, Caldeira JC, Peabody DS: **Display of single-chain variable fragments on bacteriophage MS2 virus-like particles**. *J Nanobiotechnology* 2017, **15**(1):13-13.

78. Peabody DS, Manifold-Wheeler B, Medford A, Jordan SK, do Carmo Caldeira J, Chackerian B: **Immunogenic Display of Diverse Peptides on Virus-like Particles of RNA Phage MS2**. *Journal of Molecular Biology* 2008, **380**(1):252-263.

79. Fairhead M, Krndija D, Lowe ED, Howarth M: **Plug-and-play pairing via defined divalent streptavidins**. *Journal of molecular biology* 2014, **426**(1):199-214.

80. Nelson C, Lee C, Fremont D: **Oxidative Refolding from Inclusion Bodies**. *Methods in molecular biology (Clifton, NJ)* 2014, **1140**:145-157.

81. Ovaa H, wals k: **Unnatural amino acid incorporation in E. coli: current and future applications in the design of therapeutic proteins**. *Frontiers in Chemistry* 2014, **2**(15).

82. Normanly J, Kleina LG, Masson J-M, Abelson J, Miller JH: **Construction of Escherichia coli amber suppressor tRNA genes: III. Determination of tRNA specificity**. *Journal of Molecular Biology* 1990, **213**(4):719-726.

83. Krieg UC, Walter P, Johnson AE: **Photocrosslinking of the signal sequence of nascent preprolactin to the 54-kilodalton polypeptide of the signal recognition particle**. *Proceedings of the National Academy of Sciences* 1986, **83**(22):8604.

84. Chin JW, Santoro SW, Martin AB, King DS, Wang L, Schultz PG: **Addition of p-Azido-l-phenylalanine to the Genetic Code of Escherichia coli**. *Journal of the American Chemical Society* 2002, **124**(31):9026-9027.

85. Kohrer C RU: **Proteins Carrying One or More Unnatural Amino Acids**. In: *Madame Curie Bioscience Database*. Landes Bioscience; 2000-2013.

86. Amiram M, Haimovich AD, Fan C, Wang Y-S, Aerni H-R, Ntai I, Moonan DW, Ma NJ, Rovner AJ, Hong SH *et al*: **Evolution of translation machinery in recoded bacteria enables multi-site incorporation of nonstandard amino acids**. *Nat Biotechnol* 2015, **33**(12):1272-1279.

87. Bessette PH, Åslund F, Beckwith J, Georgiou G: **Efficient folding of proteins with multiple disulfide bonds in the Escherichia coli cytoplasm**. *Proceedings of the National Academy of Sciences* 1999, **96**(24):13703.

88. **Cu-Free Click Chemistry (SPAAC)** [https://clickchemistrytools.com/cu-free-click-chemistry-spaac/]

89. Hein CD, Liu X-M, Wang D: **Click chemistry, a powerful tool for pharmaceutical sciences**. *Pharm Res* 2008, **25**(10):2216-2230.

90. Duncan R: **The dawning era of polymer therapeutics**. *Nature Reviews Drug Discovery* 2003, **2**(5):347-360.

91. Zakeri B, Fierer JO, Celik E, Chittock EC, Schwarz-Linek U, Moy VT, Howarth M: **Peptide tag forming a rapid covalent bond to a protein, through engineering a bacterial adhesin**. *Proceedings of the National Academy of Sciences* 2012, **109**(12):E690.

92. Cabral-Miranda G, Lim SM, Mohsen MO, Pobelov IV, Roesti ES, Heath MD, Skinner MA, Kramer MF, Martina BEE, Bachmann MF: **Zika Virus-Derived E-DIII Protein Displayed on Immunologically Optimized VLPs Induces Neutralizing Antibodies without Causing Enhancement of Dengue Virus Infection**. *Vaccines* 2019, **7**(3).

93. Yang M, Lai H, Sun H, Chen Q: **Virus-like particles that display Zika virus envelope protein domain III induce potent neutralizing immune responses in mice**. *Scientific Reports* 2017, **7**(1):7679.

94. Bachmann MF, Zinkernagel RM: **NEUTRALIZING ANTIVIRAL B CELL RESPONSES**. *Annual Review of Immunology* 1997, **15**(1):235-270.

95. Metzger H: **Transmembrane signaling: the joy of aggregation**. *The Journal of Immunology* 1992, **149**(5):1477.

96. Brezski R.J. MJG: **B-Cell Receptor**. In: *Multichain Immune Recognition Receptor Signaling Advances in Experimental Medicine and Biology*. Edited by A.B. S, vol. 640. New York, NY: Springer; 2008.

97. Galaway FA, Stockley PG: **MS2 Viruslike Particles: A Robust, Semisynthetic Targeted Drug Delivery Platform**. *Molecular Pharmaceutics* 2013, **10**(1):59-68.

98. Golmohammadi R, Valegård K, Fridborg K, Liljas L: **The Refined Structure of Bacteriophage MS2 at 2·8 Å Resolution**. *Journal of Molecular Biology* 1993, **234**(3):620-639.

99. Ni C-Z, Syed R, Kodandapani R, Wickersham J, Peabody DS, Ely KR: **Crystal structure of the MS2 coat protein dimer: implications for RNA binding and virus assembly**. *Structure* 1995, **3**(3):255-263.

100. Kuzmanovic DA, Elashvili I, Wick C, O'Connell C, Krueger S: **Bacteriophage MS2: Molecular Weight and Spatial Distribution of the Protein and RNA Components by Small-Angle Neutron Scattering and Virus Counting**. *Structure* 2003, **11**(11):1339-1348.

101. **Dengue and Severe Dengue** [https://www.who.int/news-room/fact-sheets/detail/dengue-and-severe-dengue]

102. Sirohi D, Chen Z, Sun L, Klose T, Pierson TC, Rossmann MG, Kuhn RJ: **The 3.8 Å resolution cryo-EM structure of Zika virus**. *Science* 2016, **352**(6284):467-470.

103. Kostyuchenko VA, Lim EX, Zhang S, Fibriansah G, Ng TS, Ooi JS, Shi J, Lok SM: **Structure of the thermally stable Zika virus**. *Nature* 2016, **533**(7603):425-428.

104. Pierson TC, Fremont DH, Kuhn RJ, Diamond MS: **Structural Insights into the Mechanisms of Antibody-Mediated Neutralization of Flavivirus Infection: Implications for Vaccine Development**. *Cell Host & Microbe* 2008, **4**(3):229-238.

105. Barouch DH, Thomas SJ, Michael NL: **Prospects for a Zika Virus Vaccine**. *Immunity* 2017, **46**(2):176-182.

106. Yang C, Gong R, de Val N: **Development of Neutralizing Antibodies against Zika Virus Based on Its Envelope Protein Structure**. *Virol Sin* 2019, **34**(2):168-174.

107. Slon Campos JL, Mongkolsapaya J, Screaton GR: **The immune response against flaviviruses**. *Nature Immunology* 2018, **19**(11):1189-1198.

108. Barba-Spaeth G, Dejnirattisai W, Rouvinski A, Vaney MC, Medits I, Sharma A, Simon-Loriere E, Sakuntabhai A, Cao-Lormeau VM, Haouz A *et al*: **Structural basis of potent Zika-dengue virus antibody cross-neutralization**. *Nature* 2016, **536**(7614):48-53.

109. Nambala P, Su W-C: **Role of Zika Virus prM Protein in Viral Pathogenicity and Use in Vaccine Development**. *Front Microbiol* 2018, **9**:1797-1797.

110. Heinz FX, Stiasny K, Püschner-Auer G, Holzmann H, Allison SL, Mandl CW, Kunz C: **Structural Changes and Functional Control of the Tick-Borne Encephalitis Virus Glycoprotein E by the Heterodimeric Association with Protein prM**. *Virology* 1994, **198**(1):109-117.

111. Metz S, Gallichotte E, Brackbill A, Premkumar L, Miley M, Baric R, Silva A: **In Vitro Assembly and Stabilization of Dengue and Zika Virus Envelope Protein Homo-Dimers**. *Scientific Reports* 2017, **7**.

112. Kudlacek ST, Premkumar L, Metz SW, Tripathy A, Bobkov AA, Payne AM, Graham S, Brackbill JA, Miley MJ, de Silva AM *et al*: **Physiological temperatures reduce dimerization of dengue and Zika virus recombinant envelope proteins**. *J Biol Chem* 2018, **293**(23):8922-8933.

113. Metz SW, Thomas A, Brackbill A, Forsberg J, Miley MJ, Lopez CA, Lazear HM, Tian S, de Silva AM: **Oligomeric state of the ZIKV E protein defines protective immune responses**. *bioRxiv* 2019:674424.

114. Slon-Campos JL, Dejnirattisai W, Jagger BW, López-Camacho C, Wongwiwat W, Durnell LA, Winkler ES, Chen RE, Reyes-Sandoval A, Rey FA *et al*: **A protective Zika virus E-dimer-based subunit vaccine engineered to abrogate antibody-dependent enhancement of dengue infection**. *Nature immunology* 2019, **20**(10):1291-1298.

115. Rey FA, Stiasny K, Vaney M-C, Dellarole M, Heinz FX: **The bright and the dark side of human antibody responses to flaviviruses: lessons for vaccine design**. *EMBO Rep* 2018, **19**(2):206-224.

116. Gunnoo SB, Madder A: **Chemical Protein Modification through Cysteine**. *ChemBioChem* 2016, **17**(7):529-553.

117. Kim Y, Ho SO, Gassman NR, Korlann Y, Landorf EV, Collart FR, Weiss S: **Efficient site-specific labeling of proteins via cysteines**. *Bioconjugate chemistry* 2008, **19**(3):786-791.

118. Kim YC, Lopez-Camacho C, Nettleship JE, Rahman N, Hill ML, Silva-Reyes L, Ortiz-Martinez G, Figueroa-Aguilar G, Mar MA, Vivanco-Cid H *et al*: **Optimization of Zika virus envelope protein production for ELISA and correlation of antibody titers with virus neutralization in Mexican patients from an arbovirus endemic region**. *Virol J* 2018, **15**(1):193-193.

119. Rouvinski A, Dejnirattisai W, Guardado-Calvo P, Vaney M-C, Sharma A, Duquerroy S, Supasa P, Wongwiwat W, Haouz A, Barba-Spaeth G *et al*: **Covalently linked dengue virus envelope glycoprotein dimers reduce exposure of the immunodominant fusion loop epitope**. *Nature communications* 2017, **8**:15411-15411.

120. Veggiani G, Nakamura T, Brenner MD, Gayet RV, Yan J, Robinson CV, Howarth M: **Programmable polyproteams built using twin peptide superglues**. *Proceedings of the National Academy of Sciences* 2016, **113**(5):1202.

121. Holm C, Joanny J, Kremer K, Netz R, Reineker P, Seidel C, Vilgis T, Winkler R: **Polyelectrolyte Theory**. In., vol. 166; 2004: 3-17.

122. Hsieh S-C, Tsai W-Y, Nerurkar VR, Wang W-K: **Characterization of the ectodomain of the envelope protein of dengue virus type 4: expression, membrane association, secretion and particle formation in the absence of precursor membrane protein**. *PLoS One* 2014, **9**(6):e100641-e100641.

123. Cherrier MV, Kaufmann B, Nybakken GE, Lok S-M, Warren JT, Chen BR, Nelson CA, Kostyuchenko VA, Holdaway HA, Chipman PR *et al*: **Structural basis for the preferential recognition of immature flaviviruses by a fusion-loop antibody**. *The EMBO journal* 2009, **28**(20):3269-3276.

124. Roberson JA, Crill WD, Chang G-JJ: **Differentiation of West Nile and St. Louis encephalitis virus infections by use of noninfectious virus-like particles with reduced cross-reactivity**. *J Clin Microbiol* 2007, **45**(10):3167-3174.

125. Lai C-Y, Tsai W-Y, Lin S-R, Kao C-L, Hu H-P, King C-C, Wu H-C, Chang G-J, Wang W-K: **Antibodies to envelope glycoprotein of dengue virus during the natural course of infection are predominantly cross-reactive and recognize epitopes containing highly conserved residues at the fusion loop of domain II**. *J Virol* 2008, **82**(13):6631-6643.

126. Tsai W-Y, Lai C-Y, Wu Y-C, Lin H-E, Edwards C, Jumnainsong A, Kliks S, Halstead S, Mongkolsapaya J, Screaton GR *et al*: **High-Avidity and Potently Neutralizing Cross-Reactive Human Monoclonal Antibodies Derived from Secondary Dengue Virus Infection**. *J Virol* 2013, **87**(23):12562.

127. Beltramello M, Williams KL, Simmons CP, Macagno A, Simonelli L, Quyen NT, Sukupolvi-Petty S, Navarro-Sanchez E, Young PR, de Silva AM *et al*: **The human immune response to Dengue virus is dominated by highly cross-reactive antibodies endowed with neutralizing and enhancing activity**. *Cell Host Microbe* 2010, **8**(3):271-283.

128. Berneck BS, Rockstroh A, Fertey J, Grunwald T, Ulbert S: **A Recombinant Zika Virus Envelope Protein with Mutations in the Conserved Fusion Loop Leads to Reduced Antibody Cross-Reactivity upon Vaccination**. *Vaccines* 2020, **8**(4).

129. Tsai W-Y, Driesse K, Tsai J-J, Hsieh S-C, Sznajder Granat R, Jenkins O, Chang G-J, Wang W-K: **Enzyme-linked immunosorbent assays using virus-like particles containing mutations of conserved residues on envelope protein can distinguish three flavivirus infections**. *Emerging Microbes & Infections* 2020, **9**(1):1722-1732.

130. **COVID-19 Map** [https://coronavirus.jhu.edu/map.html]

131. **Coronavirus Vaccine Tracker** [https://www.nytimes.com/interactive/2020/science/coronavirus-vaccine-tracker.html]

132. Health NIo: **Fourth large-scale COVID-19 vaccine trial begins in the United States**. In.; 2020.

133. Mahase E: **Covid-19: Pfizer and BioNTech submit vaccine for US authorisation**. *BMJ* 2020, **371**:m4552.

134. Mahase E: **Covid-19: Moderna vaccine is nearly 95% effective, trial involving high risk and elderly people shows**. *BMJ : British Medical Journal (Online)* 2020, **371**.

135. Cohen J: **Effective vaccine offers shot of hope for pandemic**. *Science* 2020, **370**(6518):748.

136. Huang C, Wang Y, Li X, Ren L, Zhao J, Hu Y, Zhang L, Fan G, Xu J, Gu X *et al*: **Clinical features of patients infected with 2019 novel coronavirus in Wuhan, China**. *The Lancet* 2020, **395**(10223):497-506.

137. Zhang J-j, Dong X, Cao Y-y, Yuan Y-d, Yang Y-b, Yan Y-q, Akdis CA, Gao Y-d: **Clinical characteristics of 140 patients infected with SARS-CoV-2 in Wuhan, China**. *Allergy* 2020, **75**(7):1730-1741.

138. Fanelli V, Fiorentino M, Cantaluppi V, Gesualdo L, Stallone G, Ronco C, Castellano G: **Acute kidney injury in SARS-CoV-2 infected patients**. *Critical Care* 2020, **24**(1):155.

139. Wu L, O'Kane AM, Peng H, Bi Y, Motriuk-Smith D, Ren J: **SARS-CoV-2 and cardiovascular complications: From molecular mechanisms to pharmaceutical management**. *Biochemical Pharmacology* 2020, **178**:114114.

140. Xu L, Liu J, Lu M, Yang D, Zheng X: **Liver injury during highly pathogenic human coronavirus infections**. *Liver International* 2020, **40**(5):998-1004.

141. Zhang C, Shi L, Wang F-S: **Liver injury in COVID-19: management and challenges**. *The Lancet Gastroenterology & Hepatology* 2020, **5**(5):428-430.

142. Kirkcaldy RD, King BA, Brooks JT: **COVID-19 and Postinfection Immunity: Limited Evidence, Many Remaining Questions**. *JAMA* 2020, **323**(22):2245-2246.

143. Tillett RL, Sevinsky JR, Hartley PD, Kerwin H, Crawford N, Gorzalski A, Laverdure C, Verma SC, Rossetto CC, Jackson D *et al*: **Genomic evidence for reinfection with SARS-CoV-2: a case study**. *The Lancet Infectious Diseases*.

144. Zhang K, Lau JY-N, Yang L, Ma Z-G: **SARS-CoV-2 reinfection in two patients who have recovered from COVID-19**. *Precision Clinical Medicine* 2020.

145. Chi X, Yan R, Zhang J, Zhang G, Zhang Y, Hao M, Zhang Z, Fan P, Dong Y, Yang Y *et al*: **A neutralizing human antibody binds to the N-terminal domain of the Spike protein of SARS-CoV-2**. *Science (New York, NY)* 2020, **369**(6504):650-655.

146. Llanes A, Restrepo CM, Caballero Z, Rajeev S, Kennedy MA, Lleonart R: **Betacoronavirus Genomes: How Genomic Information has been Used to Deal with Past Outbreaks and the COVID-19 Pandemic**. *Int J Mol Sci* 2020, **21**(12):4546.

147. Rota PA, Oberste MS, Monroe SS, Nix WA, Campagnoli R, Icenogle JP, Peñaranda S, Bankamp B, Maher K, Chen M-h *et al*: **Characterization of a Novel Coronavirus Associated with Severe Acute Respiratory Syndrome**. *Science* 2003, **300**(5624):1394.

148. Zhong NS, Zheng BJ, Li YM, Poon LLM, Xie ZH, Chan KH, Li PH, Tan SY, Chang Q, Xie JP *et al*: **Epidemiology and cause of severe acute respiratory syndrome (SARS) in Guangdong, People's Republic of China, in February, 2003**. *The Lancet* 2003, **362**(9393):1353-1358.

149. Xiao X, Chakraborti S, Dimitrov AS, Gramatikoff K, Dimitrov DS: **The SARS-CoV S glycoprotein: expression and functional characterization**. *Biochemical and Biophysical Research Communications* 2003, **312**(4):1159-1164.

150. Lu R, Zhao X, Li J, Niu P, Yang B, Wu H, Wang W, Song H, Huang B, Zhu N *et al*: **Genomic characterisation and epidemiology of 2019 novel coronavirus: implications for virus origins and receptor binding**. *The Lancet* 2020, **395**(10224):565-574.

151. Wang C, Li W, Drabek D, Okba NMA, van Haperen R, Osterhaus ADME, van Kuppeveld FJM, Haagmans BL, Grosveld F, Bosch B-J: **A human monoclonal antibody blocking SARS-CoV-2 infection**. *Nature Communications* 2020, **11**(1):2251.

152. Li F, Li W, Farzan M, Harrison SC: **Structure of SARS Coronavirus Spike Receptor-Binding Domain Complexed with Receptor**. *Science* 2005, **309**(5742):1864.

153. Li W, Zhang C, Sui J, Kuhn JH, Moore MJ, Luo S, Wong S-K, Huang IC, Xu K, Vasilieva N *et al*: **Receptor and viral determinants of SARS-coronavirus adaptation to human ACE2**. *The EMBO Journal* 2005, **24**(8):1634-1643.

154. Hoffmann M, Kleine-Weber H, Schroeder S, Krüger N, Herrler T, Erichsen S, Schiergens TS, Herrler G, Wu N-H, Nitsche A *et al*: **SARS-CoV-2 Cell Entry Depends on ACE2**

and TMPRSS2 and Is Blocked by a Clinically Proven Protease Inhibitor. *Cell* 2020, **181**(2):271-280.e278.

155. Yan R, Zhang Y, Li Y, Xia L, Guo Y, Zhou Q: **Structural basis for the recognition of SARS-CoV-2 by full-length human ACE2**. *Science* 2020, **367**(6485):1444.

156. Liu Z, Xiao X, Wei X, Li J, Yang J, Tan H, Zhu J, Zhang Q, Wu J, Liu L: **Composition and divergence of coronavirus spike proteins and host ACE2 receptors predict potential intermediate hosts of SARS-CoV-2**. *Journal of Medical Virology* 2020, **92**(6):595-601.

157. Wrapp D, Wang N, Corbett KS, Goldsmith JA, Hsieh C-L, Abiona O, Graham BS, McLellan JS: **Cryo-EM structure of the 2019-nCoV spike in the prefusion conformation**. *Science* 2020, **367**(6483):1260.

158. Tortorici MA, Veesler D: **Chapter Four - Structural insights into coronavirus entry**. In: *Advances in Virus Research.* Edited by Rey FA, vol. 105: Academic Press; 2019: 93-116.

159. Ejemel M, Li Q, Hou S, Schiller ZA, Tree JA, Wallace A, Amcheslavsky A, Kurt Yilmaz N, Buttigieg KR, Elmore MJ *et al*: **A cross-reactive human IgA monoclonal antibody blocks SARS-CoV-2 spike-ACE2 interaction**. *Nature Communications* 2020, **11**(1):4198.

160. Shang J, Ye G, Shi K, Wan Y, Luo C, Aihara H, Geng Q, Auerbach A, Li F: **Structural basis of receptor recognition by SARS-CoV-2**. *Nature* 2020, **581**(7807):221-224.

161. Walls AC, Park Y-J, Tortorici MA, Wall A, McGuire AT, Veesler D: **Structure, Function, and Antigenicity of the SARS-CoV-2 Spike Glycoprotein**. *Cell* 2020, **181**(2):281-292.e286.

162. Starr TN, Greaney AJ, Hilton SK, Ellis D, Crawford KHD, Dingens AS, Navarro MJ, Bowen JE, Tortorici MA, Walls AC *et al*: **Deep Mutational Scanning of SARS-CoV-2 Receptor Binding Domain Reveals Constraints on Folding and ACE2 Binding**. *Cell* 2020, **182**(5):1295-1310.e1220.

163. Chen W-H, Strych U, Hotez PJ, Bottazzi ME: **The SARS-CoV-2 Vaccine Pipeline: an Overview**. *Curr Trop Med Rep* 2020:1-4.

164. Chen W-H, Tao X, Agrawal A, Algaissi A, Peng B-H, Pollet J, Strych U, Bottazzi ME, Hotez PJ, Lustigman S *et al*: **Yeast-Expressed SARS-CoV Recombinant Receptor-Binding Domain (RBD219-N1) Formulated with Alum Induces Protective Immunity and Reduces Immune Enhancement**. *bioRxiv : the preprint server for biology* 2020:2020.2005.2015.098079.

165. Mulligan MJ, Lyke KE, Kitchin N, Absalon J, Gurtman A, Lockhart SP, Neuzil K, Raabe V, Bailey R, Swanson KA *et al*: **Phase 1/2 Study to Describe the Safety and**

Immunogenicity of a COVID-19 RNA Vaccine Candidate (BNT162b1) in Adults 18 to 55 Years of Age: Interim Report. *medRxiv* 2020:2020.2006.2030.20142570.

166. Quinlan BD, Mou H, Zhang L, Guo Y, He W, Ojha A, Parcells MS, Luo G, Li W, Zhong G *et al*: **The SARS-CoV-2 receptor-binding domain elicits a potent neutralizing response without antibody-dependent enhancement**. *bioRxiv* 2020:2020.2004.2010.036418.

167. Ravichandran S, Coyle EM, Klenow L, Tang J, Grubbs G, Liu S, Wang T, Golding H, Khurana S: **Antibody signature induced by SARS-CoV-2 spike protein immunogens in rabbits**. *Science Translational Medicine* 2020, **12**(550):eabc3539.

168. Yang J, Wang W, Chen Z, Lu S, Yang F, Bi Z, Bao L, Mo F, Li X, Huang Y *et al*: **A vaccine targeting the RBD of the S protein of SARS-CoV-2 induces protective immunity**. *Nature* 2020.

169. Zang J, Gu C, Zhou B, Zhang C, Yang Y, Xu S, Bai L, Zhang R, Deng Q, Yuan Z *et al*: **Immunization with the receptor-binding domain of SARS-CoV-2 elicits antibodies cross-neutralizing SARS-CoV-2 and SARS-CoV without antibody-dependent enhancement**. *Cell Discovery* 2020, **6**(1):61.

170. Zheng M, Song L: **Novel antibody epitopes dominate the antigenicity of spike glycoprotein in SARS-CoV-2 compared to SARS-CoV**. *Cellular & Molecular Immunology* 2020, **17**(5):536-538.

171. Huo J, Le Bas A, Ruza RR, Duyvesteyn HME, Mikolajek H, Malinauskas T, Tan TK, Rijal P, Dumoux M, Ward PN *et al*: **Neutralizing nanobodies bind SARS-CoV-2 spike RBD and block interaction with ACE2**. *Nature Structural & Molecular Biology* 2020, **27**(9):846-854.

172. Yi C, Sun X, Ye J, Ding L, Liu M, Yang Z, Lu X, Zhang Y, Ma L, Gu W *et al*: **Key residues of the receptor binding motif in the spike protein of SARS-CoV-2 that interact with ACE2 and neutralizing antibodies**. *Cellular & Molecular Immunology* 2020, **17**(6):621-630.

173. Ou X, Liu Y, Lei X, Li P, Mi D, Ren L, Guo L, Guo R, Chen T, Hu J *et al*: **Characterization of spike glycoprotein of SARS-CoV-2 on virus entry and its immune cross-reactivity with SARS-CoV**. *Nature Communications* 2020, **11**(1):1620.

174. Tai W, He L, Zhang X, Pu J, Voronin D, Jiang S, Zhou Y, Du L: **Characterization of the receptor-binding domain (RBD) of 2019 novel coronavirus: implication for development of RBD protein as a viral attachment inhibitor and vaccine**. *Cellular & Molecular Immunology* 2020, **17**(6):613-620.

175. Tian X, Li C, Huang A, Xia S, Lu S, Shi Z, Lu L, Jiang S, Yang Z, Wu Y *et al*: **Potent binding of 2019 novel coronavirus spike protein by a SARS coronavirus-specific human monoclonal antibody**. *Emerging microbes & infections* 2020, **9**(1):382-385.

176. Menachery VD, Yount BL, Debbink K, Agnihothram S, Gralinski LE, Plante JA, Graham RL, Scobey T, Ge X-Y, Donaldson EF *et al*: **A SARS-like cluster of circulating bat coronaviruses shows potential for human emergence**. *Nature Medicine* 2015, **21**(12):1508-1513.

177. Datta PK, Liu F, Fischer T, Rappaport J, Qin X: **SARS-CoV-2 pandemic and research gaps: Understanding SARS-CoV-2 interaction with the ACE2 receptor and implications for therapy**. *Theranostics* 2020, **10**(16):7448-7464.

178. Wrapp D, De Vlieger D, Corbett KS, Torres GM, Wang N, Van Breedam W, Roose K, van Schie L, Hoffmann M, Pöhlmann S *et al*: **Structural Basis for Potent Neutralization of Betacoronaviruses by Single-Domain Camelid Antibodies**. *Cell* 2020, **181**(5):1004-1015.e1015.

179. Tortorici MA, Beltramello M, Lempp FA, Pinto D, Dang HV, Rosen LE, McCallum M, Bowen J, Minola A, Jaconi S *et al*: **Ultrapotent human antibodies protect against SARS-CoV-2 challenge via multiple mechanisms**. *Science* 2020:eabe3354.

180. Huo J, Zhao Y, Ren J, Zhou D, Duyvesteyn HME, Ginn HM, Carrique L, Malinauskas T, Ruza RR, Shah PNM *et al*: **Neutralization of SARS-CoV-2 by Destruction of the Prefusion Spike**. *Cell Host & Microbe* 2020, **28**(3):445-454.e446.

181. Yuan M, Wu NC, Zhu X, Lee C-CD, So RTY, Lv H, Mok CKP, Wilson IA: **A highly conserved cryptic epitope in the receptor binding domains of SARS-CoV-2 and SARS-CoV**. *Science* 2020, **368**(6491):630.

182. Gui M, Song W, Zhou H, Xu J, Chen S, Xiang Y, Wang X: **Cryo-electron microscopy structures of the SARS-CoV spike glycoprotein reveal a prerequisite conformational state for receptor binding**. *Cell Research* 2017, **27**(1):119-129.

183. Kirchdoerfer RN, Wang N, Pallesen J, Wrapp D, Turner HL, Cottrell CA, Corbett KS, Graham BS, McLellan JS, Ward AB: **Stabilized coronavirus spikes are resistant to conformational changes induced by receptor recognition or proteolysis**. *Scientific Reports* 2018, **8**(1):15701.

184. Pallesen J, Wang N, Corbett KS, Wrapp D, Kirchdoerfer RN, Turner HL, Cottrell CA, Becker MM, Wang L, Shi W *et al*: **Immunogenicity and structures of a rationally designed prefusion MERS-CoV spike antigen**. *Proceedings of the National Academy of Sciences* 2017, **114**(35):E7348.

185. Xiong X, Qu K, Ciazynska KA, Hosmillo M, Carter AP, Ebrahimi S, Ke Z, Scheres SHW, Bergamaschi L, Grice GL *et al*: **A thermostable, closed SARS-CoV-2 spike protein trimer**. *Nature Structural & Molecular Biology* 2020.

186. Wrobel AG, Benton DJ, Hussain S, Harvey R, Martin SR, Roustan C, Rosenthal PB, Skehel JJ, Gamblin SJ: **Antibody-mediated disruption of the SARS-CoV-2 spike glycoprotein**. *Nature Communications* 2020, **11**(1):5337.

187. ter Meulen J, van den Brink EN, Poon LLM, Marissen WE, Leung CSW, Cox F, Cheung CY, Bakker AQ, Bogaards JA, van Deventer E *et al*: **Human Monoclonal Antibody Combination against SARS Coronavirus: Synergy and Coverage of Escape Mutants**. *PLOS Medicine* 2006, **3**(7):e237.

188. Lv Z, Deng Y-Q, Ye Q, Cao L, Sun C-Y, Fan C, Huang W, Sun S, Sun Y, Zhu L *et al*: **Structural basis for neutralization of SARS-CoV-2 and SARS-CoV by a potent therapeutic antibody**. *Science* 2020, **369**(6510):1505.

189. Pinto D, Park Y-J, Beltramello M, Walls AC, Tortorici MA, Bianchi S, Jaconi S, Culap K, Zatta F, De Marco A *et al*: **Cross-neutralization of SARS-CoV-2 by a human monoclonal SARS-CoV antibody**. *Nature* 2020, **583**(7815):290-295.

190. Brooks SA: **Protein glycosylation in diverse cell systems: implications for modification and analysis of recombinant proteins**. *Expert Review of Proteomics* 2006, **3**(3):345-359.

191. Rao RSP, Bernd W: **Do N-glycoproteins have preference for specific sequons?** *Bioinformation* 2010, **5**(5):208-212.

192. Blom N, Sicheritz-Pontén T, Gupta R, Gammeltoft S, Brunak S: **Prediction of post-translational glycosylation and phosphorylation of proteins from the amino acid sequence**. *PROTEOMICS* 2004, **4**(6):1633-1649.

193. Bruun TUJ, Andersson A-MC, Draper SJ, Howarth M: **Engineering a Rugged Nanoscaffold To Enhance Plug-and-Display Vaccination**. *ACS Nano* 2018, **12**(9):8855-8866.

194. Böhm M, Bohne-Lang A, Frank M, Loss A, Rojas-Macias MA, Lütteke T: **Glycosciences.DB: an annotated data collection linking glycomics and proteomics data (2018 update)**. *Nucleic Acids Res* 2019, **47**(D1):D1195-D1201.

195. Lütteke T, Bohne-Lang A, Loss A, Goetz T, Frank M, von der Lieth C-W: **GLYCOSCIENCES.de: an Internet portal to support glycomics and glycobiology research**. *Glycobiology* 2006, **16**(5):71R-81R.

196. Bohne-Lang A, von der Lieth C-W: **GlyProt: in silico glycosylation of proteins**. *Nucleic Acids Res* 2005, **33**(Web Server issue):W214-W219.

197. Tabish S, Raza A, Nasir A, Zafar S, Bokhari H: **Analysis of glycosylation motifs and glycosyltransferases in Bacteria and Archaea**. *Bioinformation* 2011, **6**(5):191-195.

198. Chuang G-Y, Boyington JC, Joyce MG, Zhu J, Nabel GJ, Kwong PD, Georgiev I: **Computational prediction of N-linked glycosylation incorporating structural properties and patterns**. *Bioinformatics* 2012, **28**(17):2249-2255.

199. Marie Nguyen WS: **Application of the Experion Automated Electrophoresis System to Glycoprotein Visualization and Analysis**

In.; 2007.

200. Peters TN: **Gel electrophoresis of proteins: A practical approach (second edition); Edited by B D Hames and D Rickwood. pp 383. IRL press at Oxford University Press, Oxford. 1990. £25 (pbk), also available spiralbound ISBN 0-19-963075-5**. *Biochemical Education* 1991, **19**(1):39-39.

201. Wang G, de Jong RN, van den Bremer ETJ, Parren PWHI, Heck AJR: **Enhancing Accuracy in Molecular Weight Determination of Highly Heterogeneously Glycosylated Proteins by Native Tandem Mass Spectrometry**. *Anal Chem* 2017, **89**(9):4793-4797.

202. Stanley P SH, Taniguchi N: **N-Glycans**. In: *Essentials of Glycobiology, 2nd edition.* Edited by Varki A CR, Esko JD, et al. Cold Spring Harbor (NY): Cold Spring Harbor Laboratory Press; 2009.

203. Hsia Y, Bale JB, Gonen S, Shi D, Sheffler W, Fong KK, Nattermann U, Xu C, Huang P-S, Ravichandran R *et al*: **Design of a hyperstable 60-subunit protein icosahedron**. *Nature* 2016, **535**(7610):136-139.

204. Veneziano R, Moyer TJ, Stone MB, Wamhoff E-C, Read BJ, Mukherjee S, Shepherd TR, Das J, Schief WR, Irvine DJ *et al*: **Role of nanoscale antigen organization on B-cell activation probed using DNA origami**. *Nature Nanotechnology* 2020, **15**(8):716-723.

205. Kato Y, Abbott RK, Freeman BL, Haupt S, Groschel B, Silva M, Menis S, Irvine DJ, Schief WR, Crotty S: **Multifaceted Effects of Antigen Valency on B Cell Response Composition and Differentiation In Vivo**. *Immunity* 2020, **53**(3):548-563.e548.